UNIVERSITÀ
DEGLI STUDI
DI PADOVA

UNIVERSITÀ DEGLI STUDI DI PADOVA

Dipartimento di salute della donna e del bambino

CORSO DI DOTTORATO DI RICERCA IN: MEDICINA DELLO SVILUPPO E SCIENZE DELLA PROGRAMMAZIONE SANTITARIA

Curricolo: Emato-oncologia, genetica, malattie rare e medicina predittiva

XXX CICLO

PHARMACOLOGICAL STUDIES OF NOVEL ANTITUMORAL COMPOUNDS

Tesi redatta con il contributo finanziario: Borsa Legge 170 - Salute dell'uomo (studio e trattamento dei tumouri e delle malattie degenerative con nuovi approcci derivati dalla conoscenza del genoma umano)

Coordinatore: Ch.mo Prof. Carlo Giaquinto
Supervisori: Ch.mo Prof. Giuseppe Basso
Ch.mo Prof. Giampietro Viola

Dottorando: Elena Mattiuzzo

ACKNOWLEDGEMENTS

Special thanks go to Professor Giuseppe Basso, my supervisor Professor Giampietro Viola and to Dr. Roberta Bortolozzi, Dr. Maria Rosaria Esposito and Dr. Pina Fusco.
An important thank you also to my family.

Summary

Over the years biomedical research was focused on the development of new anticancer agents able to selectively target cancer cells at low concentration efficacy. Based on the idea that oncogenes and tumour suppressor genes are a critical force in the malignant transformation of cells, research efforts have focused on developing drugs that directly target these genes. In this context my PhD thesis, focused on the study of new molecules endowed with antiproliferative activity and different mechanisms of action.

In the first study we focused on B-cell acute lymphoblastic leukaemia (B-ALL), that is one of the most common paediatric malignant disorders characterized by an accumulation of B-cell blasts reminiscent of normal stages of differentiation and by infiltration of various extramedullary sites.

Excessive cell proliferation induced by aberrant entry into the cell cycle is considered an hallmark of cancer. Recent findings have revealed that CDK4/6 and its regulatory subunit cyclin D1 are potentially oncogenes and are overexpressed in a diverse set of human cancers, including B-cell acute lymphoblastic leukemia (B-ALL). Moreover, CDK6 is essential for MLL-rearranged leukemias. These findings suggest that CDK4/6 may be effective targets for therapeutic intervention. To test this possibility, we have inhibited CDK4 and CDK6 in four cell lines of B-ALL, characterized by different genetic rearrangements, using Ribociclib, an orally bioavailable, small molecule inhibitor of both CDK4 and CDK6. At low concentration, Ribociclib potently inhibit CDK4/6 without induction of apoptosis; therefore, standard treatment for newly diagnosed childhood B-ALL patients includes glucocorticoids (GC) treatment, but the molecular basis of GC sensitivity and resistance remains largely unknown; for this reason we have tested if Ribociclib in combination with Dexamethasone, a glucocorticoid that is currently used as antitumour agent in the treatment of leukemia, may lead to synergistic killing of leukemia cells.

B-ALL patients that respond poorly to glucocorticoid therapy when diagnosed are usually predicted to undergo relapse. Therefore, understanding the biological mechanisms underlying this poor responsiveness is crucial for the development of more effective therapies.

In the second study we focused our attention on multidrug resistance (MDR) that is one of the most frequent causes of failure of cancer; MDR can lead to the reduction of intracellular drug levels and consequent drug insensitivity, often to multiple

agents. A well-established cause of MDR involves the increased expression of members of the ATP binding cassette (ABC) transporter superfamily, many of which efflux various chemotherapeutic compounds from cells.

Recent discoveries have provided clear evidence that cancer stem cells are present in several cancerous tissues, such as medulloblastoma, neuroblastoma, colon and breast cancers. These cancer stem cells represent only a small percentage of total cell populations and efficiently efflux Hoechst dye resulting in the dye-negative phenotype, also known as side population (SP) phenotype. Further investigations revealed that Hoechst dye efflux is attributable to increased levels of expression of the ABC transporters, which are capable of extruding certain chemotherapeutic agents, and have been implicated in drug resistance. Several approaches have been taken to overcome ABC transportes mediated drug resistance. Recent studies found that certain ecdysteroids derivative, such as the most common 20-hydroxyecdysone, significantly decrease the resistance of a multi-drug resistant (MDR) murine leukemia cell line expressing the human ABCB1 transporter to doxorubicin. This has prompted us to study new candidates structures as P-gp inhibitors derived from ecdysone. We found that these new synthetic P-gp inhibitors could be promising in overcoming multidrug resistance in association with standard chemoterapeutic agents and in eradicating the side population portion that is one of the most resistant cell population to chemotherapy in solid tumours such as medulloblastoma.

In the third study we focused our attention on antitubulinic agents because the most common features of human cancer are the cell cycle deregulation that leads to hyper proliferation pattern. Several therapeutic strategies have been proposed for targeting the tubulin polymerization in cancer. Tubulin binding agents constitute an important class of compounds with broad activity in both solid and in hematologic neoplasia. These agents are believed to block cell division by interfering with the function of the mitotic spindle, blocking cells at the metaphase/anaphase junction of mitosis. In this work we evaluated the antiproliferative activity, interactions with tubulin and cell cycle effects of a new class of simple synthetic inhibitors of tubulin polymerization based on the molecular skeleton of 2-alkoxycarbonyl-3-(3',4',5'-trimethoxyanilino) thiophene. The results we obtained indicated that compound **4c** possessed the highest overall potency and displayed high antiproliferative activities at submicromolar concentrations; we found that it could induce tumour cell apoptosis through reducing the mitochondrial membrane potential and regulating the expression of apoptosis-related proteins in tumour cells.

Publications

The following publications and submitted papers are associated with this dissertation:

- Lesma G., Luraghia A., Rainoldi G., **Mattiuzzo E.**, Bortolozzi R., Viola G., Silvani A. (2016) Multicomponent Approach to Bioactive Peptide– Ecdysteroid Conjugates: Creating Diversity at C6 by Means of the Ugi Reaction *Synthesis* 48: 3907-3916
- Romagnoli R., Kimatrai Salvador M., Santiago Schiaffino O., Baraldi P. G., Oliva P., Baraldi S., Lopez-Cara L. C., Brancale A., Ferla S., Hamel E., Balzarini J., Liekense S., **Mattiuzzo E.**, Basso G. and Viola G. 2-Alkoxycarbonyl-3-arylamino-5-substituted thiophenes as a novel class of antimicrotubule agents. Design, synthesis, cell growth and tubulin polymerization inhibition activity *European Journal of Medicinal Chemistry 143: 683-698*
- Bortolozzi R.*, **Mattiuzzo E.***, Trentin L., Accordi B., Basso G., Viola G. Ribociclib, a CDK4/CDK6 inhibitor, enhances glucocorticoid sensititvity in B-acute lymphoblastic leukemia (B-ALL) *Submitted to Biochemical Pharmacology November 2017*

  ***equal contributing authors**

The following publications have been contributed during the course of this degree, but are not included in this work:

- Romagnoli R., Baraldi PG., Prencipe F., Oliva P., Baraldi S., Kimatrai Salvador M., Lopez-Cara LC., Bortolozzi R., **Mattiuzzo E.**, Basso G. and Viola G. (2017) Design, Synthesis and Biological Evaluation of 3-Substituted-2-Oxindole Hybrid Derivatives as Novel Anticancer Agents *European Journal of Medicinal Chemistry* 134: 258-270
- Bortolozzi R.*, **Mattiuzzo E.***, Hamel E., Carta D, Viola G., Ferlin M.G. Targeting tubulin polymerization by novel 7-aryl-pyrroloquinolinones derivatives, synthesis and SARs *European Journal of Medicinal Chemistry* 143: 244-258

  ***equal contributing authors**

Abbreviations

B-ALL	B-Acute Lymphoblastic Leukaemia
Bcl-2	B-cell lymphoma 2
BSA	Bovine Serum Albumin
CA-4	Combretastatin A4
CDK	Cyclin-Dependent Kinase
CI	Combination Index
CIS	Cis-platin
DEX	Dexamethasone
DOXO	Doxorubicine
GC	Glucocorticoid
GR	Glucocorticoid receptor
H_2-DCFDA	2,7-dichlorodihydrofluorescein diacetate
IC50	Half maximal inhibitory concentration
Mcl-1	Induced Myeloid Leukemia Cell Differentiation protein
MDR	Multidrug Resistance
MTT	3-(4,5-dimethylthiazol-2-yl)-2,5-diphenyltetrazodium bromide
PARP	PolyADP-ribose Polymerase
PBS	Phosphate-buffered saline
P-gp	P-glycoprotein
PI	Propidium Iodide
p-Rb (S780)	Phosphorylated retinoblastoma (S780)
Rb	Retinoblastoma
Rho123	Rhodamine 123
RIBO	Ribociclib
RPPA	Reverse Phase Protein Array
SDS-PAGE	Sodium dodecyl sulfate polyacrylamide gel electrophoresis
VBL	Vinblastine
VCR	Vincristine
WBC	White Blood Cells Count

TABLE OF CONTENTS

CHAPTER 1

TARGETING CYCLIN D1-CDK4/CDK6 COMPLEX

1.1. General introduction

During the mammalian cell cycle, progression through the first gap (G1) phase and initiation of DNA synthesis (S) phase is cooperatively regulated by several cyclins and their associated cyclin dependent kinase (CDKs) (1). The principal kinases involved during G1 phase are CDK4, CDK6 and CDK2 (2). CDK4 and CDK6 form active complexes with one of the three D-type cyclins (D1, D2 or D3) while CDK2 associates with cyclin E; these complexes promote G1-S transition by phosphorylating retinoblastoma tumour suppressor protein (RB). Phosphorylation of RB disables its function as transcriptional repressor to allow activation of the E2F-dependent transcriptional program, an important mediator of S-phase entry and initiation of DNA synthesis (3).

To prevent abnormal proliferation, assembly of active cyclin D-CDK4/CDK6 complexes is negatively and strictly regulated by INK4 protein family members p16, p15, p18 and p19 and by a second group of protein including p21 and p27 (4).

In cancer, cell cycle is dysregulated causing excessive cell proliferation that promotes tumourigenesis and disease progression. Therefore, dysregulation of cell cycle is a hallmark of cancer.

CDK4/CDK6 are frequently hyperactivated or overexpressed in a wide variety of cancers; in particular, it has been found that CDK6 is a direct target of MLL fusion protein in MLL-rearranged acute lymphoblastic leukemia (5).

Based on this, CDK4/CDK6 may be attractive therapeutic targets in childhood acute lymphoblastic leukemia.

1.2 Acute lymphoblastic leukemia

Acute lymphoblastic leukemia (ALL) is a malignant clonal proliferation of lymphoid progenitor cells and it is one of the four main categories of human leukemia; the majority of ALLs are of the B-cell type, characterized by an accumulation of blast B-cells (6). Although ALL can occur at any age, it is more prevalent among children, particularly those aged 3–6 years old. Children treated on modern protocols have survival rates exceeding 90%. Despite significant advances in treatment, approximately 15% to 20% of patients with ALL suffer relapsed disease, the most common cause of treatment failure with an overall survival rate of only 30% (7).

Standard treatment options for newly diagnosed childhood B-ALL patients include chemotherapy treatment and, more commonly, a four-drug induction regimen,

composed of vincristine, glucocorticoids (Dexamethasone or prednisone), L-asparaginase, Ara-c (Cytarabine) and either doxorubicin or daunorubicin (8). Although glucocorticoids (GC) are the most important drugs used in the treatment of ALL for more than 50 years, the molecular basis of GC sensitivity and resistance remains largely unknown. Elucidating the molecular mechanisms related to GC cytotoxicity is crucial for understanding a major part of treatment success or failure in childhood ALL and for the exploration of possibilities to modulate GC resistance (9).

1.3 p16-Cyclin D1-CDK4/CDK6-retinoblastoma axis

The p16-Cyclin D1-CDK4/CDK6-retinoblastoma (RB) axis critically regulates G1 to S phase progression. In response to mitogenic signaling, Cyclin D1-CDK4/CDK6 and Cyclin E/CDK2 complexes cooperate to phosphorylate the tumour suppressor retinoblastoma protein on multiple serine and threonine residues. These phosphorylation events disrupt RB-mediated transcriptional repression and facilitate progression into S-phase (10) (**Fig.1).**

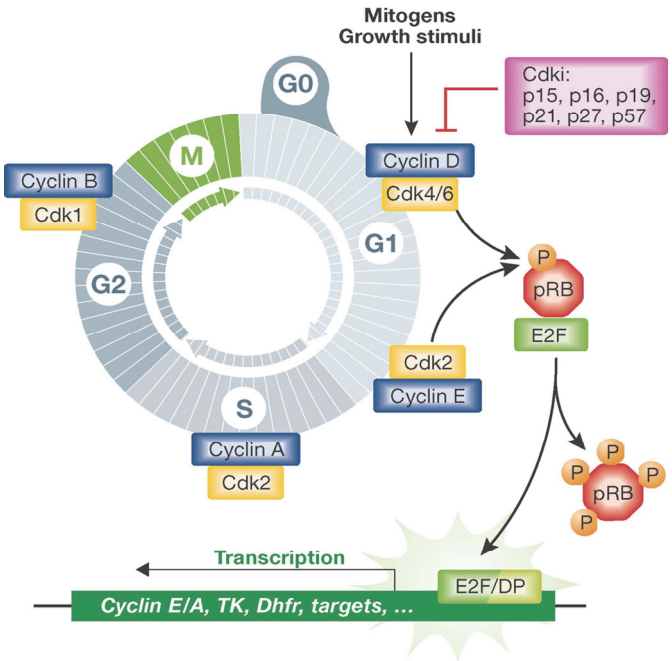

Fig. 1 Overview of p16-Cyclin D-CDK4/CDK6 pathway (11).

INK4 protein family: p16

p16 is the principal member of the INK4 family of CDK inhibitors and it is codified by a gene localized on chromosome 9p21 within the INK4a/ARF locus, which encodes for

two different proteins with different promoters: p16/INK4a and p19/ARF. Both proteins have antiproliferative biological activity, and are involved in the retinoblastoma protein and p53 pathways, respectively (12).

The principal function of p16 is the binding to CDK4 and CDK6 inhibiting their catalytic activity; in addition, to become functional, CDK4/CDK6 require cytoplasmic, post-translational folding in a complex involving heat shock protein (HSP) 90, an interaction that is disrupted by p16. The INK4a locus (also known as CDKN2a) appears to be inactivated in a wide variety of tumours including melanoma, pancreatic adenocarcinoma, glioblastoma, certain leukemias (T-ALL and B-cell ALL), non-small cell lung cancer and bladder carcinoma; among mechanisms that inactivate p16 in tumour cells, homozygous deletion may predominantly contribute to tumourigenesis or disease progression (13;14). Frequency of p16 deletions in B-cell acute lymphoblastic leukemia is around 20% (15).

1.3.1 Cyclin D

Cyclin D (CCND1) promotes cell proliferation as a regulatory partner for CDK4 or CDK6. The resulting cyclin D-CDK complexes display two distinct functions: 1-in the kinase-dependent function, cyclin D-CDK4/CDK6 complex phosporilates the retinoblastoma protein; 2-in the kinase-independent function, D-type cyclins physically bind and activate or repress the activity of several transcription factors (16). There are three D-type cyclins: cyclin D1, cyclin D2 and cyclin D3; cyclin D2 and cyclin D3 proteins are 62% and 51%, respectively, identical to cyclin D1, and 62% identical to each other. Of the three D-type cyclins, cyclin D1 is a known oncogene which overexpression is predominantly associated with human tumourigenesis and cellular metastasis; this overexpression is commonly associated with copy number alterations, or more rarely with mutation, or as a consequence of the dysregulation of mitogenic signalling (17).

1.3.2 Cyclin-dependent kinases (CDKs)

The family of cyclin-dependent kinases (CDKs) contains over 20 members; in particular, CDK4/CDK6 are homologous proteins with overlapping functions in the initiation of the cell cycle. Unbound CDKs are catalytically inactive but when bound to the appropriate D-type cyclins (D1, D2 and D3) the proteins acquire a kinase activity, which is necessary to drive progression of the cell cycle. Cyclin D-CDK4/6 complexes also exert direct regulatory effects on other transcriptional programs to

govern cell proliferation. A prominent example is FOXM1, which enhances the expression of G1/S genes and is activated by CDK4/6–cyclin-dependent phosphorylation (18).

CDK6 or CDK4 overexpression has been demonstrated in several malignancies, including certain types of leukemia and lymphomas. In particular, CDK6, but not CDK4, has been proposed as a direct target of MLL fusion proteins and it has been found that MLL-rearranged ALL cells may gain a proliferative advantage from MLL fusion driven upregulation of CDK6 (19).

1.4 TARGETING CYCLIN D1-CDK4/CDK6 COMPLEX

Dysregulation of the cyclin D1-CDK4/CDK6 complex is frequently observed in cancer and contributes to aberrant cell proliferation and consequent tumourigenesis (20). These findings suggest that CDK4/CDK6 may be effective targets for therapeutic intervention. In particular, the fact that CDK6 is a direct target of MLL rearranged B-cell acute lymphoblastic leukemia prompted us to investigate if pharmacological inhibition of CDK4/CDK6 could increase the efficiency of chemotherapeutic treatment and overcome drug resistance in this haematological malignancy.

In the past, the first-generation CDK inhibitors, denominated pan-inhibitors, were nonselective CDK inhibitors that blocked CDK6 and CDK4 but also had significant off-target effects (21).

However, new selective ATP-competitive inhibitors of CDK4 and CDK6 that have the potential to cause dose-dependent decrease of retinoblastoma phosphorylation and G1 arrest in cancers cells are currently in clinical trials: Palbociclib (PD0332991; Pfizer Inc., FDA-approved), Ribociclib (LEE011; Novartis), and Abemaciclib (LY2835219; Lilly, FDA Breakthrough Therapy status) (22) **(Fig.2)**.

A)

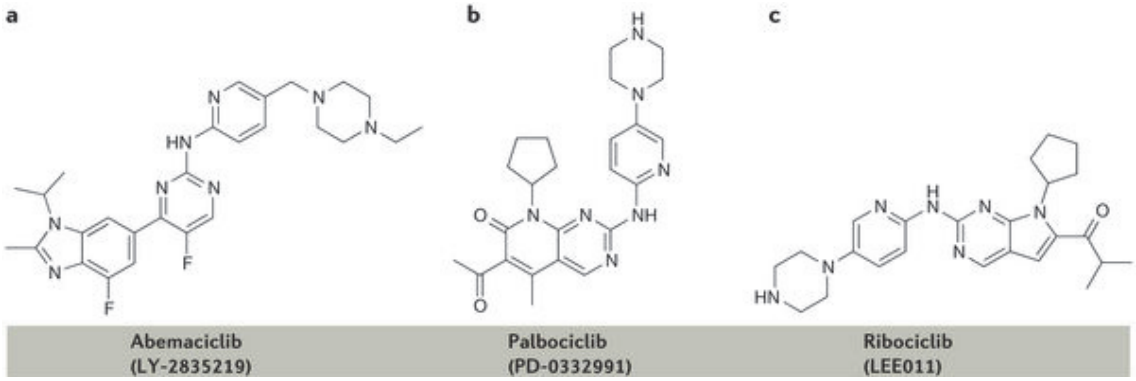

B)

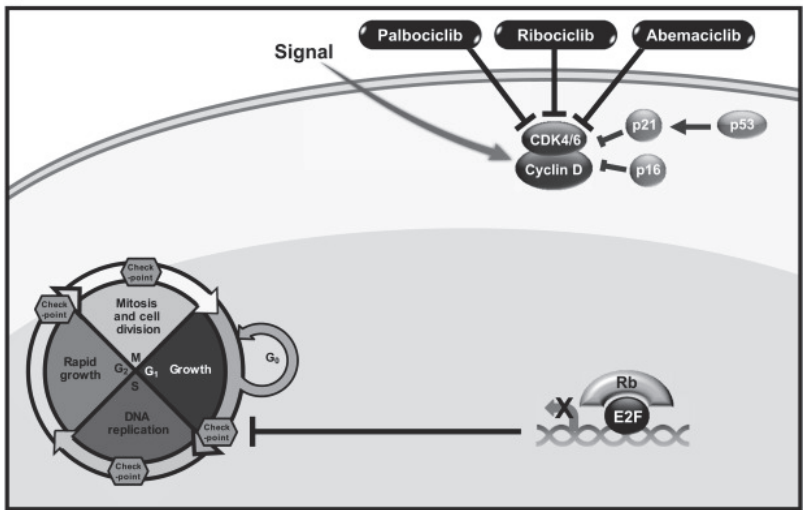

Fig. 2 Inhibiting CDK4/CDK6 in cancer. A) Chemical structure of selective CDK4/CDK6 inhbitors (13) B) new selective ATP-competitive inhibitors of CDK4/CDK6: - Amebaciclib, - Palbociclib and – Ribocilcib (20).

1.4.1 Ribociclib (LEE011)

Ribociclib is an orally bioavailable small molecule that is a dual selective inhibitor of CDK4/CDK6 at nanomolar concentrations (23). The effectiveness of oral Ribociclib monotherapy is being investigated in subjects with breast cancer, glioblastoma, and liposarcoma (24). For example, Rader et al. reported that Ribociclib significantly reduced proliferation in 12 of 17 human neuroblastoma-derived cell lines by inducing cytostasis at nanomolar concentrations (25). Successful implementation of Ribociclib in the clinical settings will need to be done in combination with other agents because Ribociclib doesn't induce cell death. Often, new targeted drugs have been introduced to patients with leukemia in combination with standard chemotherapy (26). The combination of Ribociclib with other drugs is under study. Ribociclib recently granted Food and Drug Administration priority review as first-line treatment of postmenopausal women with hormone-receptor positive, human epidermal growth factor receptor-2 negative (HR+/HER2-) advanced or metastatic breast cancer in combination with letrozole (27).

1.5 Aim of the project

Excessive cell proliferation induced by aberrant entry into the cell cycle is considered an hallmark of cancer. Recent findings have revealed that CDK4/6 and its regulatory subunit cyclin D1 are oncogenes and are overexpressed in a diverse set of human cancers, including B-cell acute lymphoblastic leukemia (B-ALL) (3). Moreover, CDK6 is essential for MLL-rearrenged leukemias (19). These findings suggest that CDK4/6 may be effective targets for therapeutic intervention. To test this possibility, we will inhibit CDK4 and CDK6 in four cell lines of B-cell acute lymphoblastic leukemia, characterized by different genetic rearrangements, using Ribociclib, an orally bioavailable, small molecule inhibitor of both CDK4 and CDK6. At low concentration, Ribociclib potently inhibit CDK4/6 without induction of apoptosis; therefore, standard treatment for newly diagnosed childhood B-ALL patients includes glucocorticoids (GC) treatment, but the molecular basis of GC sensitivity and resistance remains largely unknown; for this reason we will test if Ribociclib in combination with Dexamethasone, a glucocorticoid that is currently used as antitumour agent in the treatment of leukemia, may lead to synergistic killing of leukemia cells (28).

RIBOCICLIB, A CDK4/CDK6 KINASE INHIBITOR, ENHANCES GLUCOCORTICOID SENSITIVITY IN B-ACUTE LYMPHOBLASTIC LEUKEMIA (B-ALL)

Elena Mattiuzzo[a], Roberta Bortolozzi[a], Benedetta Accordi[a], Luca trentin[a], Giuseppe Basso[a], Giampietro Viola[a]

[a]*Dipartimento di Salute della Donna e del Bambino, Laboratorio di Oncoematologia, Università di Padova, 35131 Padova, Italy*

1.6 Abstract

Background

Dysregulation of the cyclin D1-CDK4/CDK6 complex contributes to aberrant cell proliferation and consequent tumourigenesis. Among the CDKs that control cell cycle progression, cyclin D-dependent kinases CDK4 and CDK6 are considered important oncogenic drivers in many cancers. CDK6 is a direct target of MLL rearranged B-cell acute lymphoblastic leukemia (B-ALL) and this prompted us to investigate if pharmacological inhibition of CDK4/CDK6 could increase the efficiency of chemotherapy and overcome drug resistance.

Gene expression analysis performed in a cohort of childhood patients showed that CDK4 and CDK6 are highly expressed; therefore, Reverse Phase Protein Array (RPPA) analysis showed that cyclin D1 expression is higher in High Risk-MRD patients. These results suggest specific inhibition of cyclin D/CDK4/CDK6 axis as an attractive strategy to improve the effect of common chemotherapy on B-ALL patients.

Standard treatment for newly diagnosed childhood B-ALL patients include chemotherapy treatment and although glucocorticoids (GC) are the most important drugs used in the treatment of acute lymphoblastic leukemia, the molecular basis of GC sensitivity and resistance remain largely unknown; understanding the molecular mechanisms related to GC cytotoxicity is crucial for modulating GC resistance.

Materials and Methods

To evaluate the effect of dual inhibition of CDK4/CDK6 in B-ALL, we used Ribociclib, an orally bioavailable highly specific CDK4/6 inhibitor. For this study we used four cell lines of B-cell acute lymphoblastic leukemia (B-ALL), characterized by different genetic rearrangements and different response to glucocorticoids; we treated them with Ribociclib alone and in combination with Dexamethasone (DEX), a glucocorticoid currently used in B-ALL treatment. MTT assay was performed to analyze the effects of treatment on cell proliferation; moreover, cell cycle analysis and annexin V/PI were carry on by flow citometry to assess cell cycle modification and cell viability. Western Blot analysis were performed to evaluate changing in signaling pathways induced by the treatment.

Results

Treatment with Ribociclib induced a strong cell cycle arrest in G1 phase in a time-

dose dependent manner along with a dose-dependent decrease in phosphorylated retinoblastoma (Rb). We investigated whether treatment with Ribociclib could induce growth inhibition of B-ALL cell lines: we observed, in SEM and RCH-ACV, a strong growth inhibition at all drug concentration after continuous treatment; moreover, wash out of the inhibitor after 48h hours of treatment showed that both cell lines didn't restore cell growth. These results show that Ribociclib could have an irreversible activity. A strong dose-dependent reduction of clonogenic potential was also observed in SEM cell line. Ribociclib exposure strongly synergize (CI<1) with DEX in SEM and RCH-ACV resistant cell lines with a strong decrease of proliferation and a significant increase of apoptotic cell death. Immunoblot analysis showed a decrease in phosphorylated Rb and Cyclin D1 starting from 48h of co-treatment and an increase in p27. Preliminary experiments showed a modest increase in glucocorticoid receptor (GR) after Ribociclib and combination treatment in SEM and RCH-ACV cells. To further confirm the synergistic effect, we evaluated mRNA level of GR targets and we found that GR, BTG1 and GILZ are overexpressed in combination treatment in SEM and RCH-ACV. The synergistic effect of Ribociclib-DEX combination was also confirmed on primary cultures derived from pediatric patients affected by B-acute lymphoblastic leukemia. Our findings support the concept that pharmacological inhibition of CDK4/CDK6 may represent a useful therapeutic strategy to control cell proliferation in B-ALL and provide new insight in understanding potential mechanism of glucocorticoid resistance.

Keywords**:** CDK4/CDK6; cell cycle; B-acute lymphoblastic leukemia; chemotherapy; drug resistance; Ribociclib; glucocorticoid receptor

1.7 Materials and methods

Cell culture

The human leukemia cell lines RS 4;11, SEM, RCH-ACV and NALM6 were purchased from the American Type Culture Collection. Cells were cultured in RPMI 1640 (Life Technologies, Italy) supplemented with 10% fetal bovine serum (FBS), glutamine (2 mM; Life Technologies, Italy), penicillin (100 U/ml; Life Technologies, Italy) and streptomycin (100 µg/ml; Life Technologies, Italy), and maintained at 37°C in a humidified atmosphere with 5% CO_2.

Primary leukemia cell cultures

BCP-ALL patient samples were obtained after informed consent following the tenets of the Declaration of Helsinki. The study was approved by the ethical committee board of the University of Padova, the Padova Academic Hospital and the Italian Association of Pediatric Onco-Hematology (AIEOP). Diagnosis was made according to standard cytomorphology, cytochemistry and immunophenotypic criteria (31). All analyzed BCP-ALL samples were obtained at the time of diagnosis before treatment.

Drug treatment

Cells were grown to 60% confluence and then treated with Dexamethasone (Sigma-Aldrich) and Ribociclib (Selleckchem), at a stock concentration of 10 mM and then used at different concentrations. Cells were treated for 72 h using scalar dilutions of Ribociclib (Sellekchem), combined with Dexamethasone (Sigma-Aldrich). Ribociclib was also added to drug solutions at fixed combination ratios. The effectiveness of various drug combinations was analyzed by the Calcusyn Version 2.1 software (Biosoft). The combination index (CI) was calculated according to the Chou-Talalay method (29-30). A combination index of 1 indicates an additive effect of the 2 drugs. Combination index values less than 1 indicate synergy, and combination index values more than 1 indicate antagonism.

MTT assay

Proliferation was assessed by MTT (3-(4,5-dimethylthiazol-2-yl)-2,5-diphenyl tetrazolium bromide) assay after treatment. Equal concentrations of cells were plated in triplicate in a 96-well plate and incubated with 10 µl MTT (Sigma-Aldrich, St Louis, MO, USA) for 4 h. Absorbance was measured at 560 nm using Victor3TM 1420

Multilabel Counter (PerkinElmer, Waltham, MA, USA). The growth inhibition$_{50}$ (GI_{50}=compound concentration required to inhibit cell proliferation by 50%) was calculated by plotting the data as a logarithmic function of (x) when viability was 50%. DMSO-treated cells viability was set to 100%.

Measurement of cell growth inhibition

Cell growth inhibition was determined by trypan blue exclusion assay plating SEM and RCH-ACV ($2,5*10^5$ cells/well) in 6 wells plate a day before treatment with Ribociclib 5 μM and 10 μM. The following day, the starting cell number was calculated (T= 0h) and until the 3_{th} day, every 24h cell number was calculated in continuous presence of the drug.

To determine the persistence of the effects of drug exposure, SEM and RCH-ACV cells ($2,5*10^5$ cells/well) were plated in 6 well plate a day before treatment with Ribociclib 5 μM and 10 μM. After 48h of treatment, cells were collected and resuspended in complete fresh medium. Proliferation was measured using trypan blue exclusion assay and until the 3_{th} day, every 24h cell number was calculated.

Annexin V/Pi assay

Surface exposure of phosphatidylserine on apoptotic cells was measured by flow cytometry with a Coulter Cytomics FC500 (Beckman Coulter) by adding Annexin V conjugated to fluorescein isothiocyanate (FITC) to cells according to the manufacturer's instructions (Annexin V Fluos, Roche Diagnostic). Simultaneously, the cells were stained with PI. Excitation was set at 488 nm, and the emission filters were at 525 and 585 nm, respectively, for FITC and PI.

Flow cytometric analysis of cell cycle distribution

Cell cycle distribution was measured by flow cytometry with a Coulter Cytomics FC500 (Beckman Coulter) by using propidium iodide in propidium iodide/RNase A staining.

At 24h and 48h after drugs treatment, cells were harvested, washed with phosphate-buffered saline solution (PBS) and fixed in 70% EtOH overnight at 4°C. After fixation, cells were washed twice with PBS before resuspension in 0.1% Triton X-100/propidium iodide/RNase A solution (1mg/mL of PI and 4mg/mL RNase-A). Cells were incubated at room temperature in the dark light for 30 min and then processed for analysis. Samples were analyzed on a Cytomic FC500 flow cytometer (Beckman

Coulter). DNA histograms were analyzed using MultiCycle for Windows (Phoenix Flow Systems).

Cell colony-formation assay

Cells were harvested for 24h after drug treatment and were seeded in a fresh 12-well plate (1200 cells/well) and kept in culture undisturbed for 15 days, during which time the surviving cells spawned colonies of proliferating cells. Colony formation was analysed by staining the cells with diluted MTT.

Immunoblotting

Total protein extracts were isolated in lysis buffer prepared as follows: TPER Reagent (Pierce, Milano, Italy), NaCl 300 mM, orthovanadate 1 mM (Sigma, Milano, Italy), AEBSF 2 mM (PEFABLOC, Roche Biochemicals, Milano, Italy), Aprotinin 1 µg/ml (Sigma–Aldrich, Milano, Italy), Pepstatin-A 5 µg/ml (Sigma–Aldrich, Milano, Italy) and Leupeptin 1 µg/ml (Sigma–Aldrich, Milano, Italy). The protein concentration in the supernatant was determined using the BCA protein assay (Pierce, Milano, Italy). Equal amounts of protein (10 µg) were resolved using SDS-PAGE gels and transferred to Immobilon-P membrane (Millipore). Membranes were blocked with 3% BSA in tween 0.1% in PBS 1X (phosphate buffered saline) for at least 2 h under rotation at room temperature. Membranes were then incubated with primary antibodies overnight. Membranes were then incubated with peroxidase-conjugated secondary antibodies (Perkin Elmer, Italy) for 60 min. All membranes were visualized using ECL Select (GE Healthcare, Italy).

Reverse-phase protein arrays (RPPA)

Cell lysates were diluted to 1 mg/ml in Tris–Glycine SDS Sample Buffer (Invitrogen) containing 5% of ®-mercaptoethanol and boiled for 5 min immediately prior to array printing. Lysates were loaded into a 384-well plate and serially diluted with lysis buffer into four-point with the primary antibodies on anautomated slide stainer (Dako Autostainer Plus) using the CSA kit (Dako). Each antibody was previously subjected to extensive validation for single-band specificity by Western blot. Slides were air-dried and scanned on a Epson Perfection V300 Photo at 600 dpi. The TIF images of antibody- and Fast Green FCF stained slides were analyzed using Microvigene Software (VigeneTech Inc, Boston, MA, USA) to extract numeric intensity values from the array images dilution curves ranging from undiluted to 1:8. Protein

lysates were printed in duplicate in each array set onto nitrocellulose-coated slides (FAST slides) with the 2470 Arrayer (Aushon BioSystems). Printed slides were stored desiccated at -20°C until use. For RPPA analysis, one slide was stained with Fast Green FCF dye (Sigma) according to the manufacturer's instruction, in order to estimate the total protein amount of each printed sample. Before antibody staining, the arrays were blocked for 3 h RT in blocking solution (2% I-Block in T-PBS). Arrays were then stained with the primary antibodies on anautomated slide stainer (Dako Autostainer Plus) using the CSA kit (Dako). Each antibody was previously subjected to extensive validation for single-band specificity by Western blot. Slides were air-dried and scanned on an Epson Perfection V300 Photo at 600 dpi. The TIF images of antibody- and Fast Green FCF stained slides were analyzed using Microvigene Software (VigeneTech Inc, Boston, MA, USA) to extract numeric intensity values from the array images.

RNA interference with small interfering RNAs (siRNAs)

To achieve a suitable gene silencing, SEM and RCH-ACV cells were transfected with 300pmol of Cdk6 small interfering RNA (siRNA) purchased from Santa Cruz Biotechnology (sc-29264) as well as non targeting siRNA (siNEG, Thermofisher Scientific) confirmed to have minimal targeting of known genes using the Lonza's Nucleofector™ Technology according to the manufacturer's instructions. All siRNA pools were resuspended to 20 μM in 1X siRNA buffer.

RNA isolation and Reverse transcriptase polymerase chain reaction (RT-PCR)

Total cellular RNA from cell lines and patient bone marrow was extracted with TRIzol reagent (Invitrogen). RNA quality was controlled using Nanodrop spectrophotometer. Subsequently, 1μg of total RNA was reversely transcribed using random hexamers and Superscript II (Invitrogen), according to the manufacturer's instructions.

Real time PCR

Real-time quantitative (RQ-PCR) was performed on an Applied Biosystems 7900 HT Sequence Detection System using SYBR Green PCR Master Mixture Reagents (Applied Biosystems; Forest City, CA). Experiments were performed minimum as triplicate and used for relative quantity study. Primers used for RQ-PCR analysis were for GR gene (glucocorticoid receptor), BTG1, GILZ and CDK6. All expression values were normalized using expression of GUS as an endogenous control **(Table 1)**.

Table 1. Primer sequences used for RQ-PCR analysis of B-ALL cells treated with combination treatment

	Forward	Reverse
GR	5'-CCTTCTGCGTTCACAAGCTA-3'	5'-TTCTTTGGAGTCCATCAGTG-3'
BTG1	5'-TGTTCAGGCTTCTCCCAAGT-3'	5'-CTACCATTTGCACGTTGGTG-3'
GILZ	5'-GAAGGAGCAGATCCGAGAGC-3'	5'-GGCTCAGACAGGACTGGAAC-3'
CDK6	5'-ACTTCGGCCTTGCCCGCATC-3'	5'-GGGGGTGGCGTAGCTGGACT-3'
GUS	5'-GAAAATATGTGGTTGGAGAGC-3'	5'-CGAGTGAAGATCCCCTTTTTA-3'

Statistical analysis

All experiments were performed with a minimum of three technical and three biological replicates, and values reported are the mean of the three biological replicates, unless otherwise indicated. Error bars represent the standard deviation (SD) from the mean, unless otherwise indicated. When comparing data from experiments with multiple groups, a multicomparison ANOVA was used with the Newman-Keuls. For all tests, differences were considered statistically significant at a *P* value of 0.05 or less. All statistical analyses were performed using the GraphPad Prism software.

1.8 Results

Cyclin D1-CDK4/6 complex is dysregulated in B lymphoblastic leukaemic patients

To investigate if Cyclin D1-CDK4/6 complex plays a role in childhood B-cell acute lymphoblastic leukemia (B-ALL) we performed some analysis to understand the status of this complex in a cohort of pediatric patients. We evaluated gene expression of CDK4 and CDK6 and we observed a significantly overexpression of CDK4 in MLL-rearrenged leukemia respect to normal bone marrow and a significantly overexpression of CDK6 in all leukemia subtypes respect to normal bone marrow confirming that these kinases are dysregulated in B-ALL **(Fig.3)**.

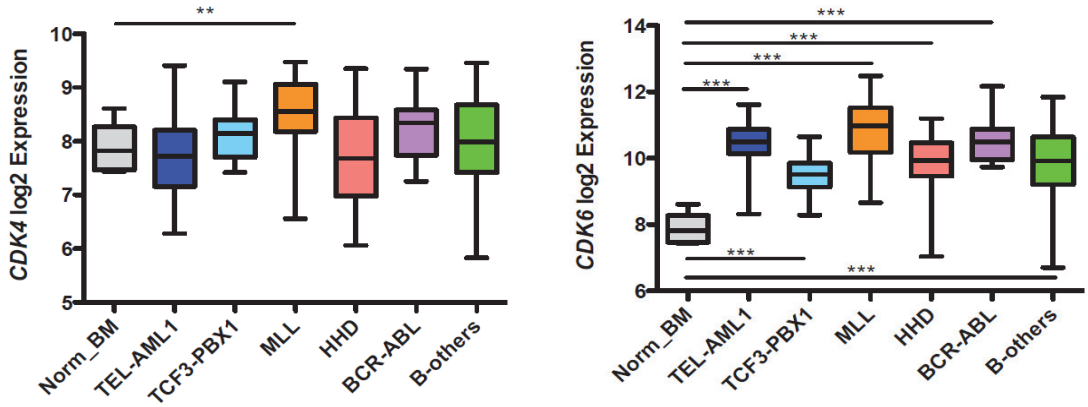

Fig. 3 CDK4/CDK6 are overexpressed in B-ALL patients compared to normal bone marrow. CDK4/CDK6 gene expression level was analyzed in 299 patients and compared to bone marrow of healthy donors.

For what concern Cyclin D1, Reverse phase protein microarray (RPPA) analysis, in a cohort of pediatric patients, showed that there are high levels of Cyclin D1, in high risk patients. Among childhood ALL patients, white blood cells counts (WBC) and minimal residue disease (SR, standard risk; HR, high risk) represent independent predictors of an adverse outcome. We determined whether high levels of Cyclin D1 expression were associated with increased WBC at diagnosis. To do this, we compared infant ALL patients with “low” (<50,000) and “high” (>50,000) WBC counts, and found that patients expressing high WBC presented higher Cyclin D1 levels at diagnosis. We also determined whether high levels of Cyclin D1 expression were correlated with minimal residue disease at diagnosis; we observed that there were higher levels of Cyclin D1 expression in high risk patients respect to standard risk patients. We found higher Cyclin D1 expression in relapsed patients respect to not

relapsed **(Fig.4)**. Taken together, this data demonstrate that Cyclin D1/CDK4/CDK6 complex is generally deregulated in childhood B-cell acute lymphoblastic leukemia.

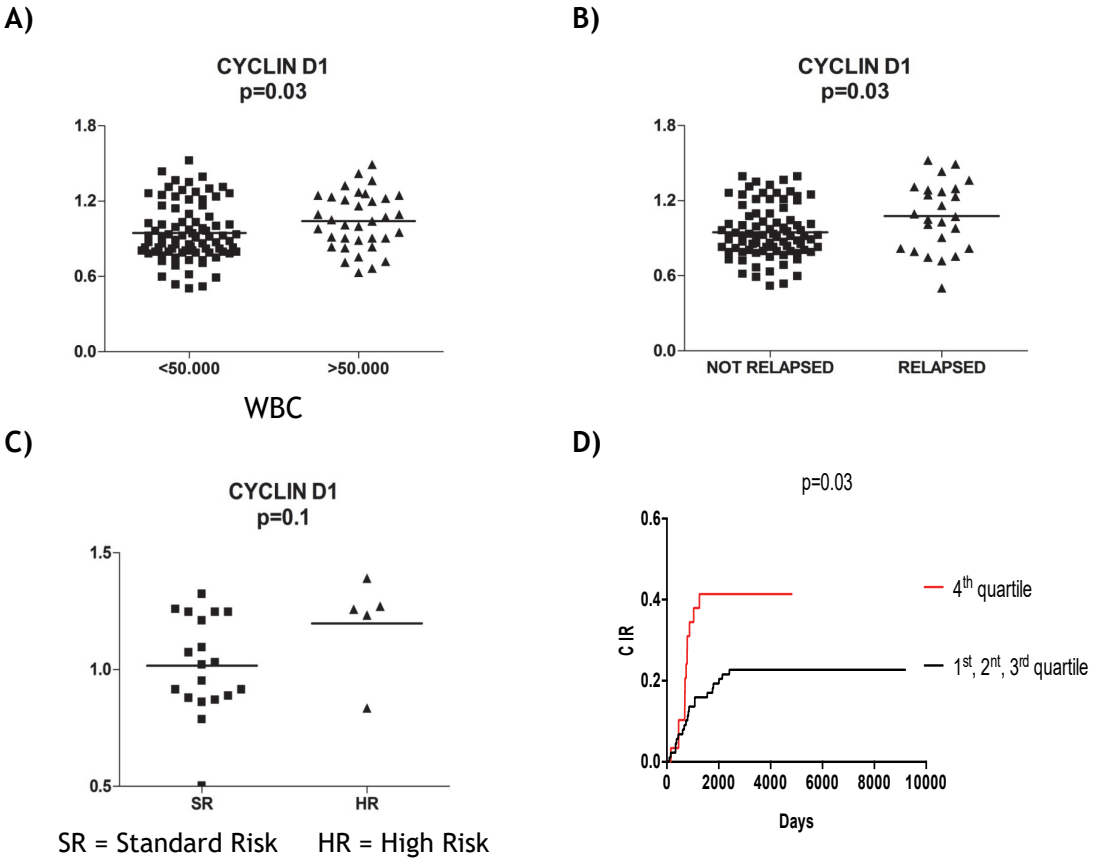

Fig. 4 High levels of Cyclin D1 in B-ALL patients that relapse and in high risk.
(A-C) RPPA analysis in a cohort of childhood B-ALL has revealed high levels of Cyclin D1 in relapsed and high risk patients. (D) CIR analysis showed that those patients with high levels of Cyclin D1 relapse before than those patients with low levels of Cyclin D1.

Knockdown of Cdk6 decreases cell proliferation in B-ALL cell lines and induces a G1 cell cycle arrest

Since our preliminary observation indicate that CDK4/CDK6 signaling is hyperactivated in B-ALL patients, in order to assess the effective role of CDK4/CDK6-cyclin D1 signal in B-ALL in maintaining hyperphosphorylated RB and in supporting cell proliferation, we evaluate the effect of CDK4/CDK6 gene silencing on B-ALL cell line RCH-ACV. Cells were transiently transfected with a CDK6 and CDK4 siRNA pool and cell proliferation was measured after 48 h by MTT assay. Silencing of CDK4/CDK6 was confirmed by western blot analysis **(Fig.5 A,B)**. The best characterized direct phosphorylation targets of cyclin D-dependent kinase are RB proteins (pRB), SMAD2, SMAD3 and FOXM1 transcription factor. As expected, CDK4/CDK6 silencing induced

strong dephosphorylation of pRB (S780), FOXM1 (T600) and SMAD2/3 (T8), followed by the activation of the cell cycle inhibitor p21 **(Fig 5A,B)**. Moreover, a decrease of pRB total protein was also observed, as previously demonstrated by Rader et al. (25). Considering that the phosphorylation of RB, FOXM1 and SMAD2/3 are essential to the activation of the cell transcriptional activity that promotes G1-S transition, we evaluate CDK4/CDK6 depletion effects on cell proliferation. Flow cytometric analysis has revealed a significant retention of cell in G1-phase of the cell cycle **(Fig.5C)** along with a remarkable decrease of cell proliferation **(Fig.5D)**.

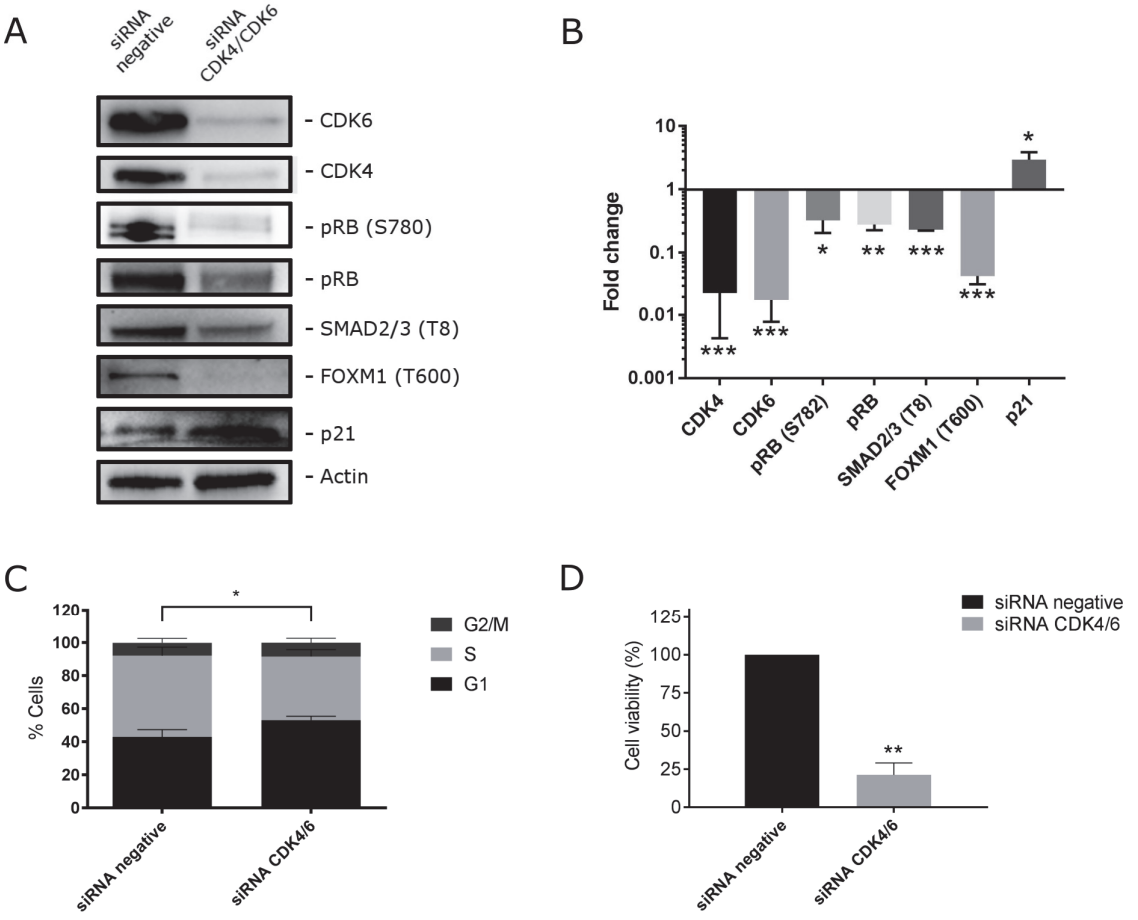

Fig. 5 Ckd4 and Cdk6 knockdown in RCH-ACV cells induces a significant decrease in cell proliferation and a G1 phase arrest. RCH-ACV were transfected with a specific CDK/CDK6 siRNA and a negative siRNA as a control. (A) Western blot analysis confirmed the knockdown of endogenous both CDK4 and CDK6 and the reduced expression of pRB, pRB (s780), SMAD2/3 (T8) and FOXM1 (T600). (B) Densitometric analysis of immunoblots. (C) Cell cycle analysis of RCH-ACV cells after 48 h from the transfection. (D) Cell viability analysis, was performed by MTT assay, after 72 h after transfection. All the data are presented as mean ± SEM of three independent experiments. *, p <0.05: ** p < 0.01, ***p<0.001.

To further analyze the role of CDK6 on cell cycle progression in B-ALL, we analyzed

the cell-cycle phase distribution in SEM and RCH-ACV cells following Cdk6 knockdown. As shown in **Fig.6** in both cell lines, there was an increase of the percentage of cells in G1 and a corresponding decrease of cells in S phase compared with non-specific (NSC) control cells.

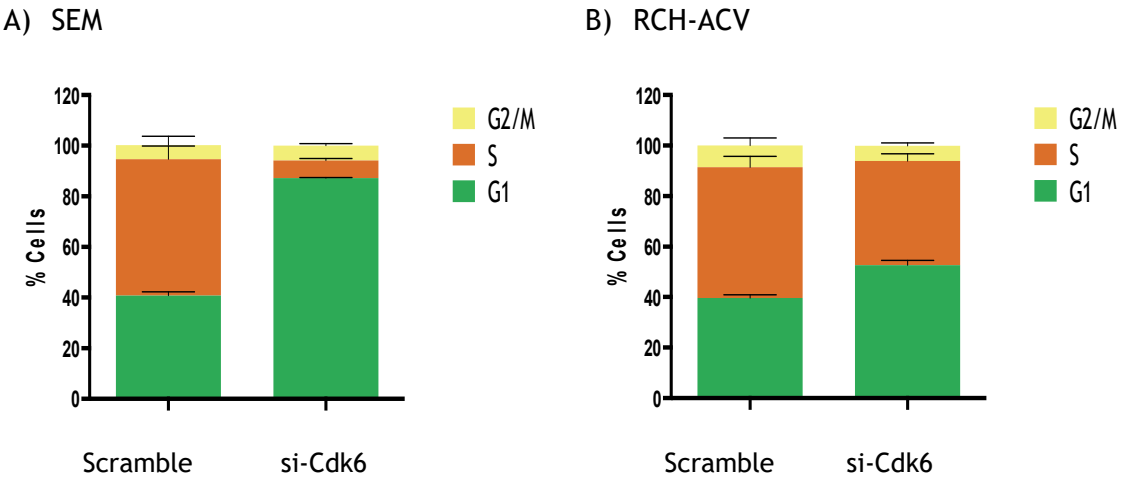

Fig. 6 Cdk6 downregulation in SEM and RCH-ACV cells by a specific Cdk6 siRNA pool induces a G1 cell cycle arrest. In SEM (A) and RCH-ACV cell (B) lines the endogenous Cdk6 expression was blocked by knockdown performed by using Cdk6 transient silencing. After 48h of knockdown, cell cycle analysis was performed to investigate the effect of Cdk6 inhibition in cell cycle-phase progression. Results are the average ± SD of three independent experiments in triplicate.

Ribociclib induces cell growth inhibition in B-ALL cell lines

To explore the effect of Ribociclib on cell proliferation in B-ALL, we choose 4 B-ALL cell lines including RS4;11, NALM6, SEM and RCH-ACV. Cells were exposed to the inhibitor for 72 h at concentrations ranging from 0.001 to 100 µM. The GI_{50} evaluated by MTT assay after 72 h was in the micromolar range for all cell lines treated **(Fig.7)**.

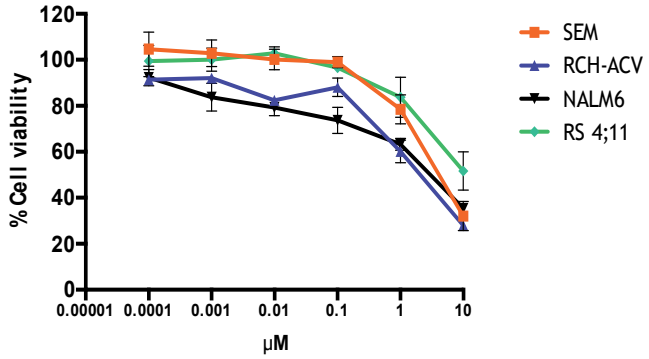

CELL LINE	GI_{50}
NALM-6	2.8 ± 0.5
SEM	6.1 ± 0.8
RCH-ACV	2.7 ± 0.6
RS4;11	4.1 ± 0.6

Fig. 7 Ribociclib has a modest effect on cell viability. Cells were treated at the indicated concentration and cell viability was assessed by MTT test after 72 h of incubation. GI_{50} is in the micromolar range for all cell lines treated. Data are expressed as mean ± SEM of three independent experiments.

Since we have found that Ribociclib induces growth inhibition in B-ALL cell lines; in this context, we treated both SEM and RCH-ACV cell lines with Ribociclib 5 μM and 10 μM for 24, 48, and 72 h. Cell growth inhibition was evaluated by Trypan Blue exclusion and we observed, in both cell lines, a strong growth inhibition at all drug concentrations. Removal of the inhibitor after 48 h hours from the medium showed that both cell lines didn't restore cell growth **(Fig.8a-b)**

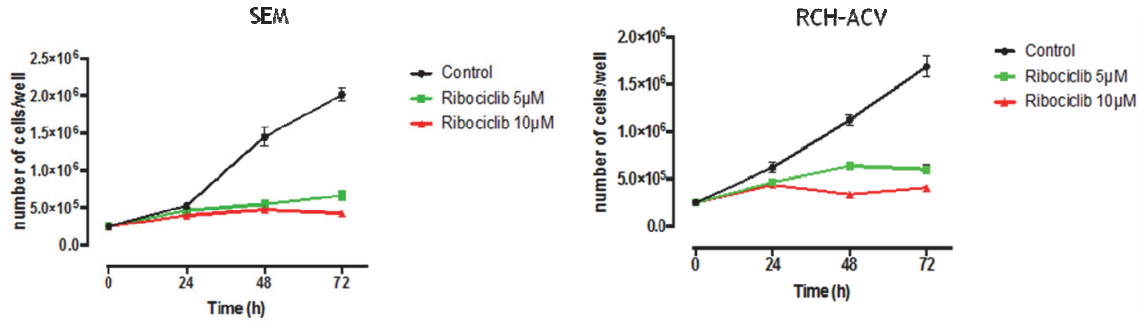

Fig. 8a Ribociclib induces growth inhibition in B-ALL cell lines after continuous treatment of the inhibitor.

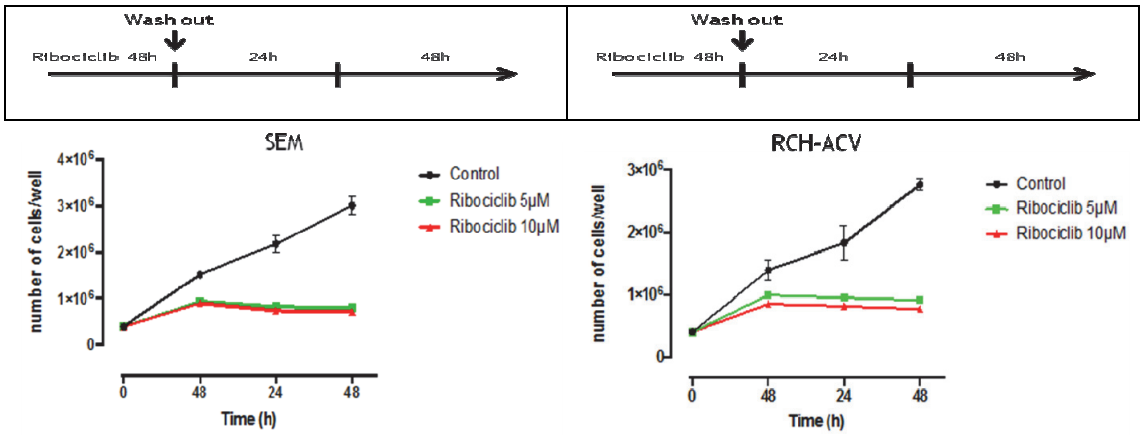

Fig. 8b Ribociclib induces growth inhibition in B-ALL cell lines after wash out of the inhibitor.

To determine whether Ribociclib affected the colony formation ability of B-ALL cell lines, we performed colony formation assay in SEM cell line. After a treatment of 24h with Ribociclib at the concentration of 5 μM and 10 μM, we washed out cells and we performed colony formation assay in methocult for 15 days. Colony numbers were

then quantified in each group. Consistently, we found that Ribociclib dramatically reduced the ability to form colonies in treated SEM cell lines, compared to the control group in a dose-dependent manner **(Fig.8c)**.

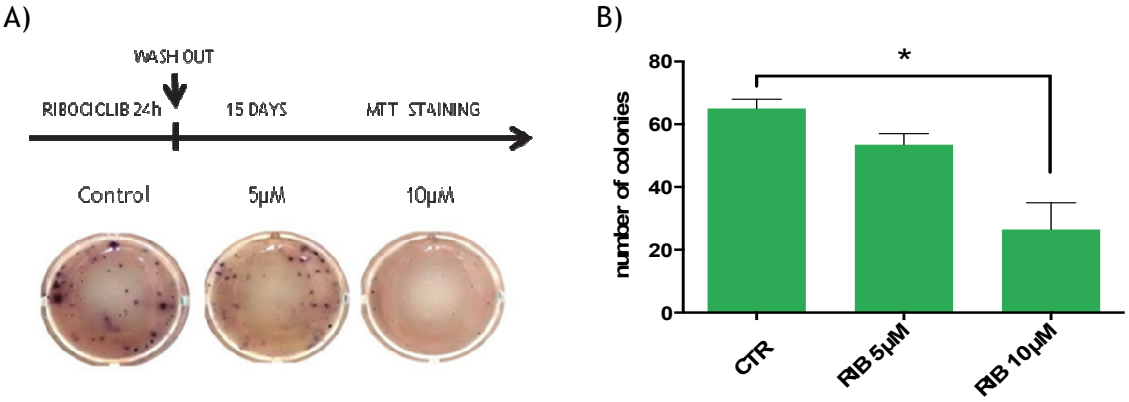

Fig. 8c Ribociclib affected the colony formation ability of B-ALL cell lines: A) Clonogenic assay in SEM cells treated with 5 μM and 10 μM of Ribociclib, washed out after 24 h of treatment and recovery for 15 days; B) colony counting to assess growth of cells treated with Ribociclib that statistically reduced the ability to form colonies in treated SEM cell lines, compared to the control group in a dose-dependent manner. Data are expressed as mean ± SEM of three independent experiments. Statistical analysis was performed using ANOVA multicomparison test against the cells treated with the non-treated control; * $p \leq 0.05$.

Ribociclib induces G1 arrest but not apoptosis in B-ALL cell lines

Cell cycle analysis was undertaken on SEM and RS4;11 treated with Ribociclib at 5 and 10 μM for 24 and 48 h. As shown in **Fig.9a** Ribociclib induces a significant increase in G1 phase along with a decrease in S phase in both cell lines.

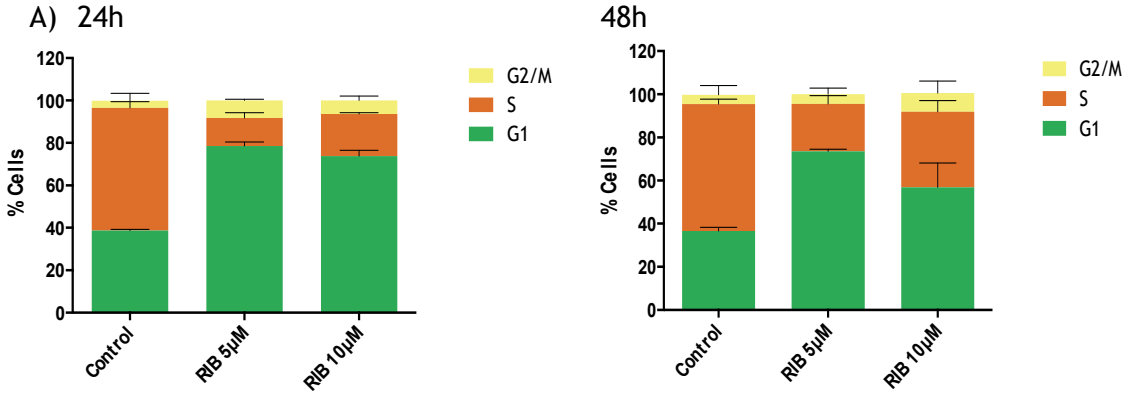

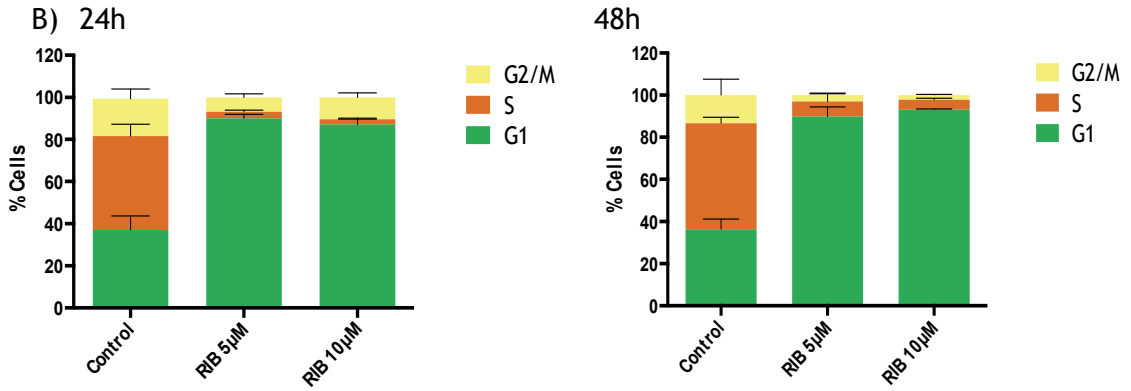

Fig. 9a CDK4/CDK6 inhibition in SEM and RS4;11 cells by Ribociclib treatment induces a G1 cell cycle arrest. (A) SEM and (B) RS4;11 cell lines were treated with the indicated concentration of Ribociclib. After 24 and 48 h of treatment, cell cycle analysis was performed to investigate the effect of CDK4/CDK6 inhibition in cell cycle-phase progression. Results are the average ± SD of three independent experiments in triplicate.

Moreover, flow cytometric analysis carried out after different times of treatment indicate that Ribociclib doesn't induce apoptosis as demonstrated by non significant appearance of annexin-V positive cells in both cell lines when treated with Ribociclib even at the concentration of 10 μM for 24 and 48 h **(Fig.9b).**

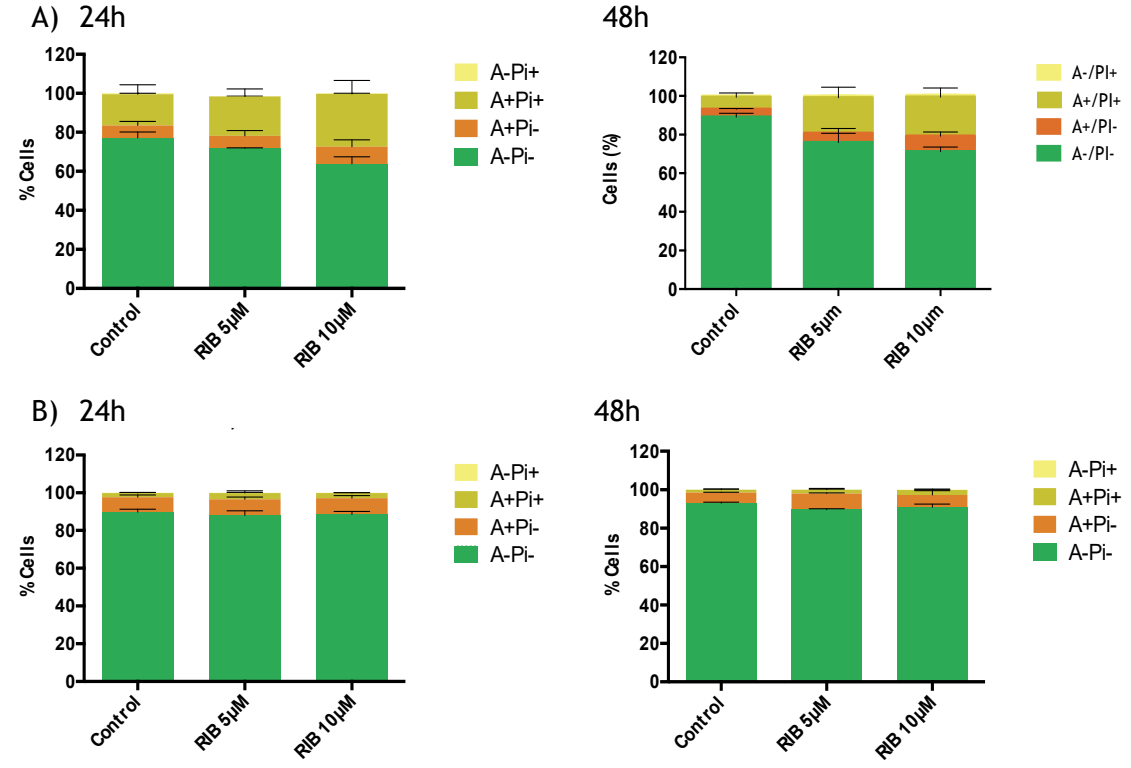

Fig. 9b CDK4/CDK6 inhibition in SEM and RS4;11 cells by Ribociclib treatment doesn't induce apoptosis. A) SEM and B) RS4;11 cells were treated with Ribocliclib at the

concentration of 5 μM and 10 μM, for 24 and 48 h. Induction of apoptosis was assessed by flow cytometry after staining of the cells with Annexin-V-FITC and propidium iodide (PI). Dual staining permits discrimination between live cells (annexin-V^-/PI^-), early apoptotic cells (annexin-V^+/PI^-), late apoptotic cells (annexin-V^+/PI^+) and necrotic cells (annexin-V^-/PI^+). Shown are the mean ± standard error of mean (SEM) of 3 separate experiments.

To confirm that the growth inhibition observed in B-ALL cell lines was due to a targeted impairment of CDK4/6 signaling, we analyzed the levels of phosphorylated retinoblastoma following treatment with Ribociclib. The mechanism by which CDK4/CDK6 promote cell proliferation and G1-S cell cycle transition depend on the phosphorylation of critical substrate proteins. As depicted in Fig 4B-C in all studied B-ALL cell lines, treatment with ribociclib induced a rapid and dramatic decrease of pRB phosphorylation at S780 already at the lowest concentration of inhibitor, together with a dephosphorylation of FOXM1 (T600) (delayed in RS 4;11) and at later time of SMAD3 (T8). By these dephosphorylation, the signaling that drive the transition through G1-S phase is arrested **(Fig.10)**

A)

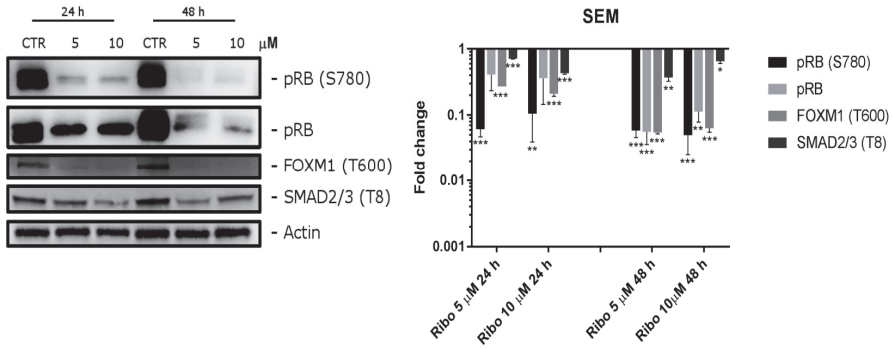

B)

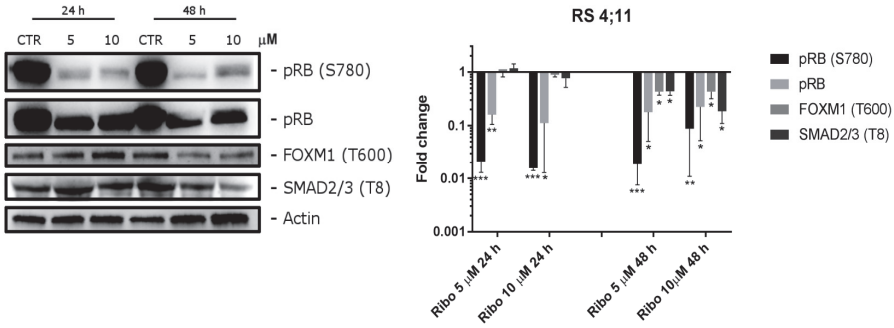

Fig. 10 Effect of CDK4/CDK6 inhibition on the expression of proteins involved in G1 phase of cell cycle. Ribociclib treatment decreases protein levels of pRB, pRB (s780) SMAD2/3 (T8) and FOXM1 (T600) in A) SEM and B) RS4;11 cell lines after 24 and 48 h; cells were collected, and protein extracts were subjected to western blot analysis for the indicated antibodies. Actin was used as loading control. The right part of the table shows densitometric analysis of immunoblot. All the data are presented as mean ± SEM of three independent experiments. *, $p < 0.05$: ** $p < 0.01$, ***$p < 0.001$.

Ribociclib synergizes with dexamethasone in inhibiting B-ALL proliferation

Since CDK4/CDK6 pharmacological inhibition induces a strong G1 phase arrest in B-ALL cell lines, we investigated if this effect could enhance killing of B-ALL cells. in combination with the most commonly used chemotherapeutics in B-ALL treatment.

Four different B-ALL cell lines, two glucocorticoid-resistant (RCH-ACV, SEM) and two glucocorticoid-sensitive (NALM-6, RS4;11) were treated for 72 h with Ribociclib in combination with chemotherapeutic agents (i.e. Dexamethasone, asparaginase, daunorubicin and vincristine) used normally to treat pediatric B-ALL patients. More specifically, Ribociclib was combined with different drugs at fixed molar combination ratio, and cell viability analyzed by MTT assay The obtained results indicate that among the different drugs, only Dexamethasone in association with Ribociclib induces synergism **(Fig.11A)**. These results are in well agreement with that reported recently by (30) in T-cell acute lymphoblastic leukemia. Another thing that is to note is that we observed synergism also in Dexamethasone resistant cell lines.

In light of the strong synergy with Ribociclib in combination with glucocorticoids we focused our further study on this combination.

As demonstrated by the values of combination index (CI) according to Chou and Talalay (28,29) **(Fig.11B)** in all cell lines tested, Ribociclib has a synergistic effect with Dexamethasone ($CI<1$). Glucocorticoids (GC) are the most important drugs used in the treatment of acute lymphoblastic leukemia, but the molecular basis of GC resistance remains largely unknown and understanding the molecular mechanisms related to GC cytotoxicity is crucial for modulating GC resistance.

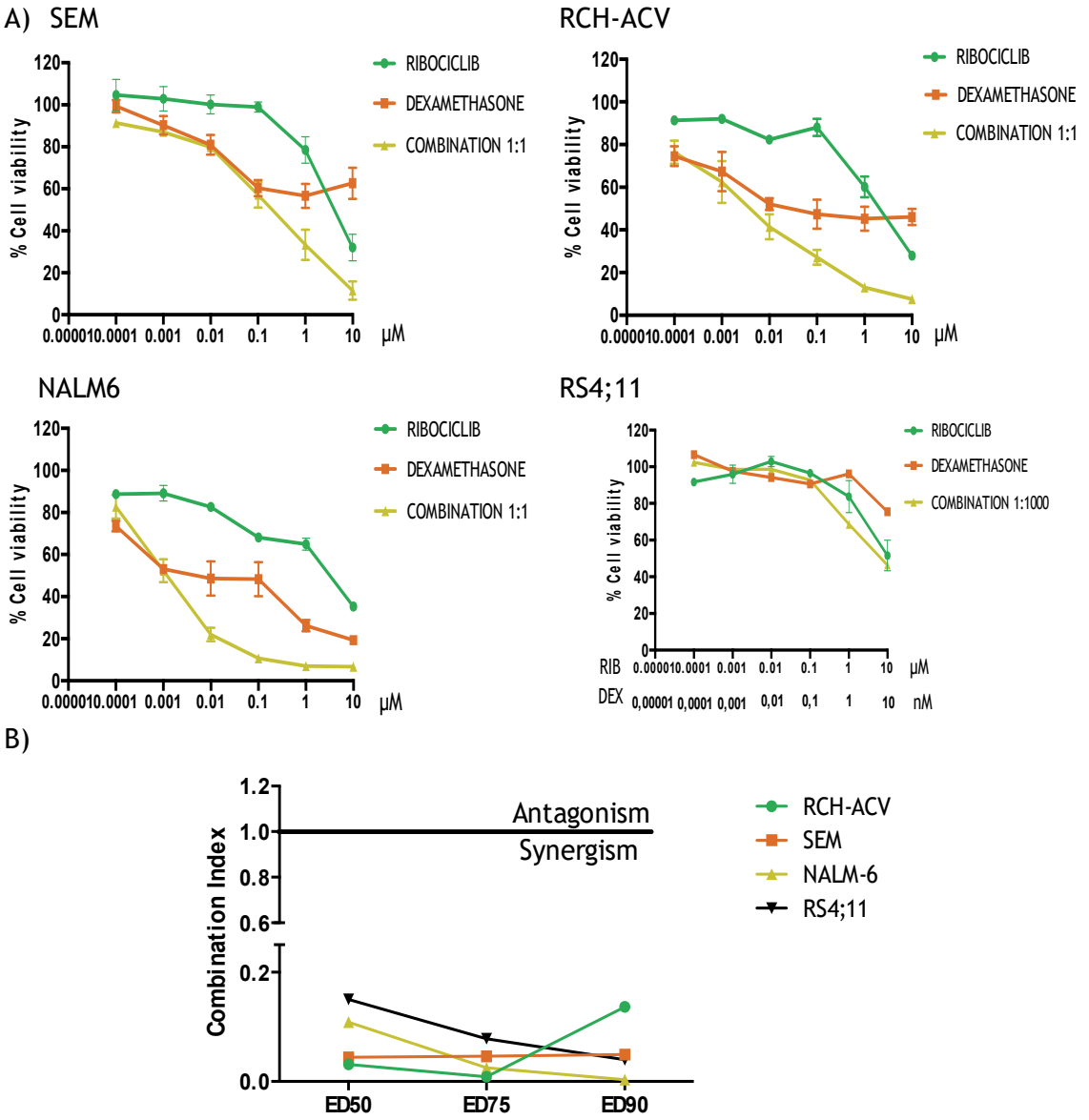

Fig. 11 Ribociclib strongly synergizes with Dexamethasone in B-ALL cell lines. A) Cells were treated at the indicated concentration and at fixed combination ratio 1:1 in SEM, RCH-ACV and NALM6 (0.0001-10 µM for both drugs) and 1:1000 in RS4;11 (0.0001-10 µM for Ribociclib and 0.0001-10 nM for Dexamethasone); cell viability was assessed by MTT test after 72 h of incubation. Data are expressed as mean ± SEM of three independent experiments. B) Combination index values (CI) in B-ALL cell lines treated with Ribociclib in combination with Dexamethasone.

The synergistic effect of Ribociclib-Dexamethasone combination was also confirmed on primary cultures derived from pediatric patients affected by B-acute lymphoblastic leukemia **(Fig.12).**

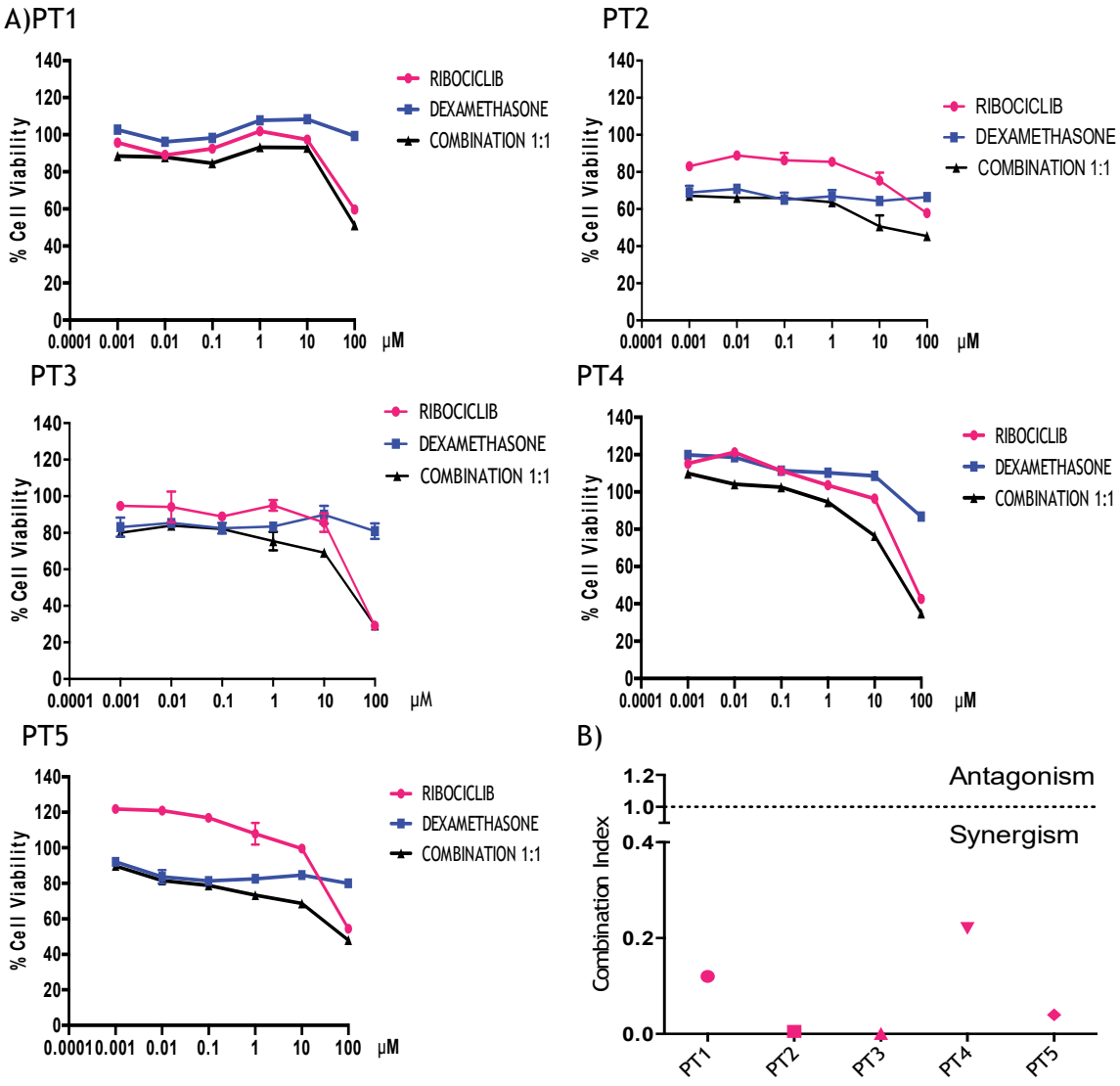

Fig. 12 Synergistic effect of Ribociclib-Dexamethasone combination in B-ALL primary cultures. A) Cells were treated at the indicated concentration and at fixed combination ratio 1:1 (0.001-100 μM for both drugs); viability was assessed by MTT test after 48 hours of incubation; B) combination index values (CI) at ED50 in B-ALL primary cultures treated with Ribociclib in combination with Dexamethasone.

Combination of Ribociclib and Dexamethasone induces G1 arrest and apoptosis in B-ALL cell lines

To explore the potential role of Ribociclib and Dexamethasone combination in Dexamethasone resistant B-ALL, we next studied the effects of this combination on cell cycle and cell viability of Dexamethasone resistant cell lines, SEM and RCH-ACV.

The cell cycle analysis showed that there was a significant shift in cell cycle distribution of both cell lines in response to combination treatment after 24 and 48

h; in particular, we observed a considerable increase in G1 phase arrest and a consequent decrease in S phase, in combination treatment respect to control and single treatment group (**Fig.13A-B**).

As demonstrated by western blot, this arrest of cell cycle upon combined treatment, could be mediated by a reinforced dephosphorylation of CDK4/CDK6 target. In particular, combined treatment induce a significant decrease of pRB (S780), SMAD2/3 (T8), FOXM1(T600) along with a strong increase of CDK4/CDK6 inhibitor p16 (**Fig.13C-D**).

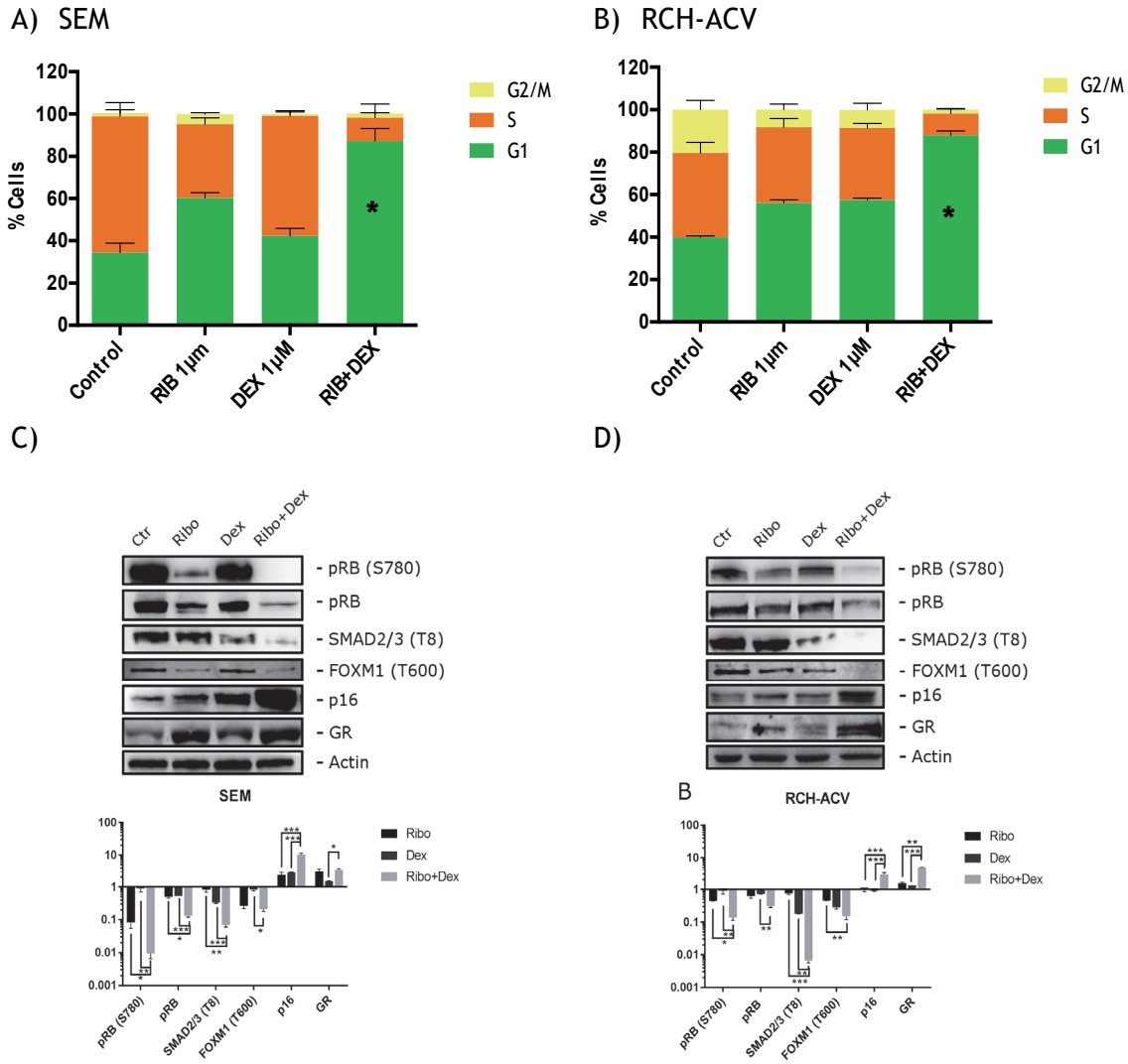

Fig. 13 CDK4/CDK6 inhibition in SEM and RCH-ACV cells by combination treatment induces a stronger G1 cell cycle arrest respect to single treatment. (A) SEM and B) RCH-ACV cell lines were treated with the indicated concentration of Ribociclib, Dexamethasone and combination between Ribociclib and Dexamethasone. After 48 h of treatment, cell cycle analysis was performed to investigate the effect of the drug combination in cell cycle-phase progression. Results are the average ± SD of three independent experiments. Combination

treatment enhances the decrease of cell cycle protein expression of S780 phosphorylated retinoblastoma, retinoblastoma, SMAD2/3 (T8) and FOXM1 (T600) in SEM (C) and RCH-ACV (D) cell lines; after 48 h cells were collected, and protein extracts were subjected to western blot analysis for the indicated antibodies.

Next, we asked whether the synergistic effects of Ribociclib plus Dexamethasone reflect enhanced apoptotic responses to glucocorticoids therapy. Annexin V-propidium iodide (PI) staining indicated increased apoptosis in SEM and RCH-ACV cell treated with Ribociclib 1 and Dexamethasone 1 for 72 h **(Fig.14).**

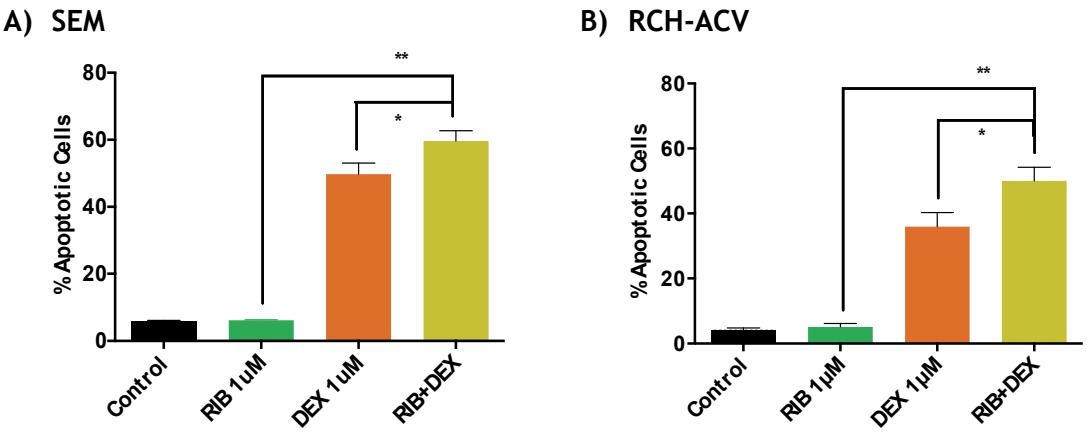

Fig. 14 Combination treatment of Ribociclib and Dexamethasone induces strong apoptosis in SEM and RCH-ACV. Annexin V staining of cells following 72 h treatment with Ribociclib at 1 µM and Dexamethasone 1 µM compared with controls. A) SEM, B) RCH-ACV. The % of apoptotic cells is referred to the sum of early (A+/PI-) and late (A+/PI+) apoptotic cells. Data are expressed as mean ± SEM of three independent experiments. Statistical analysis was performed using ANOVA multicomparison test against the cells treated with the non-treated control; * $p \leq 0.05$; $p \leq 0.001$.

Combination of Ribociclib and Dexamethasone induces an increase in Glucocorticoid receptor expression in B-ALL cell lines

To further test the efficacy of combination treatment and to assess the therapeutic role of CDK4/CDK6 inhibition in the treatment of glucocorticoid-resistant leukemias, we treated SEM and RCH-ACV with combination of Ribociclib and Dexamethasone. We analyzed the effects of this combination at protein level after 48 h and at transcriptional level after 24 h to explore the mechanisms mediating the reversal of glucocorticoid resistance upon CDK4/CDK6 inhibition. We found a modest increase in glucocorticoid receptor expression in SEM and RCH-ACV treated with Ribociclib or Dexamethasone for 48 h. In contrast, Ribociclib plus Dexamethasone treatment resulted in a higher upregulation of glucocorticoid receptor protein levels **(Fig.16A-**

C). At the transcriptional level, quantitative real time PCR showed a synergistic and significative upregulation of glucocorticoid-regulated genes such as GILZ and BTG1 in SEM and RCH-ACV treated with combination of Ribocilib and Dxamethasone for 24 h. There is also a moderate increase in glucocorticoid receptor in SEM cell line and a significative increase in glucocorticoid receptor expression in RCH-ACV cell line **(Fig.16B-D)**. These results suggest that pharmacological inhibition of CDK4/CDK6 enhances glucocorticoid receptor autoregulation and glucocorticoid expression, suggesting an increased in glucocorticoid resistant B-ALL cells.

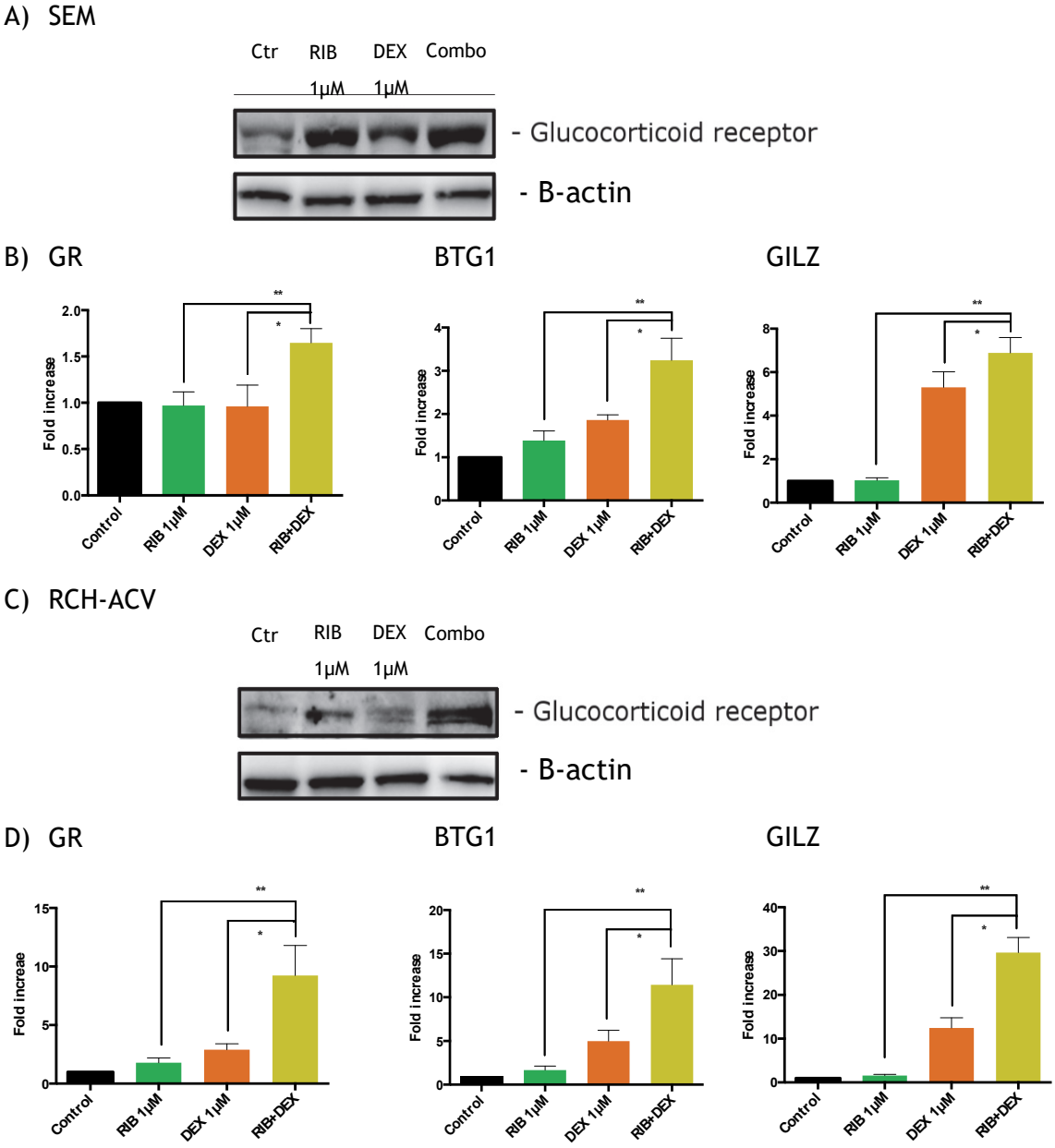

Fig. 16 Ribociclib plus dexamethasone enhances glucocorticoid receptor autoregulation and glucocorticoid sensitivity in glucocorticoid resistant B-ALL cells. In panel A) SEM and C)

RCH-ACV cells were treated with Ribociclib (1 μM), dexamethasone (1 μM) and combination treatment for 48 h. Cells were collected after treatment and were subjected to western blot analysis for Glucocorticoid receptor (GR) and housekeeping expression. In panel B) SEM and D) RCH-ACV were treated for 24 h with Ribociclib (1 μM), dexamethasone (1 μM) and combination treatment; Glucocorticoid receptor, BTG1 and GILZ mRNA levels were analyzed by RQ-PCR analysis and results were normalized to GUS mRNA levels. Data are expressed as mean ± SEM of three independent experiments. Statistical analysis was performed using ANOVA multicomparison test against the cells treated with the non-treated control; * $p \leq 0.05$; $p \leq 0.001$.

CDK4/CDK6 silencing induce GR expression and sensitize B-ALL cells to dexamethasone

In order to assess potential off-target effects induced by ribociclib treatment on GR, we evaluate its protein expression after CDK4/CDK6 gene silencing (**Fig.2A, 17A-B**). As expected, similarly to ribociclib treatment, CDK4/CDK4 silencing strongly enhanced GR expression (**Fig.17A-B**). Moreover, accordingly to pharmacological inhibition, gene silencing significantly sensitize RCH-ACV cells to dexamethasone treatment (**Fig.17C**).

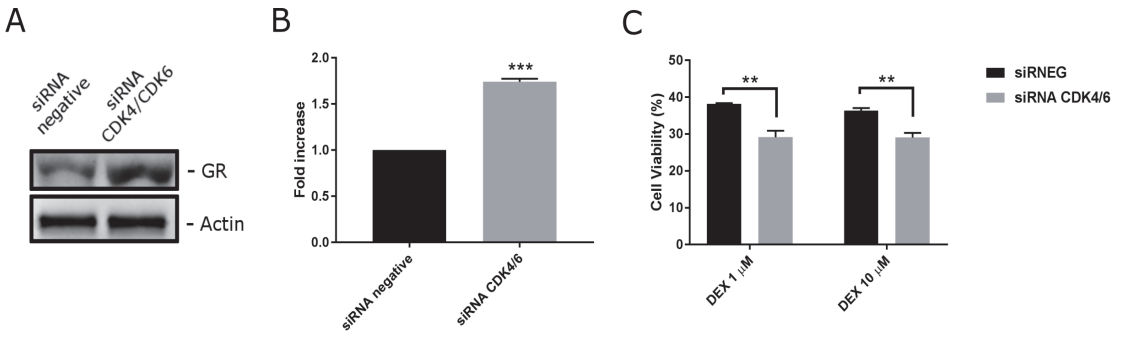

Fig. 17 Effects of specific CDK4/CDK6 silencing in RCH-ACV cells. Panel A. Knowdown of CDK4/CDK6 induce a significant increase of glucocorticoid receptor (GR) expression (Panel B) and sensitize cells to the action of dexamethasone. Panel C. Silenced cells were treated with dexamethasone (1μM and 10 μM) for 48 h and viability was assessed by MTT assay. Data are presented as mean ± SEM of three independent experiments. ** $p < 0.01$, ***$p<0.001$.

1.9 Discussion

Excessive cell proliferation induced by aberrant entry into the cell cycle is considered an hallmark of cancer. Recent findings have suggested that CDK4/6 and its regulatory subunit cyclin D1 may be potential oncogenes and are overexpressed in a diverse set of human cancers. Moreover, CDK6 is essential for MLL-rearrenged leukemias (20). Success in targeting the cell cycle in cancer with broad spectrum CDK inhibitors has been modest, mainly because lack of selectivity and high toxicity. The CDK4/CDK6 specific inhibitor Ribociclib, received FDA approval as first-line treatment for HR+/HER2- metastatic breast cancer in combination with any aromatase inhibitor (33).

Our study, for the first time, tests a CDK4/CDK6 specific inhibitor in the treatment of B-ALL, demonstrating significant efficacy in vitro as a single agent and in combination with Dexamethasone.

Gene expression analysis performed on 299 B-ALL patient samples showed that CDK4 and CDK6, are highly overexpressed in comparison to bone marrow derived from healthy donors. These preliminary results prompted us to investigate if inhibiting CDK4 and CDK6 in B-ALL could be a good strategy to sensitize resistant leukemia subtypes to chemotherapy.

This study was performed on 4 B-ALL cell lines, characterized by different chromosomal rearrengements; due to the observation that CDK4/CDK6 signaling is higly active in B-ALL, thus maintaining hyperphosphorylated retinoblastoma and supporting cell cycle progression through the G1/S checkpoint, we chose to interrogate the effect of CDK4/CDK6 depletion on B-ALL cell lines. We knocked-down CDK4/CDK6 genes ina B-ALL cell line and analyzed both cell viability and proliferation. We observed a significant reduction in cell proliferation along with a strong arrest in G1 phase of the cell cycle.

We next investigated whether pharmacological inhibition phenocopied siRNA-mediated protein depletion: we found that at low concentration, Ribociclib induced a strong G1 cell cycle arrest. As expected a strong reduction of pRB (S780) but a reduction in total protein was also observed in well agreement with CDK4/CDK6 silencing. Analougsly Ribociclib treatment induces a significative dephosphorylation of both FOXM1 (T600) and SMAD2/3 (T8), two important targets of CDK4/CDK6.

The FOXM1 transcription factor has been identified as potential target of CDK4/6 signaling and also as recently reported by our group and others, it is involved in B-

ALL proliferation (34-35). The treatment with ribociclib induced a decrease in the expression of phosphorylated form of FOXM1, suggesting its deactivation and a consequent decrease of its transcriptional activity. SMAD2/3 are the principal mediator for TGF-b antiproliferative responses and regulate the transcription of important cell cycle mediators such as c-myc, p21 and p15. SMAD2/3 are direct target of inhibitory phosphorylation by CDK4/CDK6 during cell cycle (36-37). Together with FOXM1, the decrease in T8 phosphorylation site of SMAD2/3 upon Ribociclib treatment, and thus its activation, further reinforced the antiproliferative effect of the studied drug.

We demonstrated that Ribociclib treatment causes a decrease in cell proliferation and cell colony formation; therefore, for the first time, we showed that Ribociclib acts irreversibly on cell proliferation of B-ALL cell lines after 48h of treatment and successive wash out, maybe due to the prolonged G1 arrest that negatively regulates the phosphorilation of CDK4/CDK6 downstream targets, importants for cell cycle progression.

From the point of view of the cytotoxic mechanism of action of Ribociclib, we provided evidence that the compound has a cytostatic effect and it doesn't induce apoptosis; as demonstrated by Chen-Kiang for Palbocilib (38), another CDK4/CDK6 inhibitor, it is possible that treatment of B-ALL with Ribociclib may halt gene expression in G1 and prevent the expression of genes programmed for other phases, thereby sensitizing tumour cells for cytotoxic killing. Numerous mechanisms have been proposed to explain the lack of effective glucocorticoid-induced apoptosis in prednisone poor responders; however molecular basis of glucocorticoids resistance in acute lymphoblastic leukemia remain unclear (39). To this regard we examined if combining Ribociclib with the chemotherapeutics used in B-ALL therapy could increase their efficacy. Our results clearly indicate a strong synergistic effect (CI<1) between Ribociclib and Dexamethasone in the four B-ALL cell lines tested. In particular, it is important to note that Ribociclib is able to partially reverse the glucocorticoid resistance in SEM and RCH-ACV, that are normally resistant to dexamethasone. Furthermore, these results were confirmed, in a more specific way, in the same cell lines after combination treatment of Ribociclib and Dexamethasone; we found an increase in the Glucocorticoid receptor at protein and mRNA level, we observed also a synergistic upregulation of glucocorticoid-regulated genes such as BTG1, GILZ.

Numerous studies on the mechanisms of glucocorticoids resistance have established

that an effective upregulation of Glucocorticoid receptor gene in response to glucocorticoids is required for the activation of apoptosis in human leukemias (40). Our results showed that combination treatment in SEM and RCH-ACV causes a significative increase of apoptotic cells after 72 h.

Another important finding is that the increase of GR expression is increased also when CDK4/6 are knockdown by specific siRNA indicating that the effect of Ribociclib are not due to an off-target. Importantly this occur in glucorticoid resistant cells thus these results could be important in the light of the fact that one of the negative prognostic factors in the cure of B-ALL is the resistance to glucocorticoids.

Our findings indicate that Ribociclib acts synergistically with Dexamethasone and thus might overcome potential resistance to treatment; moreover, a combinatorial strategy might also enable lower doses of glucocorticoids to be used, minimizing toxicities while maintaining therapeutic efficacy. We can conclude that targeting CDK4/CDK6 kinase activity may improve the treatment of glucocorticoid-resistant B-ALL.

1.10 References

1) Lapenna S., Giordano A. (2009) Cell cycle kinase as therapeutic targets for cancer *Nat Rev Drug Discov* 8: 547-66
2) Duronio R. J. , Yue Xiong (2013) Signaling Pathways that Control Cell Proliferation *Cold Spring Harb Perspect Biol* 5: a008904
3) Lars Anders, Nan Ke, Per Hydbring, Yoon J. Choi, Hans R. Widlund, Joel M. Chick, Huili Zhai, Marc Vidal, Stephen P. Gygi, Pascal Braun, and Piotr Sicinski (2011) A Systematic Screen for CDK4/6 Substrates Links FOXM1 Phosphorylation to Senescence Suppression in Cancer Cells *Cancer Cell* 20: 620–634
4) Konecny G.E., Winterhoff B., Kolarova T., Qi J, Manivong K., Dering J., Yang G., Chalukya M., Wang H.J., Anderson L., Kalli K.R., Finn R.S., Ginther C., Jones S., Velculescu V.E., Riehle D., Cliby W.A., Randolph S., Koehler M., Hartmann L.C., Slamon D.J. (2011) Expression of p16 and retinoblastoma determines response to cdk4/6 inhibition in ovarian cancer *Clin Cancer Res* 17: 1591-602
5) Van der Linden M.H., Willekes M., Van Roon E., Seslija L., Schneider P., Pieters R., Stam R.W. (2014) MLL fusion-driven activation of CDK6 potentiates proliferation in MLL-rearranged infant ALL *Cell Cycle* 13: 834-44
6) Cobaleda C., Sánchez-García I. (2009) B-cell acute lymphoblastic leukemia: towards understanding its cellular origin *Bioessays* 31: 600-9
7) Moorman AV. (2016) New And Emerging Prognostic And Predictive Genetic Biomarkers In B-Cell Precursor Acute Lymphoblastic Leukemia *Haematologica* 101: 407-16
8) Stacy L. Cooper and Patrick A. Brown (2015) Treatment of Pediatric Acute Lymphoblastic Leukemia *Pediatr Clin North Am* 62: 61–73
9) Tissing W.J., Meijerink J.P., Den Boer M.L., Pieters R. (2003) Molecular determinants of glucocorticoid sensitivity and resistance in acute lymphoblastic leukemia *Leukemia* 17: 17-25
10) Ling Cen, Brett L. Carlson, Mark A. Schroeder, Jamie L. Ostrem, Gaspar J. Kitange, Ann C. Mladek, Stephanie R. Fink, Paul A. Decker, Wenting Wu, Jung-Sik Kim, Todd Waldman, Robert B. Jenkins, and Jann N. Sarkaria (2012) p16-Cdk4-Rb axis controls sensitivity to a cyclin-dependent kinase inhibitor PD0332991 in glioblastoma xenograft cells *Neuro Oncol* 14: 870–881
11) Aguilar V., Fajas L. (2010) Cycling through metabolism *EMBO Mol Med* 2:338-48
12) C. Romagosa, S. Simonetti, L. López-Vicente, A. Mazo, M. E. Lleonart,

J. Castellvi and S. Ramon y Cajal (2011) p16Ink4a overexpression in cancer: a tumour suppressor gene associated with senescence and high-grade tumours *Oncogene* 30: 2087–209

13) Nakamura M., Sugita K., Inukai T., Goi K., Miyamoto N., Kagami K., Okazaki-Koyama T., Mori T., Saito M., Nakazawa S. (2001) Abnormalities of the p16INK4a gene in childhood B-precursor acute lymphoblastic leukemia without nonrandom translocations: analysis of seven matched pairs of primary leukemia and corresponding cell line *Leukemia* 15. 1136-9
14) O'Leary B., Finn R.S., Turner N.C. (2016) Treating cancer with selective CDK4/6 inhibitors *Nat Rev Clin Oncol* 13: 417-30
15) Drexler H.G. (1998) Review of alterations of the cyclin-dependent kinase inhibitor INK4 family genes p15, p16, p18 and p19 in human leukemia–lymphoma cells *Leukemia* 12: 845-59
16) Yu Q., Sicinska E., Geng Y, Ahnström M., Zagozdzon A., Kong Y., Gardner H., Kiyokawa H., Harris L.N., Stål O., Sicinski P. (2006) Requirement for cdk4 kinase function in breast cancer *Cancer Cell* 9: 23-32
17) Musgrove E.A., Caldon C.E., Barraclough J., Stone A., Sutherland R.L. (2011) Cyclin D as a therapeutic target in cancer *Nat Rev Cancer* 11: 558-72.
18) Tigan A.S., Bellutti F., Kollmann K., Tebb G., Sexl V. (2016) CDK6—a review of the past and a glimpse into the future: from cell-cycle control to transcriptional regulation *Oncogene* 35: 3083-91
19) Marieke H van der Linden, Merel Willekes, Eddy van Roon, Lidija Seslija, Pauline Schneider, Rob Pieters, and Ronald W Stam (2014) MLL fusion-driven activation of CDK6 potentiates proliferation in MLL-rearranged infant ALL *Cell Cycle* 13: 834–844
20) Hamilton E., Infante J.R. (2016) Targeting CDK4/6 in patients with cancer *Cancer Treat Rev* 45: 129-38
21) Dickson M.A. (2014) Molecular Pathways: CDK4 Inhibitors for Cancer Therapy *Clin Cancer Res* 20: 3379-83
22) Spring L., Bardia A., Modi S. (2016) Targeting the Cyclin D-Cyclin-dependent Kinase (CDK) 4/6-Retinoblastoma Pathway with Selective CDK 4/6 Inhibitors in Hormone Receptor-positive Breast Cancer: Rationale, Current Status, and Future Directions *Discov Med* 21: 65-74
23) Aleem E., Arceci R.J. (2015) Targeting cell cycle regulators in hematological malignancies *Front Cell Dev Biol* 3:16

24) Roskoski R. Jr. (2016) Cyclin-dependent protein kinase inhibitors including palbociclib as anticancer drugs *Pharmacol Res* 107: 249-75

25) Julie Ann Rader *et al*. (2013) Dual CDK4/CDK6 inhibition induces cell-cycle arrest and senescence in neuroblastoma *Clin Cancer Res* 19(22)

26) Yana Pikman *et al*. (2016) Sinergistic drug combination with a CDK4/6 inhibitors in T-cell acute lymphoblastic leukemia *Clin Cancer Res*

27) Novartis.com

28) Baughn L.B., Di Liberto M., Wu K., Toogood P.L., Louie T., Gottschalk R., Niesvizky R., Cho H., Ely S., Moore M.A., Chen-Kiang S. (2006) A novel orally active small molecule potently induces G1 arrest in primary myeloma cells and prevents tumour growth by specific inhibition of cyclin-dependent kinase 4/6. *Cancer Res*. 66: 7661-7

29) Chou T (2006) Theoretical basis, experimental design, and computerized simulation of synergism and antagonism in drug combination studies *Pharmacol Rev* 58: 621-681

30) Chou T-C (2010) Drug combination studies and their synergy quantification using the Chou-Talalay method *Cancer Res* 70: 440–446

31) Pikman Y., Alexe G., Roti G., Conway A,S., Furman A,, Lee E.S., Place A.E., Kim S., Saran C., Modiste R., Weinstock D.M., Harris M., Kung A.L., Silverman L.B., Stegmaier K. (2017) Synergistic Drug Combinations with a CDK4/6 Inhibitor in T-cell Acute Lymphoblastic Leukemia *Clin Cancer Res* 23:1 012-1024

32) Basso G., Buldini B., De Zen L., Orfao A. (2001) New methodologic approaches for immunophenotyping acute leukemias *Heamatologica* 86: 75–6

33) Hanxiao Xu, Shengnan Yu[1] Qian Liu, Xun Yuan, Sridhar Mani, Pestell R. G., Kongming Wu (2017) Recent advances of highly selective CDK4/6 inhibitors in breast cancer *J Hematol Oncol* 10: 97

34) Consolaro F., Basso G., Ghaem-Magami S., Lam E.W.F., Viola G. (2015) FOXM1 is overexpressed in B-acute lymphoblastic leukemia (B-ALL) and its inhibition sensitizes B-ALL cells to chemotherapeutic drugs *Int J Oncol* 47: 1230–1240

35) Buchner M., Park E., Geng H., Klemm L., Flach J., Passegué E., Schjerven H., Melnick A., Paietta E., Kopanja D., Raychaudhuri P., Müschen M. (2015) Identification of FOXM1 as a therapeutic target in B-cell lineage acute lymphoblastic leukaemia *Nat Commun* 6

36) Liu F., Matsuura I., (2005) Inhibition of Smad antiproliferative function by CDK phosphorylatio *Cell Cycle* 4: 63–66

37) Matsuura I., Denissova N.G., Wang G., He D., Long J., Liu F., (2004) Cyclin-dependent kinases regulate the antiproliferative function of Smads *Nature* 430: 226–231

38) Huang X., Di Liberto M., Jayabalan D., Liang J, Ely S., Bretz J., Shaffer AL 3rd, Louie T., Chen I., Randolph S., Hahn W.C., Staudt L.M., Niesvizky R., Moore M.A., Chen-Kiang S. (2012) Prolonged early G(1) arrest by selective CDK4/CDK6 inhibition sensitizes myeloma cells to cytotoxic killing through cell cycle-coupled loss of IRF4 *Blood* 120:1095-106

39) Bhadri V. A., Trahair T. N., Lock R. B. (2012) Glucocorticoid resistance in paediatric acute lymphoblastic leukaemia *J Paediatr Child Health* 48: 634–640

40) Real P.J., Tosello V., Palomero T., Castillo M., Hernando E., de Stanchina E., Sulis M.L., Barnes K., Sawai C., Homminga I., Meijerink J., Aifantis I., Basso G., Cordon-Cardo C., Ai W., Ferrando A. (2009) Gamma-secretase inhibitors reverse glucocorticoid resistance in T cell acute lymphoblastic leukemia *Nat Med* 15 50-8

CHAPTER 2

PHARMACOLOGICAL CHARACTERIZATION OF NOVEL P-GP INHIBITORS

2.1 General introduction

The failure of treatment of cancer patients often occurs as a result of intrinsic or acquired drug resistance of the tumour to chemotherapeutic agents. The resistance of tumours occurs not only to a single cytotoxic drug, but also occurs as a cross-resistance to a whole range of drugs with different structures and cellular targets (1). This phenomenon is called multiple drug resistance (MDR) and it is defined as a phenotype of the cells resistant to multiple structurally and functionally different drugs. Such resistance is multifactorial and may be due to various mechanisms (2). The most common mechanism of MDR is due to the overexpression of membrane efflux pumps called ATP-binding cassette (ABC) transporters, which can result in an increased efflux of the cytotoxic drugs from the cancer cells, thus lowering their intracellular concentrations; MDR severely limits the efficacy of cancer chemotherapy in a variety of common malignancies (1).

Cellular mechanisms of drug resistance have been intensively studied and experimental models can be easily generated by in vitro selection with cytotoxic agents, such as paclitaxel, doxorubicin, or vinblastine (3). Among several mechanisms underlying the development of MDR, the process of P-gp mediated drug efflux plays a key role **(Fig.1)**. This has prompted extensive investigations towards the development of new candidate structures as P-gp inhibitors (4).

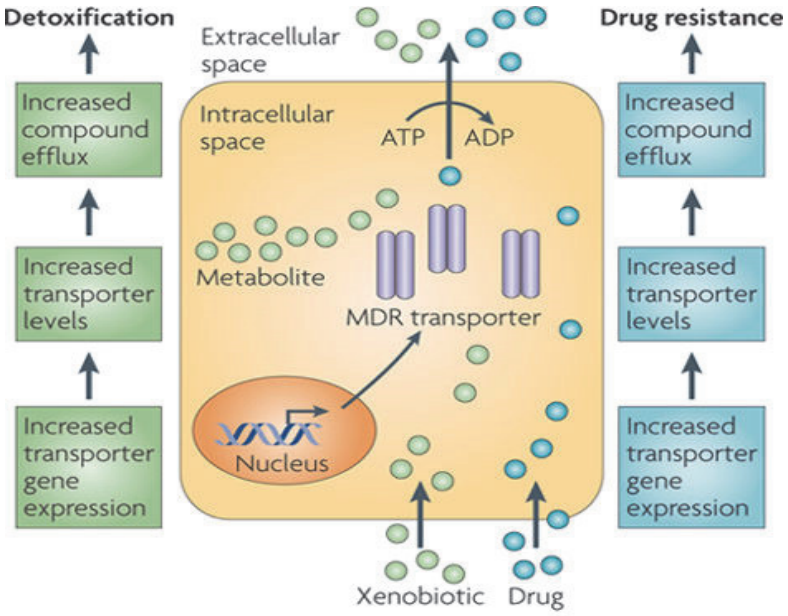

Fig. 1 Mechanisms behind multidrug resistance: The most common mechanism of MDR is due to the overexpression of ABC transporters, which can result in an increased efflux of the cytotoxic drugs from the cancer cells (6).

It is known that solid tumours are enriched of cancer stem cells that are a small subpopulation of stem-like cells and have the capability for tumour-initiation and self-renewal. This population of cells is associated with greater resistance to conventional therapy (5). We focused on medulloblastoma because it is one of the most frequent childhood brain tumours and there is the need of developing new treatment to reduce long-term toxicity of therapy.

To this regard we will investigate if overcoming/inhibiting ABC drug transporters could enhance the efficacy of current chemotherapy regimens.

2.1.1 ATP binding cassette transporters

ABC transporters are a group of plasma membrane glycoproteins consisting of both transmembrane domains and distinctive nucleotide-binding domains, which generate energy from ATP hydrolysis to actively transport a variety of compounds across (7). Currently, 49 members of the ABC transporter family have been isolated and identified (8); three members of the ABC transporter family, ABCB1 (P-glycoprotein), ABCC1 and ABCG2, appear to play an important role in the development of multidrug resistance in cancer cells **(Fig.2)** (7). All three have broad, overlapping substrate specificity and promote the elimination of various cancer chemotherapeutics such as taxanes, topoisomerase inhibitors and antimetabolites (9).

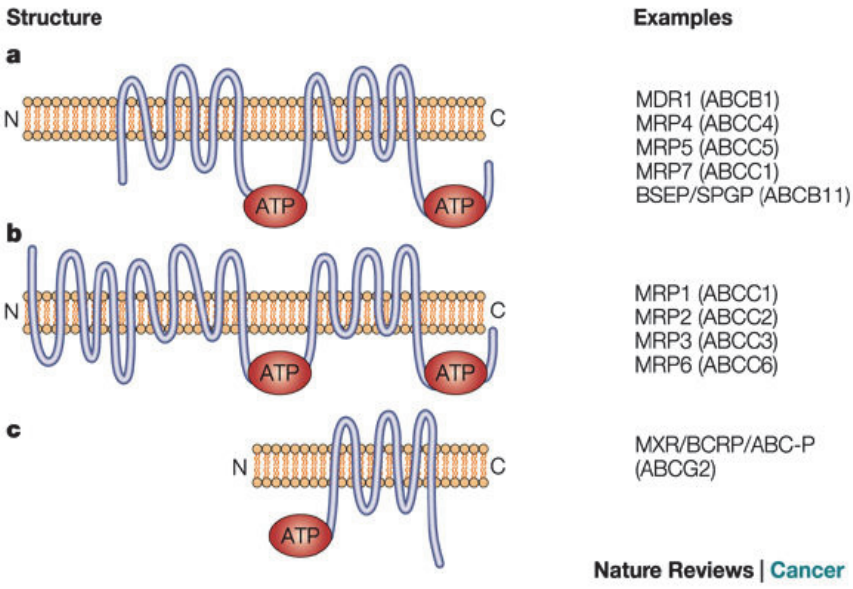

Fig. 2 The structure of three member of ABC family that play an important role in multidrug resistance. a) ABCB1 b) ABCC1 c) ABCG2 (4).

2.1.2 Targeting side population in Medulloblastoma

Medulloblastoma (MB) is a highly invasive tumour arising from embryonal cells in the cerebellum and is the most-common type of paediatric brain tumour, accounting for about 20% of all childhood brain cancers. Standard protocol therapy consists of surgical resection, craniospinal irradiation, and chemotherapy with a treatment success rate of approximately 70–75% among children aged ≥3 years (10).

The World Health Organization classifies medulloblastoma into subtypes based on histological traits, but disease prognosis is better predicted by four different non-histological subgroups, based on the global genome sequencing profile: 1) WNT; 2) Sonic hedgehog (SHH); 3) Group 3 (N-MYC amplification); and 4) Group 4 (heterogenous genes) (**Fig.3**) (11).

Despite of the efficacy of this protocol in increasing the survival rate, in particular for high-risk patients, there is the need of developing new treatment to reduce long-term toxicity of therapy such as very severe neurologic and neuroendocrine consequences.

	WNT	SHH	Group 3	Group 4
Subgroup Prevalence	7-8%	28-32%	26-27%	34-38%
Common Histology	Classic	Desmoplastic/ Nodular	Large Cell/ Anaplastic	Classic
Clinical Outcome	Very Good	Good to Intermediate	Poor	Intermediate
Gene Expression	WNT	SHH	MYC	Neuronal/ Glutamatergic
Cellular Origin/ Phenotype	Dorsal Brainstem Progenitor	Cerebellar GNP	Cerebellar Stem Cell	?

Fig. 3 Medulloblastoma subgroups (12).

The discovery of cancer stem cells in solid tumours has changed the view of carcinogenesis and chemotherapy. One particularly intriguing property of stem cells is that they express high levels of specific ABC drug transporters (13).

Within cancer stem cells there is cell population identified as “side population” (SP), based on ABC transporters-mediated efflux of Hoechst 33342 dye (14); moreover, these cells are pluripotent, have greater growth capacity and resistance to cytotoxic

drugs as compared to non-SP cells (15).

SP cells have been successfully identified in a wide range of solid tumours, including breast cancer, lung cancer, prostate cancer, ovarian cancer, pancreatic cancer, glioblastoma and medulloblastoma. This population plays a critical role in tumour initiation, maintenance, progression, and relapse (16).

We focused on MB side population because drug uptake into the brain depends on various factors, including the physical barriers presented by the blood–brain barrier (BBB) and it has been found that ABC transporters are presents at the BBB. These transporters can remove a drug from the central nervous system or prevent its entry in the BBB, thereby limiting the accumulation of such drugs in the brain (17).

Side population not only have the characteristics of tumour stem cells, it is also more resistant to the effects of drugs, and may contribute to the overall drug resistance phenotype of relapsed or resistant cancers; for these reasons, it is essential the devolopment of new drugs to eradicate SP cells. Therefore, targeting the SP cells is an attractive strategy for overcoming drug resistance in solid tumours.

2.1.3 New synthetic ecdysteroids as innovative therapeutic strategy for MDR

Ecdysteroids are hydroxysteroids with a characteristic 7-en-6- one moiety in their B-ring and these compounds are analogues of the molting hormones of arthropods (18). Quite recent studies from Hunyadi *et al.* found that certain ecdysteroid derivatives, such as the most common 20-hydroxyecdysone (Fig.4), significantly decrease the resistance of MDR murine leukemia cell line expressing the human ABCB1 transporter or P-glycoprotein to doxorubicin, a known chemotherapeutic agent that is a substrate of the ABCB1 transporter (19).

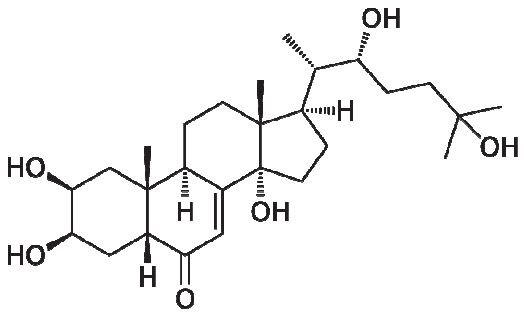

Fig. 4 Structure of 20-hydroxyecdysone.

Multicomponent reactions (MCRs) are convergent chemical processes in which more than two starting materials react to form a product, incorporating essentially most of

the atoms of the reagents. One of the most versatile MCRs is the Ugi four-component reaction (U-4CR), which is based on the exceptional reactivity of the isocyanide functional group and widely applied in diversity-oriented synthetic strategies. Here we exploit the reactivity of the 6-keto-7-ene group of 20-OH-ecdysone, demonstrating it as a precursor of an amine or isocyanide functionality. Starting from 6-amino- and 6-isocyanide-containing ecdysone derivatives, we were able to prepare a small family of ecdysteroid-peptide conjugates.

The newly synthesized derivatives were evaluated in a panel of ABCB1-overexpressing drug-selected human cancer cell lines and in medulloblastoma cell lines, for their antiproliferative activity and anti-P-gp activity.

NOVEL ECDYSTEROIDS RESENSITIZE MULTIDRUG RESISTANCE CANCER CELLS TO CHEMOTHERAPEUTIC AGENTS THROUGH MODULATION OF P-GLYCOPROTEIN FUNCTIONS, EXPRESSION AND ATPASE ACTIVITY

Elena Mattiuzzo[a], Roberta Bortolozzi[a], Giuseppe Basso[a], Giampietro Viola[a]

[a]*Dipartimento di Salute della Donna e del Bambino, Laboratorio di Oncoematologia, Università di Padova, 35131 Padova, Italy*

2.2 Abstract

Background

Failure of cancer chemotherapy can occur through increased efflux of chemotherapeutic agents, leading to the reduction of intracellular drug levels and consequent drug insensitivity, often to multiple agents. A well-established cause of multidrug resistance involves the increased expression of members of the ATP binding cassette transporter superfamily, many of which efflux various chemotherapeutic compounds from cells. The most extensively characterized MDR transporters include ABCB1 (also known as MDR1 or P-glycoprotein), ABCC1 (also known as MRP1) and ABCG2 (also known as BCRP or MXR) (6).

Recent discoveries have provided clear evidence that cancer stem cells are present in several cancerous tissues, such as medulloblastoma, neuroblastoma, colon and breast cancers. These cancer stem cells represent only a small percentage of total cell populations and efficiently efflux Hoechst dye resulting in the dye-negative phenotype, also known as side population phenotype. Further investigations revealed that Hoechst dye efflux is attributable to increased levels of expression of the MDR1 and ABCG2 transporters, which are capable of extruding certain chemotherapeutic agents, and have been implicated in drug resistance (20). Several approaches have been taken to overcome P-gp mediated drug resistance. Recent studies found that certain ecdysteroids derivative, such as the most common 20-hydroxyecdysone, significantly decrease the resistance of a multi-drug resistant murine leukemia cell line expressing the human ABCB1 transporter to doxorubicin. This has prompted extensive investigations towards the development of new candidates structures as P-gp inhibitors.

Materials and methods

In this study we examined the effects of new synthetic P-gp inhibitors deriving from ecdysteroids alone and in combination with vinblastine (VBL) and doxorubicine (DOXO) in lymphoblastic leukemia CEM Vbl-100 and LOVO/DOXO respectively; these cells were exposed to VBL and LOVO/DOXO to DOXO, in the presence or absence of synthetic ecdysteroids and cell viability was analyzed by the MTT assay. The fluorescent dye, rhodamine 123, was used to evaluate the functional activity of the P-gp efflux transport system in leukemia and in medulloblastoma cell lines after treatment with P-gp inhibitors. Verapamil was used as positive control.

We tested this new compounds alone and in combination with cis-platin and vincristine also on medulloblastoma cell lines, DAOY and D425, that are enriched in cancer stem cells overexpressing P-glycoproteins.

Results

In CEM Vbl-100 and LOVO/DOXO, we observed an increase in rhodamine 123 uptake in all resistant cell lines upon incubation with the test compounds. In these cells synthetic P-gp inhibitors increased the antiproliferative effects of VBL and DOXO and combination indexes, calculated by Chou-Talalay method, showed values <1, indicating that P-gp inhibitors strongly synergizes with VBL and DOXO. Also in medulloblastoma cell lines, P-gp inhibitors synergizes with cis-platin and vincristine. Expression levels of P-glycoproteins were quantified by real-time quantitative PCR for mRNA levels in CCRF-CEM as control and CEM Vbl-100 treated with synthetic P-gp inhibitors. mRNA levels were lower in those cells treated with synthetic P-gp inhibitors respect to CEM Vbl-100 control. We investigated the side population cell levels in medulloblastoma cell lines after 24 h P-gp inhibitors treatment and we found a decrease in SP in all cell lines respect to control and verapamil treatment (positive control).

Conclusions

These new synthetic P-gp inhibitors could be promising in overcoming multidrug resistance in association with standard chemoterapeutic agents and in eradicating the side population portion that is one of the most resistant to chemotherapy in solid tumours such as medulloblastoma.

Keywords**:** P-gp, multidrug resistance, medulloblastoma, ecdysteroids, side population

2.3 Materials and methods

Cell culture

The human leukemia cell line CEM Vbl-100 is a multidrug-resistant line selected against vinblastine and supplemented with 100 ng/ml of vinblastine. LOVO/DOXO cells are a doxorubicin resistant subclone of LOVO cells and were grown in complete Ham's F12 medium supplemented with doxorubicin (0.1 μg/mL). LOVO/DOXO and CEM Vbl-100 were a kind gift of Dr. G. Arancia (Istituto Superiore di Sanità, Rome, Italy) (20).
Medulloblastoma cell lines DAOY and D425 were purchased from the American Type Culture Collection. Cells were cultured in RPMI 1640 or DMEM (Life Technologies, Italy) supplemented with 10% fetal bovine serμM (FBS), glutamine (2 mM; Life Technologies, Italy), penicillin (100 U/ml; Life Technologies, Italy) and streptomycin (100 μg/ml; Life Technologies, Italy), and maintained at 37°C in a humidified atmosphere with 5% CO_2.

Flow cytometric analysis of rhodamine 123

Functional activity of P-gp was measured with the fluorescent dye rhodamine 123 (Rho 123, Pierce, Rockford IL, USA) that is a substrate of P-gp (4). Briefly, after different times of treatment, the cells were collected by centrifugation and resuspended in Hank's Balanced Salt Solution (HBSS) containing 0.1 μM Rho 123. The cells were then incubated for 20 min at 37°C, centrifuged and resuspended in HBSS. The fluorescence was directly recorded by flow cytometry with a Coulter Cytomics FC500 (Beckman Coulter).

Flow cytometric analysis of side population

The protocol of SP analysis was based on Goodell and colleagues. Briefly, cells (10^6/mL) were incubated in DMEM and RPMI containing 2% FCS (Life Technologies) and 5 μg/mL Hoechst 33342 dye (Sigma-Aldrich) for 90 min at 37°C, either alone or in the presence of 50 μmol/L verapamil (Sigma). At the end of incubation, cells were washed and then incubated in PBS supplemented with 2% FCS and 2 μg/mL propidium iodide (Sigma), at 4°C for 10 min, to discriminate dead cells. The cells were then analyzed in a FACSVantage fluorescence-activated cell sorter (Becton Dickinson) by using a dual wavelength analysis (blue, 424–444 nm; red, 675 nm) after excitation with 350-nm UV light.

P-glycoprotein activity assay

P-gp ATPase activity after ecdysteroids treatment was estimated by P-gp-Glo assay system (Promega, Madison, WI). This method relies on the ATP dependence of the light-generating reaction of firefly luciferase where ATP consumption is detected as a decrease in luminescence. In a 96 well plate, recombinant human P-gp (25 µg) was incubated with P-gp-Glo assay buffer™ (20 µl), verapamil (200 µM) as positive control, sodium orthovanadate (100 µM) as a P-gp ATPase inhibitor, and test compounds (1 µM-10 µM). The reaction was initiated by addition of MgATP (10 mM), then stopped 40 min later by addition of 50 µL of firefly luciferase reaction mixture (ATP detection reagent) that initiated an ATP-dependent luminescence reaction. Signals were measured 60 min later by Victor3TM 1420 Multilabel Counter (PerkinElmer, Waltham, MA, USA).

Drug treatment

Cells were grown to 60% confluence and then treated with synthetic P-gp inhibitors at a stock concentration of 10 mM, Cells were treated for 72 h using scalar dilutions of P-gp inhibitors AL10c and AL23b, combined with vinblastine, doxorubicine, vincristine at a stock concentration of 10 mM, cis-platino at a stock concentration of 5mM (Sigma-Aldrich) and then used at different concentrations. Doxorubicine, vincristine and cis-platin were added to drug solutions at fixed combination ratios while vinblastine was addes at fixed concentrations of 1 µM. The effectiveness of various drug combinations was analyzed by the Calcusyn Version 2.1 software (Biosoft). The combination index (CI) was calculated according to the Chou-Talalay method (29). A combination index of 1 indicates an additive effect of the 2 drugs. Combination index values less than 1 indicate synergy, and combination index values more than 1 indicate antagonism.

MTT assay

Proliferation was assessed by MTT (3-(4,5-dimethylthiazol-2-yl)-2,5-diphenyl tetrazolium bromide) assay after treatment. Equal concentrations of cells were plated in triplicate in a 96-well plate and incubated with 10 µl MTT (Sigma-Aldrich, St Louis, MO, USA) for 4 h. Absorbance was measured at 560 nm using Victor3TM 1420 Multilabel Counter (PerkinElmer, Waltham, MA, USA). The growth inhibition50 (GI_{50}=compound concentration required to inhibit cell proliferation by 50%) was calculated by plotting the data as a logarithmic function of (x) when viability was

50%. DMSO-treated cells viability was set to 100%.

RNA isolation and Reverse transcriptase polymerase chain reaction (RT-PCR)

Total cellular RNA from cell lines and patient bone marrow was extracted with TRIzol reagent (Invitrogen). RNA quality was controlled using Nanodrop spectrophotometer. Subsequently, 1 μg of total RNA was reversely transcribed using random hexamers and Superscript II (Invitrogen), according to the manufacturer's instructions.

Real time PCR

Real-time quantitative (RQ-PCR) was performed on an Applied Biosystems 7900 HT Sequence Detection System using SYBR Green PCR Master Mixture Reagents (Applied Biosystems; Forest City, CA. Primer used for analysis were for ABCB1 gene (p-glycoprotein). All expression values were normalized using expression of GUS as an endogenous control **(Table 1).**

Table 1.

	Forward	Reverse
ABCB1	5'- CACCAAGGCCCTGCGCTACC -3'	5'- ACACCCGGTACCCGCGATGA -3'
GUS	5'-GAAAATATGTGGTTGGAGAGC-3'	5'-CGAGTGAAGATCCCCTTTTTA-3'

Statistical analysis

All experiments were performed with a minimum of three technical and three biological replicates, and values reported are the mean of the three biological replicates, unless otherwise indicated. Error bars represent the standard deviation (SD) from the mean, unless otherwise indicated. All statistical analyses were performed using the GraphPad Prism software.

2.4 Results

Antiproliferative effect of new synthetic ecdysteroids on ABCB1 overexpressing drug-selected cell lines

To explore the effect of these new synthetic ecdysteroids we choose CCRF CEM as wild type cells and CEM Vbl-100 as ABCB1 overexpressing cell lines. Cells were exposed to 13 synthetic ecdysteroids **(Fig.4a)** for 72 h at concentrations ranging from 0.001 to 100 μM. We treated also with vinblastine to verify the resistance or sentitivity in CEM Vbl-100 and wild type cell line respectively. The GI_{50} measured by MTT assay after 72 h was in the micromolar range for all cell lines treated as shown in **Fig.4b**: GI_{50} of CEM Vbl-100 is lower respect to GI_{50} of CCRF CEM cell line for many of the compounds investigated in particular compounds AL10c, AL23b, AL26 and PON3 showd the lowest GI_{50} in this resistant cell line.

AL05a	AL09b	AL10c
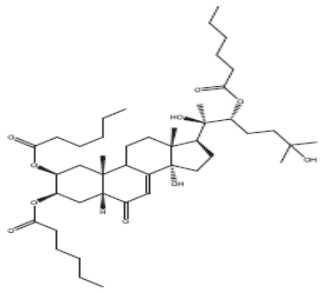	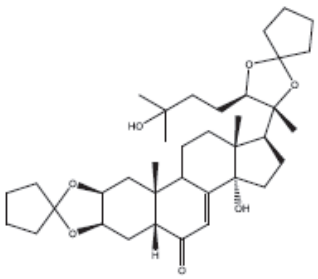	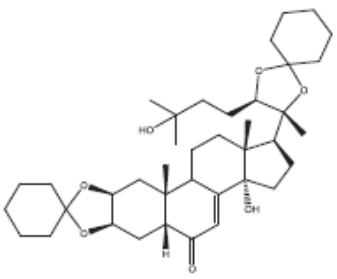
AL23b	**AL26**	**AL05b**
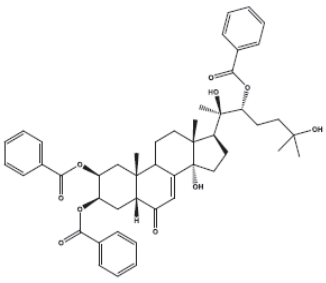	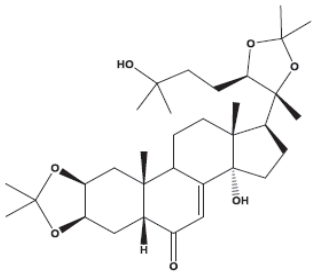	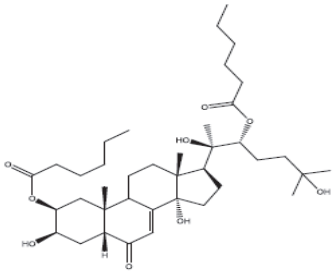

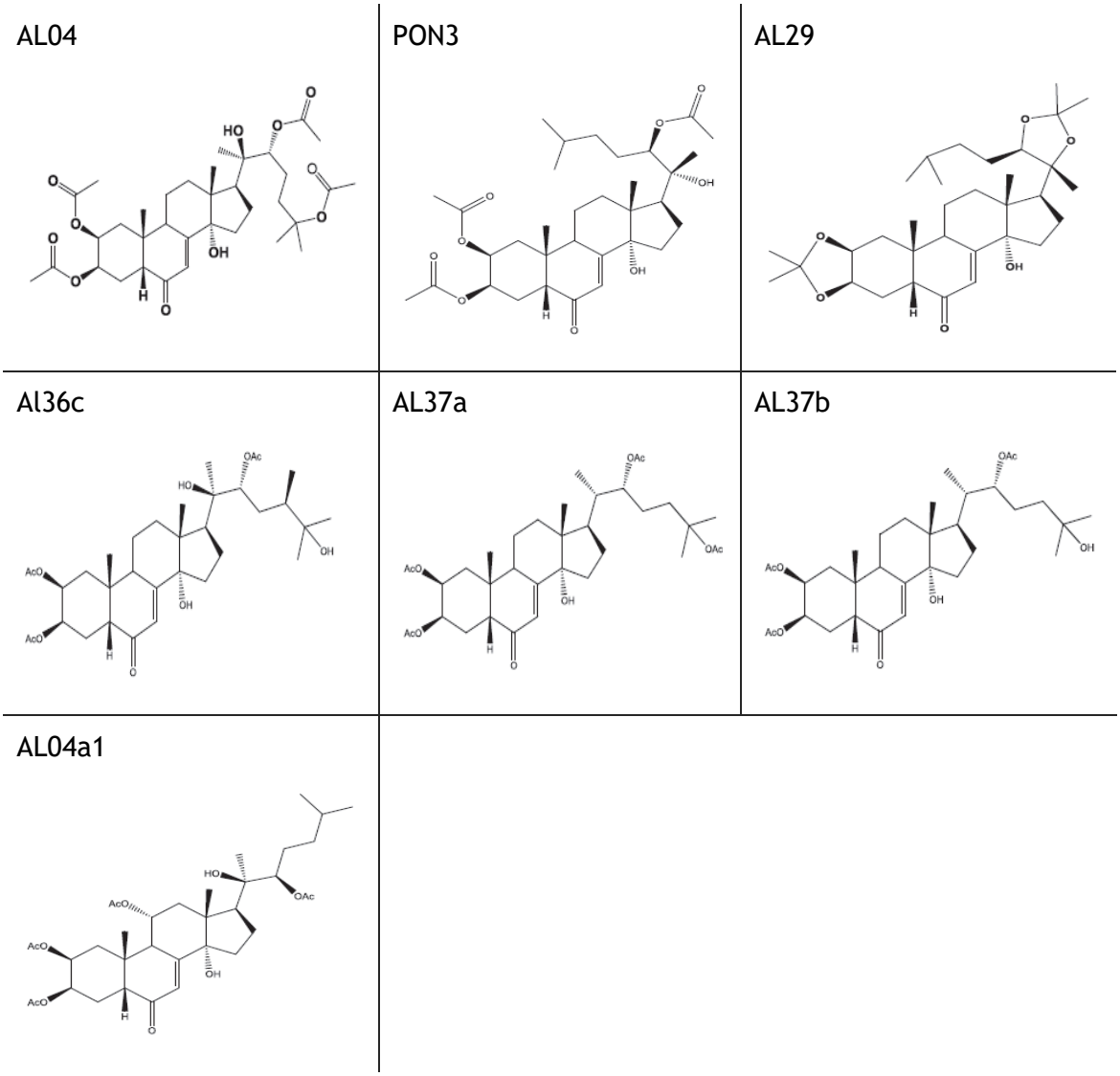

Fig. 4a Structure of new 13 synthetic ecdysteroids.

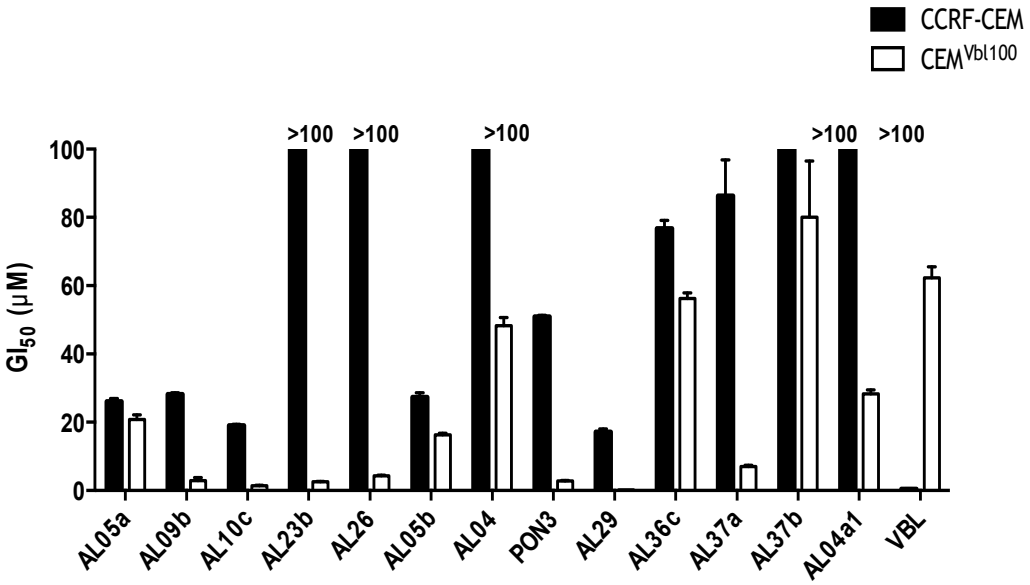

Fig. 4b In vitro cell growth inhibitory effects of ecdysteroid compounds against CCRF-CEM and CEM Vbl-100 cell line. GI_{50}= compound concentration required to inhibit tumour cell proliferation by 50%. Data are expressed as the mean ± SE from the dose-response curves of at least three independent experiments.

Rhodamine 123 accumulation in CEM Vbl-100 and LOVO/DOXO cells

Rhodamine 123 (Rho123) has been known to be substrate for P-gp, that could be used to determine whether the ecdysteroids modulate intracellular drug levels by inhibiting P-gp function. The accumulation of Rho123 was determined using flow cytometry. We performed a first rho123 analysis with those ecdysteroids that had the lower GI_{50} to understand their activity on the accumulation of rho123 in CEM Vbl-100 cell line. As shown in **Fig.5** there is a stronger intracellular accumulation of Rho123 in correspondence of cells treated with **AL10c** and **AL23b** for two hours; for this reason, we choose these two compounds for successive analysis.

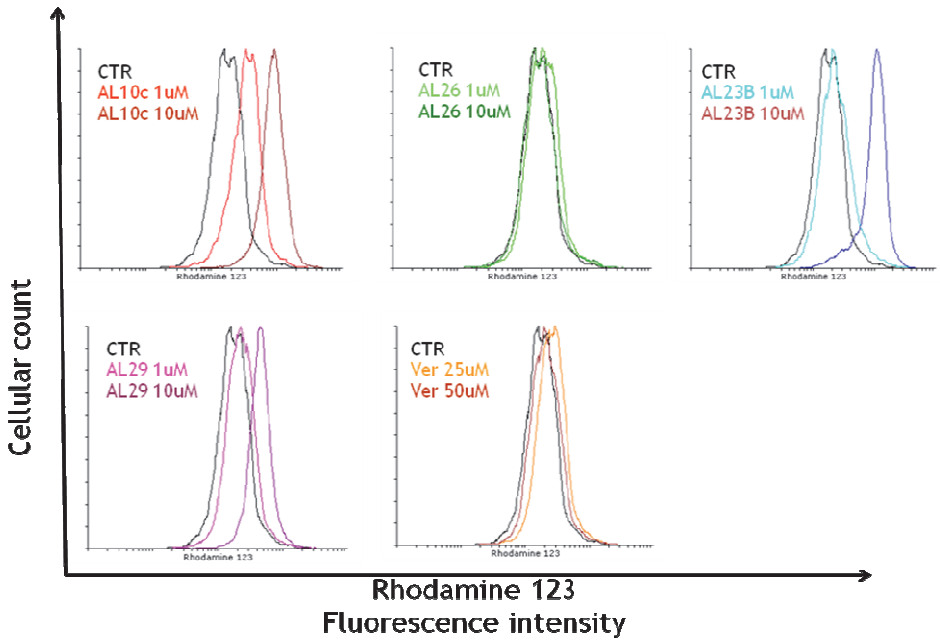

Fig. 5 Rhodamine123 accumulation in CEM Vbl-100 cell line. Cells were treated with the indicated concentration of **AL10c, AL23b, AL26, AL29** (1 and 10 μM), 25 and 50 μM verapamil (positive control). Inhibitors were incubated for 2 h; then, Rho123 was added and cells were incubated for 30 min at 37° in the dark. Cells were then harvested and used immediately to measure Rho123 fluorescence using Beckman Coulter FC500.

It was found that new synthetic ecdysteroids, **AL10c** and **AL23b**, dramatically increased Rho123 accumulation in CEM Vbl-100 cells; verapamil, known to fully inhibit P-gp activity, was used as positive control at 25 μM concentration. As shown

in **Fig.6A** the accumulation was enhanced when the cells were treated for 2 hours with 10 μM of **AL10c** and **AL23b** respect to control and verapamil. In LOVO/DOXO cells **(Fig.6B)**, we used doxorubicine as substrate for P-gp at the concentration of 1 μM, and also in this case we found that there was an accumulation of doxorubicine in those cells treated with 10 μM of **AL10c** and **AL23b** for 4 hours; verapamil was used as positive control at 25 μM concentration.

A)

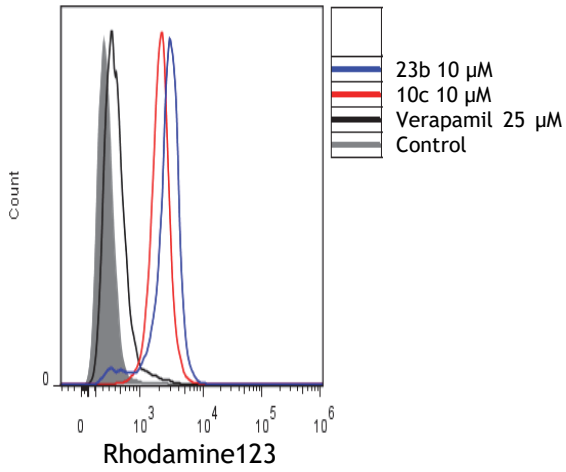

B)

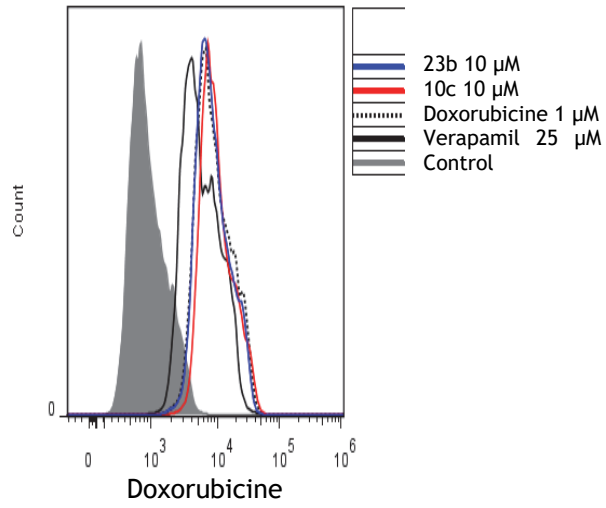

Fig. 6 Effect of new synthetic ecdysteroids on the accumulation of Rho123 in CEM Vbl-100 and of Doxorubicine in LOVO/DOXO cells. Cells were treated with the indicated concentration of **AL10c** and **AL23b** (10 μM) and 25 μM verapamil (positive control). A) In CEM Vbl-100, inhibitors were incubated for 2 h; then, Rho123 was added and cells were incubated for 30 min at 37° in the dark. Cells were then harvested and used immediately to measure Rho123 fluorescence using Beckman Coulter FC500; b) In LOVO/DOXO cell line, inhibitors were incubated for 4h; then, doxorubicine was added and cells were incubated for 15 min at 37° in the dark. Cells were then harvested and used immediately to measure doxorubicine fluorescence using Beckman Coulter FC500.

Modulation of P-gp ATPase activity with new synthetic ecdysteroids compounds

The Pgp-Glo™ Assay Systems permit to perform luminescent P-gp ATPase assays. Compounds that interact with P-gp can be identified as stimulators or inhibitors of its ATPase activity. Through this assay we examined the effects of new ecdysteroids on drug-stimulated P-gp ATPase activity. This approach is primarily used to characterize inhibitors of P-gp ATPase activity. Reduction of drug-stimulated ATPase activity by a

compound indicates it is a Pgp ATPase inhibitor.

We examined the effects of **AL10c** and **AL23b** of inhibiting the P-gp ATPase activity on recombinant human Pgp in a cell membrane fraction. As positive control, we used Verapamil that is the most known inhibitor of P-gp. Our preliminary results suggest that **AL10c** and **AL23b** inhibit the P-gp ATPase activity in a stronger way and at lower concentration respect to Verapamil **(Fig.7)**.

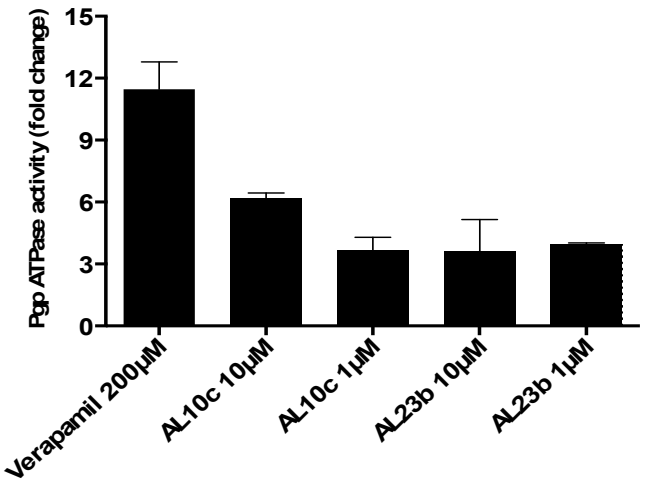

Fig. 7 New synthetic ecdysteroids compounds inhibit P-gp ATPase activity.

Treatment with AL10c and AL23b decreases P-gp expression in CEM Vbl-100

To further test the efficacy of synthetic ecdysteroids treatment and to assess the therapeutic role of P-gp inhibition in the treatment of MDR, we treated CEM Vbl-100 with **AL10c** and **AL23b** 10 µM and with verapamil 50 µM as positive control. We analyzed the effects of this treatment at transcriptional level after 24h to explore if these new compounds could induce a decrease in P-gp mRNA. Quantitative real time PCR showed a significative downregulation of P-gp expression in CEM Vbl-100 treated with **AL10c** and **AL23b** respect to control sample **(Fig.8)**.

These results suggest that pharmacological inhibition of P-gp could be promising in the treatment of MDR.

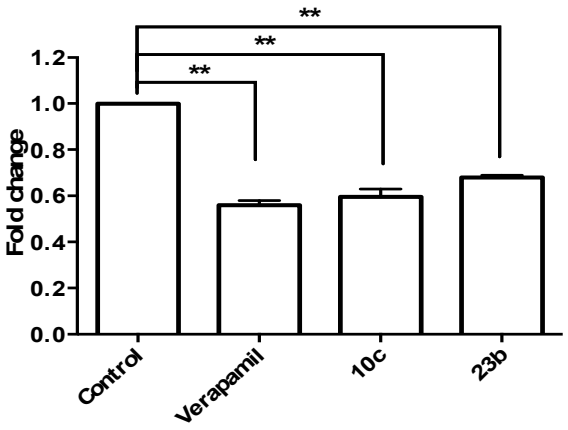

Fig. 8 Real-time PCR analysis of P-gp expression in multidrug resistant CEM vbl-100. Cells were treated with **AL10c** and **AL23b** 10 μM, and verapamil 50 μM for 24 h; P-gp expression was quantified and normalized on GUS expression, used as an internal control. The P-gp/GUS ratio for untreated samples was set as a baseline value to which all transcript levels were normalized. Error bars refer to standard deviations for three independent experiments**.** Statistical analysis was performed using ANOVA multicomparison test against the cells treated with the non-treated control; ** $p \leq 0.05$.

Synthetic ecdysteroids compounds synergize with Vinblastine in CEM Vbl-100 cell line and with Doxorubicine in LOVO/DOXO cell line

Because **AL10c** and **AL23b** inhibited P-gp efflux activity, we examined their effect on vinblastine-induced cytotoxicity to evaluate if there could be a synergistic effect in the citotoxicity effect of vinblastine. In drug-resistant CEM Vbl-100 cells, co-incubation of vinblastine at fixed concentration of 1 μM with **AL10c** and with **AL23b** resulted in a significant increase in the cytotoxicity of vinblastine **(Fig.9A-B).** In this experiment, **AL10c** and **AL23b** were added in a concentration range of 0.001-100 μM. We found that both synthetic ecdysteroids synergise with vinblastine with a combination index <1 **(Fig.9C)**.

We also performed drug combination experiments in LOVO/DOXO cell line using **AL10c** and **AL23b** in combination with Doxorubicine. Cells were treated at fixed combination ratio (1:10): **AL10c** and **AL23b** were added in a concentration range of 0.001-100 μM and Doxorubicine in a molar range of 0.0001-10 μM; also in this case we found a combination index <1 indicating a synergistic effect between our synthetic ecdysteroids and Doxorubicine **(Fig.9d Supp. Materials)**.

In all experiments cell viability was assessed by MTT test after 72 hours of incubation.

A)

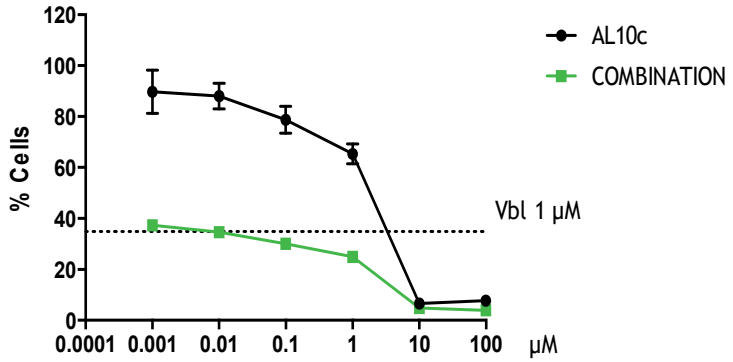

B)

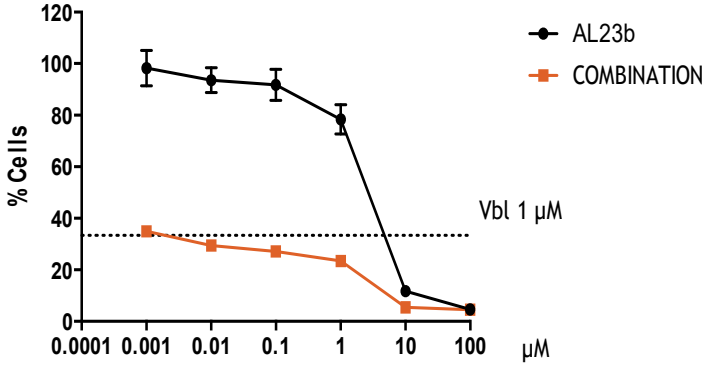

C)

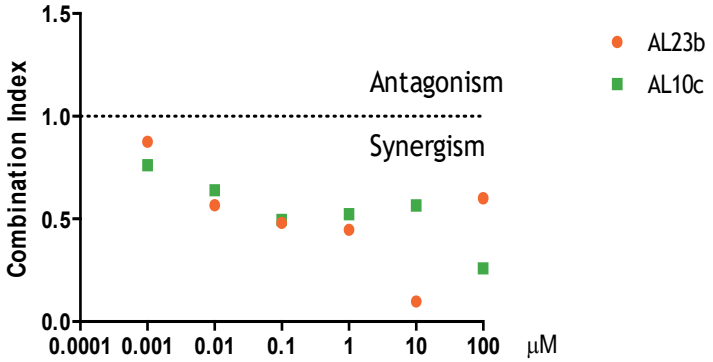

Fig. 9 Effect of AL10c and AL23b treatment alone and in combination with vinblastine in CEM Vbl-100 cells. A), B) Cells were treated at the indicated concentration and cell viability was assessed by MTT test after 72 hours of incubation. Data are expressed as mean ± SEM of three independent experiments. C) Combination index values (CI) in CEM Vbl-100 cell line treated with **AL10c** and **AL23b** in combination with vinblastine.

Synthetic ecdysteroids compounds synergize with cis-platin and vincristine in Medulloblastoma cell lines

In order to assess if these new synthetic ecdysteroids could increase the efficacy of standard medulloblastoma chemotherapy, we tested if they can be used in combination with the most commonly used chemotherapeutics. To this end, two

different medulloblastoma cell lines, DAOY and D425 were treated with **AL10C** and **AL23b** in combination with chemotherapeutic agents (cis-platin and vincristine) used normally to treat pediatric medulloblastoma patients. More specifically, as shown in **Fig.10a** in DAOY cell line, **AL10c** and **AL23b** synergize with chemotherapeutic drugs, causing a synergistic increase of their cytotoxicity; **AL10c** and **AL23b** were combined with different drugs at fixed molar combination ratio, and cell viability analyzed by MTT assay after 72 h.

As demonstrated by the values of combination index (CI) according to Chou and Talalay (20, 21) (**Fig.10b),** ED50 in DAOY cell line, **AL10c** and **AL23b** in combination with chemotherapeutic drugs acted in a synergistic fashion (CI<1).

Our results show that in general, the pharmacological inhibition of P-gp activity caused by **AL10c** and **AL23b**, can significantly increase the cell death effects provoked by the treatment with the conventional chemotherapeutic agents used alone.

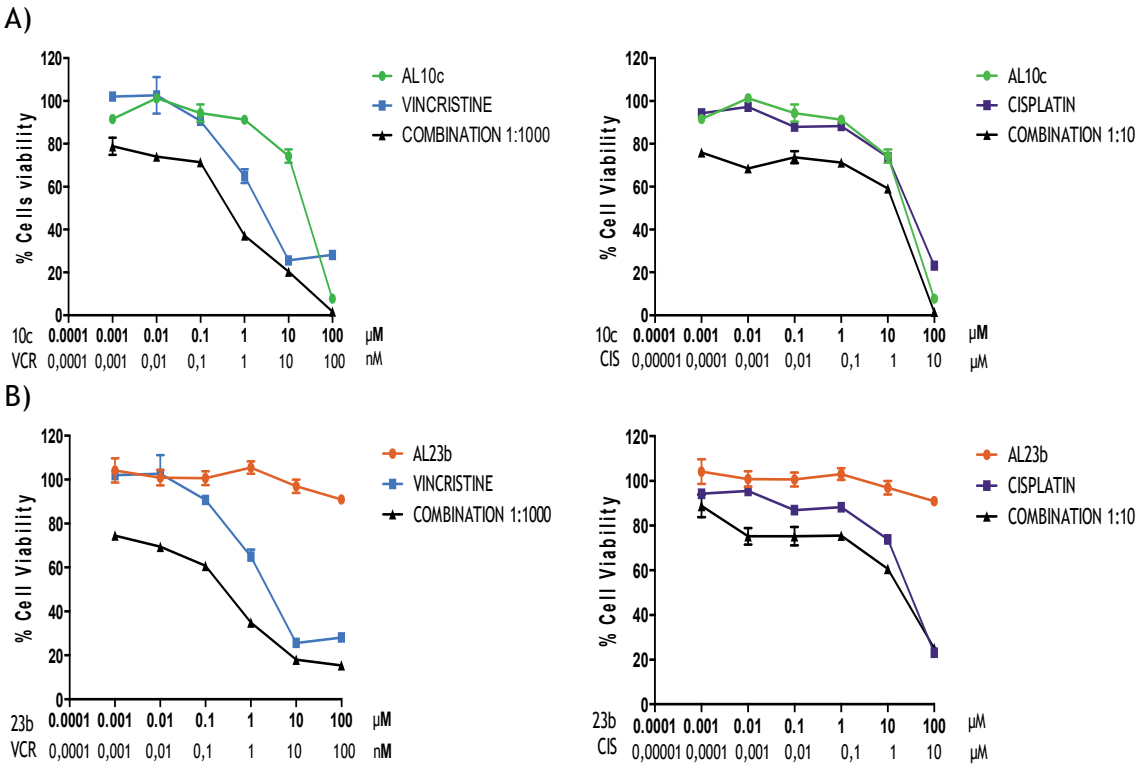

Fig. 10a Effect of AL10c and AL23b treatment in combination with different chemotherapic drugs in DAOY cells. A), B) Cells were treated at the indicated concentration and at fixed combination ratio; **AL10c** and **AL23b** (0.001-100 µM), vincristine (0.001-100 nM) and cis-platin (0.0001-10 µM); viability was assessed by MTT test after 72h of incubation. Data are expressed as mean ± SEM of three independent experiments.

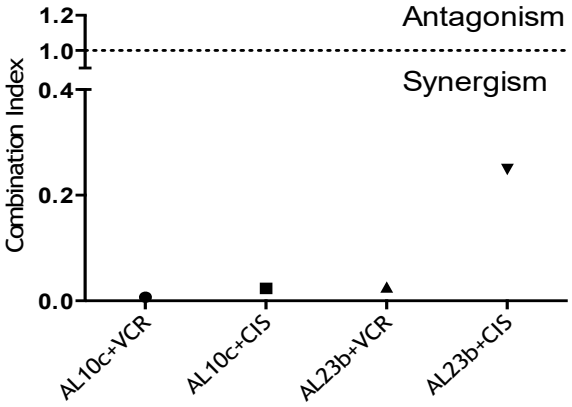

Fig. 10b Effect of AL10c and AL23b treatment in combination with different chemotherapic drugs in DAOY cells. Combination index values (CI) in DAOY cell line treated with **AL10c** and **AL23b** in combination with Vincristine and Cis-platin.

For what concern D425 cell line, **AL10c** and **AL23b** were combined with different drugs at fixed molar combination ratio, but in this case, AL10c synergizes with vincristine and cis-platin, causing a synergistic increase of their cytotoxicity while **AL23b** sinergyzes only with vincristine but not with cis-platin **(Fig.10d Supp. Materials);** as demonstrated by the values of combination index (CI) according to Chou and Talalay (20, 21) (**Fig.10e)** in D425 cell line, **AL10c** and **AL23b** in combination with chemotherapeutic drugs acted in a synergistic fashion (CI<1).

Effect of AL10c and AL23b on the side population subset in Medulloblastoma cell lines

We investigated the presence of side population in DAOY cell line. Following staining with Hoechst 33342, a SP was identified as a distinct tail extending from the main population with the characteristic low fluorescent profile in dual wavelength analysis.

We treated DAOY cell line with **AL10c** and **AL23b** 10 μM for 2 h and with Verapamil 50 μM, as an SP cell control in the Hoechst efflux, which blocks transporters of the ABC family and abrogates the ability of cells to efflux the Hoecst dye.

As shown in **Fig.11** SP disappears in those cells treated with **AL10c** and **AL23b** respect to control and Verapamil.

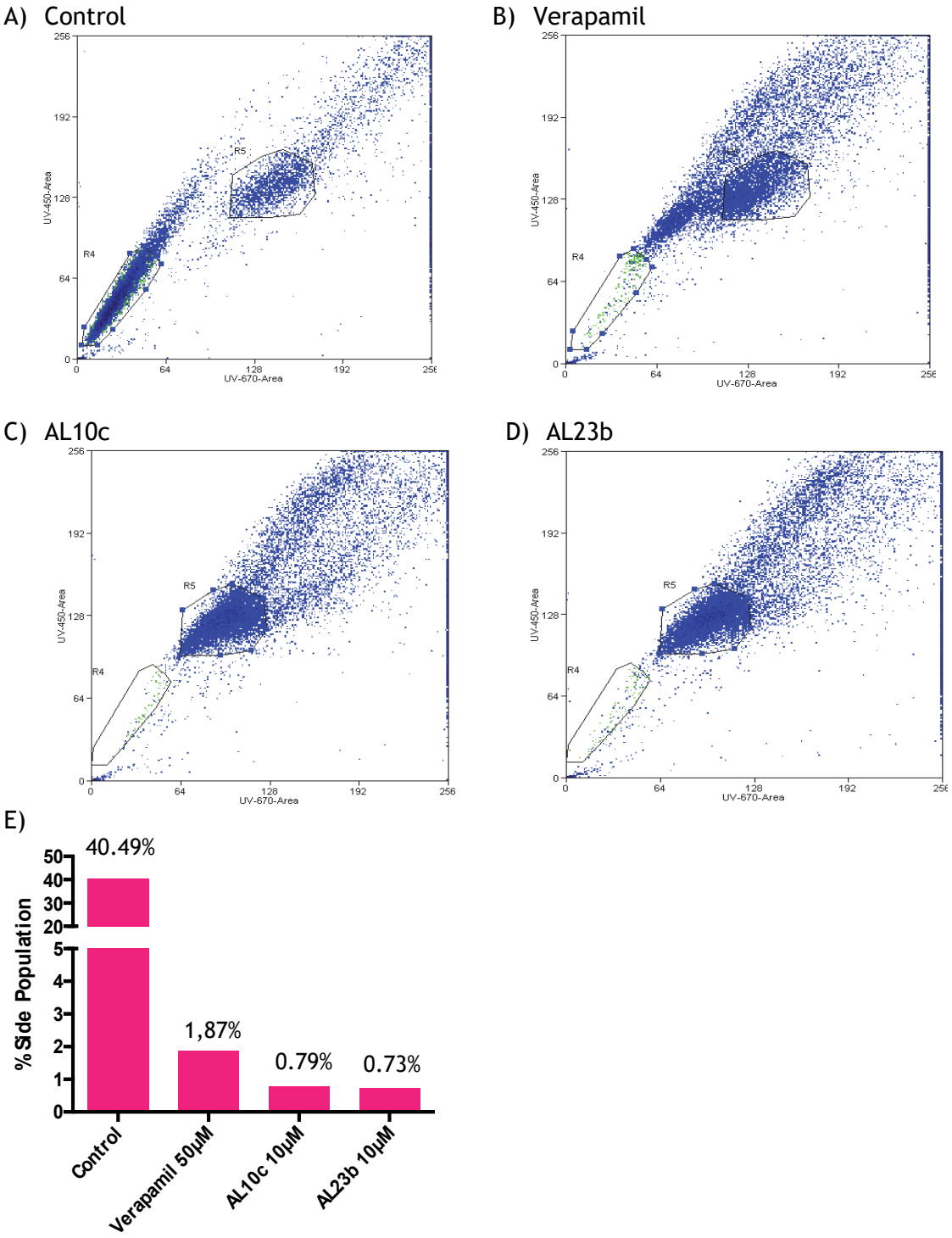

Fig. 11 Effect of AL10c and AL23b on the SP subset in DAOY cell line. A), B), C), D) The diagrams show representative analysis of the SP subpopulation in DAOY cell line treated with **AL10c** and **AL23b** 10 μM and then compared with verapamil 50 μM treated and untreated cells. Analysis was carried out after 2 h of treatment. E) Hystogram shows the percentage of side population in DAOY cell line.

2.5 Discussion

Drug resistance is a significant factor that limits the effectiveness of current chemotherapeutic drugs. In an attempt to overcome the resistance that can develop due to P-gp overexpression, P-gp inhibitors have been developed. Numerous clinical trials evaluating the effects of verapamil or valspodar in combination with chemotherapeutic agents such as doxorubicin, vincristine, dexamethasone, cyclophosphamide, paclitaxel have shown that patients given concurrent administration of P-gp inhibitors with chemotherapeutic agents have an increased toxicity and show modest or no increase in survival These results provide insight into an important limitation of P-gp inhibitors and suggest the importance of considering the development of new P-gp inhibitors.

In this study, we evaluated how new synthetic P-gp inhibitors reverse multidrug resistance in induced resistant leukemia cell line and in medulloblastoma.

In resistant leukemia cell lines CEM Vbl-100 and LOVO/DOXO both **AL10c** and **AL23b** were able to increase two P-g substrates, that are efficiently pumped out of tumour cells where P-gp is highly expressed: -rhodamine 123 and -doxorubicine respectively. Direct comparison with Verapamil, known to fully inhibit P-gp activity, demonstrated that **AL10c** and **AL23b**, at lower concentration, are more potent respect to Verapamil. Importantly the two drugs have shown lower toxicity in wild cells suggesting a preferential effect toward MDR cells.

In addition, these studies clearly indicated that reversal of multidrug resistance by **AL10c** and **AL23b** was through selective inhibition of P-gp function: in contrast to the modulatory activity in the resistant cell lines, **AL10c** and **AL23b** had no significant effect on cytotoxic drug activity in non P-gp-expressing parental cell lines (CEM and LOVO).

To understand the mechanisms of P-gp inhibition by **AL10c** and **AL23b**, P-gp ATPase activity and P-gp mRNA expression were further studied. Since the efflux function of ABC transporters is ATP-dependent, measuring ATPase activity is another approach to study the inhibition of ABC transporters. We tested **AL10c** and **AL23b** in comparison with Verapamil, used as positive control; at 1 and 10 μM our compounds showed a significant inhibitory effect on P-gp ATPase activity respect to Verapamile 200 μM. RT-PCR analysis revealed that relative ABCB1 mRNA expression was down-regulated by **AL10c** and **AL23b** after 24h treatment of resistant cell line CEM Vbl-100.

AL10c and **AL23b** were found to apparently reverse multidrug resistance in P-gp

overexpressing leukemia cells. We determined the multidrug resistance reversing of CEM Vbl-100 and LOVO/DOXO cell lines. It was found that **AL10c** and **AL23b** markedly increased the sensitivity of CEM Vbl-100 cell line to vinblastine and of LOVO/DOXO cell line to doxorubicine.

In conclusion, the first part of this study evaluated the inhibition of P-gp function in resistant leukemia cells by novel synthetic ecdysteroids

The primary treatment of Medulloblastoma consists of maximal tumour resection followed by craniospinal radiotherapy and chemotherapy. Several chemotherapeutic agents, including vincristine and cis-platin have been used against aggressive neoplasms. However, cancer cells usually develop resistance to conventional chemoterapeutics and radiation, which limits the therapeutic effectiveness of these drugs (23). In some cases, chemoresistance may result in the survival of a population of tumour cells that subsequently leads to recurrence following treatment (24). This may be particularly true for tumours that are composed of a heterogeneous population of cells such as Medulloblastoma. Within this population of cells there is side population that exhibits chemoresistance related to the ABC transporter.

In this study we clearly demonstrate that our new synthetic ecdysteroids synergistically reverse resistance to cis-platin and vincristine; in addition, they dramatically decrease the percentage of side population respect to the untreated cells and Verapamil used at higher concentration (50 μM) respect to our derivatives.

In conclusion, these new compounds may be considered as promising candidates as P-gp inhibitors and they could be used as an adjuvant therapy together with the current chemotherapies in cancer treatment, in particular to those cancers with P-gp-mediated multidrug resistance.

2.6 *Supplementary materials*

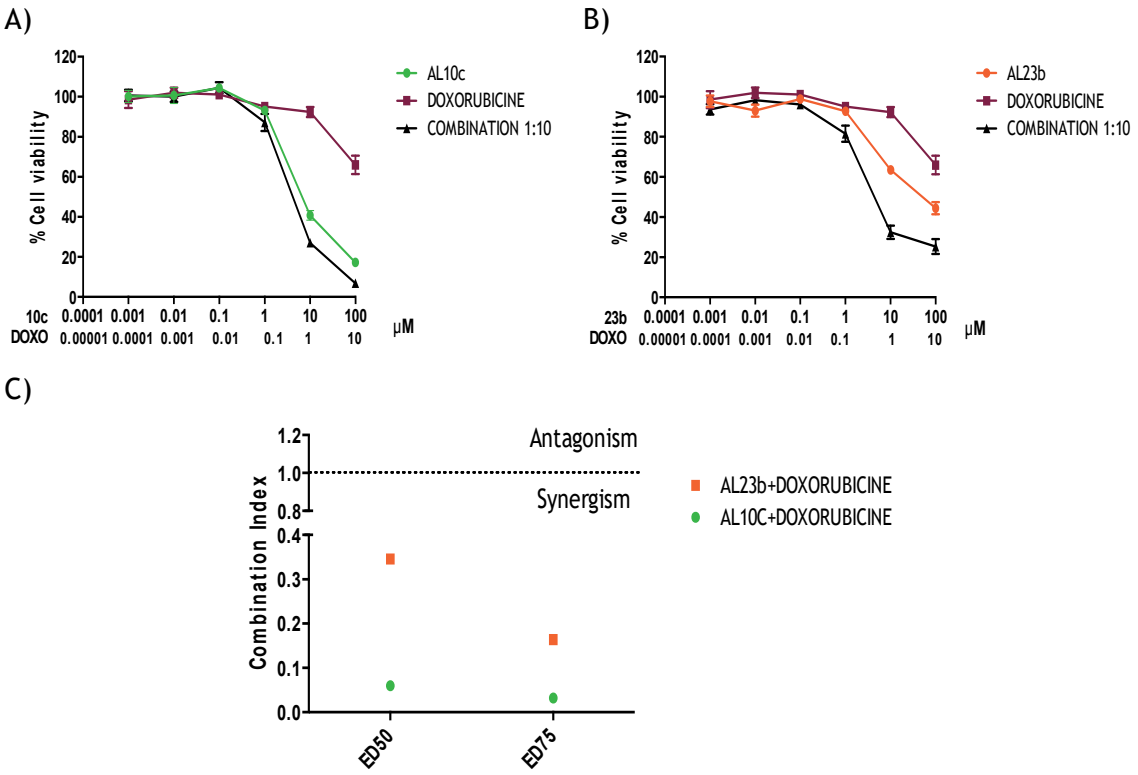

Fig. 9d Effect of AL10c and AL23b treatment in combination with Doxorubicine in LOVO/DOXO cell line. A), B) AL10c and AL23b were added in a concentration range of 0.001-100 µM and Doxorubicine in a molar range of 0.0001-10 µM. Cell viability was assessed by MTT test after 72 hours of incubation. Data are expressed as mean ± SEM of three independent experiments. C) Combination index values (CI) in LOVO/DOXO cell line treated with AL10c and AL23b in combination with Doxorubicine. CI is <1 indicating a synergistic effect between our synthetic ecdysteroids and Doxorubicine.

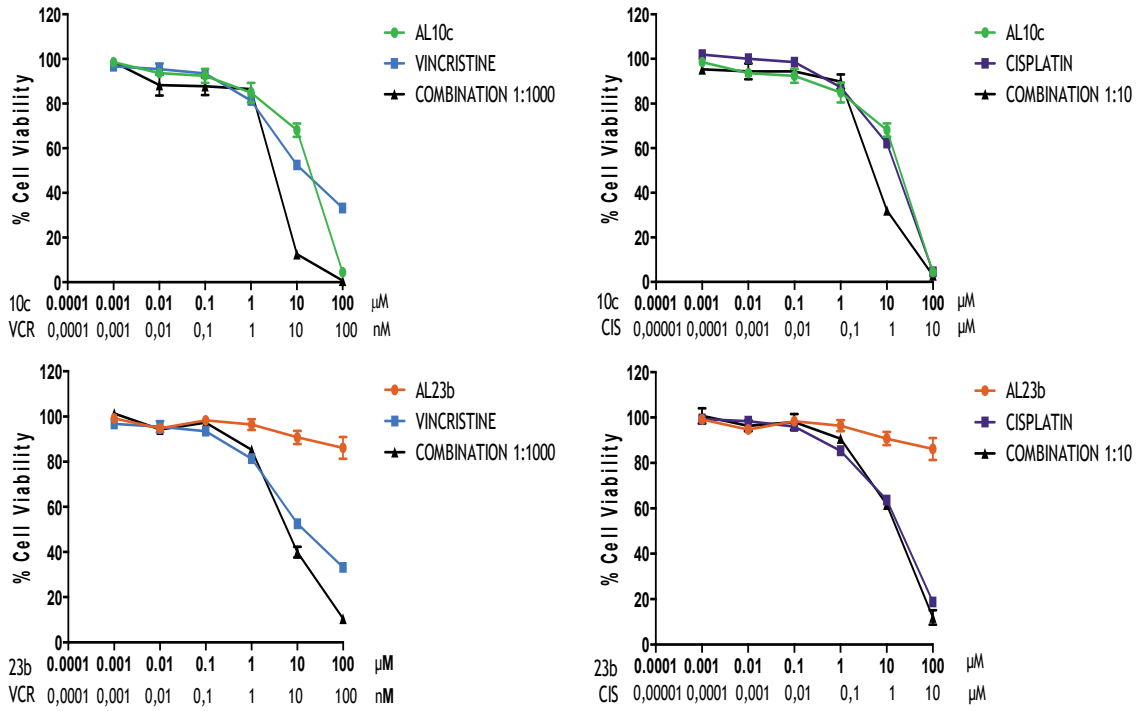

Fig. 10d Effect of AL10c and AL23b treatment in combination with different chemotherapic drugs in D425 cells. Cells were treated at the indicated concentration and at fixed combination ratio; AL10c and AL23b (0.001-100 µM), vincristine (0.001-100 nM) and cis-platin (0.0001-10 µM); viability was assessed by MTT test after 72h of incubation. Data are expressed as mean ± SEM of three independent experiments.

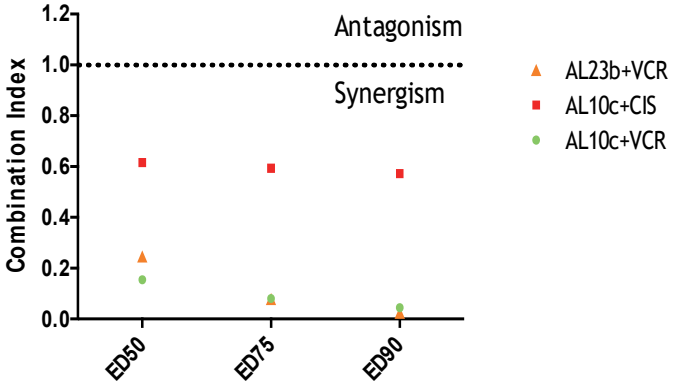

Fig. 10e Combination index values (CI) in D425 cell line treated with AL10c and AL23b in combination with Vincristine and Cis-platin. CI is <1 indicating a synergistic effect between our synthetic ecdysteroids and chemoterapeutic drugs.

2.7 References

1) Ozben T. (2006) Mechanisms and strategies to overcome multiple drug resistance in cancer *FEBS Lett* 580: 2903-9
2) Lopes-Rodrigues V., Di Luca A., Mleczko J., Meleady P., Henry M., Pesic M., Cabrera D., van Liempd S., Lima R.T., O'Connor R., Falcon-Perez J.M., Vasconcelos M.H. (2017) Identification of the metabolic alterations associated with the multidrug resistant phenotype in cancer and their intercellular transfer mediated by extracellular vesicles *Sci Rep* 7: 44541
3) Gottesman M.M., Fojo T., Bates S.E. (2002) .Multidrug resistance in cancer: role of ATP–dependent transporters *Nat Rev Cancer* 2: 48-58
4) Lesmaa G., Luraghia A., Rainoldia G., Mattiuzzo E., Bortolozzi R., Viola G., Silvani A. (2016) Multicomponent Approach to Bioactive Peptide–Ecdysteroid Conjugates: Creating Diversity at C6 by Means of the Ugi Reaction *Synthesis* 48: 3907-3916
5) Clarke M.F., Dick J.E., Dirks P.B., Eaves C.J., Jamieson C.H., Jones D.L., Visvader J., Weissman I.L., Wahl G.M. (2006) Cancer Stem Cells—Perspectives on Current Status and Future Directions: AACR Workshop on Cancer Stem Cells *Cancer Res* 6: 9339-44
6) Fletcher JI1, Haber M, Henderson MJ, Norris MD. (2010) ABC transporters in cancer: more than just drug efflux pumps *Nat Rev Cancer* 10:147-56
7) Wu C.P., Calcagno A.M., Ambudkar S.V. (2008) Reversal of ABC drug transporter-mediated multidrug resistance in cancer cells: Evaluation of current strategies *Curr Mol Pharmacol* 1: 93-105
8) Kathawala R.J., Gupta P., Ashby C.R. Jr, Chen Z.S. (2015) The modulation of ABC transporter-mediated multidrug resistance in cancer: A review of the past decade *Drug Resist Updat* 18: 1-17
9) Holohan C., Van Schaeybroeck S., Longley D.B., Johnston P.G. (2013) Cancer drug resistance: an evolving paradigm *Nat Rev Cancer* 13: 714-26
10) Gajjar A.J., Robinson G.W. (2014) Medulloblastoma—translating discoveries from the bench to the bedside *Nat Rev Clin Oncol* 11: 714-22
11) Huang S.Y., Yang J.Y. (2015) Targeting the Hedgehog Pathway in Pediatric Medulloblastoma *Cancers (Basel)* 7: 2110-23
12) Eberhart C. G. (2012) Three Down and One To Go: Modeling Medulloblastoma Subgroups *Cancer Cell* 21: 137–138

13) Dean M., Fojo T., Bates S. (2005) Tumour stem cells and drug resistance *Nat Rev Cancer* 5: 275-84

14) Bleau A.M., Hambardzumyan D., Ozawa T, Fomchenko E.I., Huse J.T., Brennan C.W., Holland E.C. (2009) PTEN/PI3K/Akt Pathway Regulates the Side Population Phenotype and ABCG2 Activity in Glioma Tumour Stem-like Cells *Cell Stem Cell* 4: 226-35

15) Hirschmann-Jax C., Foster A.E., Wulf G.G., Nuchtern J.G., Jax T.W., Gobel U, Goodell M.A., Brenner M.K (2004) A distinct "side population" of cells with high drug efflux capacity in human tumour cells *Proc Natl Acad Sci USA* 101: 14228-33

16) Wu C.P., Zhou L., Xie M., Du H.D., Tian J., Sun S,. Li J.Y. (2013) Identification of Cancer Stem-Like Side Population Cells in Purified Primary Cultured Human Laryngeal Squamous Cell Carcinoma Epithelia *PLoS One* 8: 65750

17) Löscher W., Potschka H. (2005) Drug resistance in brain diseases and the role of drug efflux transporters Nat Rev Neurosci 6: 591-602

18) Moserle L, Indraccolo S, Ghisi M, Frasson C, Fortunato E, Canevari S, Miotti S, Tosello V, Zamarchi R, Corradin A, Minuzzo S, Rossi E, Basso G, Amadori A. (2008) The side population of ovarian cancer cells is a primary target of IFN-alpha antitumour effects *Cancer Res* 68:5658-68

19) Martins A., Tóth N., Ványolós A., Béni Z., Zupkó I., Molnár J., Báthori M., Hunyadi A. (2012) Significant Activity of Ecdysteroids on the Resistance to Doxorubicin in Mammalian Cancer Cells Expressing the Human ABCB1 Transporter *J Med Chem* 55: 5034-43

20) Anju Singh, Hailong Wu, Ping Zhang, Christine Happel, Jinfang Ma, and Shyam Biswal (2010) Expression of ABCG2 (BCRP), a Marker of Stem Cells, is Regulated by Nrf2 in Cancer Cells That Confers Side Population and chemoresistance phenotype *Mol cancer Ther* 9:2365-2376

21) Chou T. (2006) Theoretical basis, experimental design, and computerized simulation of synergism and antagonism in drug combination studies *Pharmacol Rev* 58: 621-681

22) Chou T-C.(2010) Drug combination studies and their synergy quantification using the Chou-Talalay method *Cancer Res* 70: 440–446

23) Chen S-M., Li Y-Y., Tu C-H., Salazar N., Tseng Y-Y., Huang S-F., *et al.* (2016) Blockade of Inhibitors of Apoptosis Proteins in Combination with Conventional Chemotherapy Leads to Synergistic Antitumour Activity in Medulloblastoma and Cancer Stem-Like Cells *PLoS ONE* 11
24) Abdullah L.N. and Chow K-H E. (2013) Mechanisms of chemoresistance in cancer stem cells *Clinical and Translational Medicine* 2: 3

CHAPTER 3

ANTITUBULINIC AGENTS

3.1 General introduction

Compared to the normal counterpart, cancer cells are characterized by the cell cycle deregulation that leads to their hyperproliferative pattern. Tumour cells accumulate mutations that result in unscheduled proliferation, as a consequence of unresponsiveness to growth inhibitory signals, self-sufficiency in growth factors or both. Therefore, several antitumoural strategies have been proposed for targeting the cell division cycle in cancer by targeting tubulin polymerization (1).
There has been in recent years an intense effort directed at the discovery and development of novel small molecules, many of which are natural products, able to interfer with tubulin polymerization because of their anti-cancer potential (2).

3.1.1 Tubulin structure

Microtubules are a dynamic cellular compartment in both neoplastic and normal cells. The microtubule system of eukaryotic cells plays important roles in regulating cell architecture and has an essential role in cell division, since microtubules are a key component of the mitotic spindle (3). This dynamicity is characterized by the continuous turnover of αβ-tubulin heterodimers in the polymeric microtubules. Because of their key roles in cell structure and cell division, they are involved in a variety of fundamental cellular functions, such as cell formation, maintenance of cell shape, regulation of motility, cell signaling, secretion, intracellular transport and mitotic spindle elongation for the correct chromosome segregation (4).
Microtubules are built from subunits, each of which is itself a dimer composed by two very similar globular proteins called α-tubulin and ß-tubulin (5). The tubulin dimers stack together by non-covalent bonding to form the wall of the hollow cylindrical microtubules. This tube like structure is made of 13 parallel protofilaments, which are linear chains of tubulin dimers with α and ß-tubulin alternating along its length.
Each protofilament has a structural polarity, with α-tubulin exposed at one end and ß-tubulin at the other, and this polarity is the same for all protofilaments, giving a structural polarity to the microtubule as a whole. One end of the microtubule, thought to be the ß-tubulin end, is called plus end, and the other, the α tubulin end is called minus end.
The microtubule system has a dynamic behavior, known as “dynamic instability”, in which microtubules alternate between period of growing and shrinking through the addition or removal of tubulin monomers. This process is mediated by hydrolysis of

GTP: ß-tubulin has binding site for GTP and microtubule stability depend on the rate of GTP/GDP-bound tubulin. If new GTP molecules are added more rapidly than GTP is hydrolyzed, the microtubules retain a GTP-cap and growth continues. However, if the rate of polymerization is slow, GTP is hydrolyzed to GDP, GDP-bound tubulin dissociates resulting in a rapid depolymerization of microtubules **(Fig.1).** Dynamic instability is one of the key events of the cell cycle: during interphase microtubules turnover is slow but becomes rapid at the onset of mitosis with the disassembly of microtubules network, followed by the formation of a new network of spindle microtubules, that can turover 4-100 times more rapidly than interphase microtubules (6).

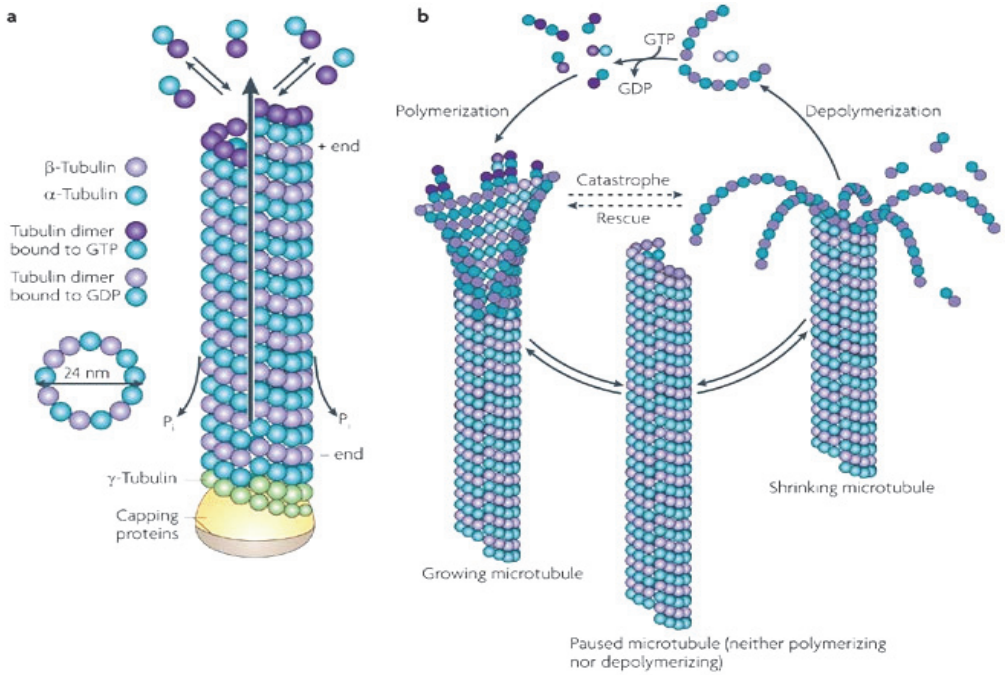

Fig. 1 The microtubule structure is composed by α and β-tubulin heterodimers (7).

The regulation of microtubules dynamics, temporal and spatial organization is a tightly regulated mechanisms to ensure the correct spindle formation and segregation of chromosomes during cell division. The main regulators of microtubules dynamics are the microtubule-sequestring protein stathmin (STMN) and microtubules-associated proteins (MAPs). Stathmin is a cytosolic phosphoprotein that regulates mitotic spindle by binding to tubulin heterodimers and inducing microtubule destabilization, while MAPs proteins can bind and stablize microtubules against depolymerization (6).

3.1.2 Tubulin targeting agents

Microtubules are extremely important in the process of mitosis, during which the duplicated chromosomes of a cell are separated into two identical sets before cleavage of the cell into two daughter cells. Their importance in mitosis and cell division makes microtubules an important target for anticancer drugs. In the context of cancer, the tubulin family of proteins is recognized as the target of the tubulin-binding chemotherapeutics, which suppress the dynamics of the mitotic spindle to cause mitotic arrest and cell death.

Microtubules may function to coordinate stress responses across the cell, resulting in enhanced cell survival in the harsh tumour microenvironment, resistance to chemotherapy treatment, and the development of more aggressive disease (8).

The tubulin-binding agents (TBA) are a very successful class of cancer drugs with therapeutic benefits in both hematopoietic and solid tumours, A large number of natural agents and/or their analogues bind to soluble tubulin and/or directly to tubulin in the microtubules. Most of these compounds are antimitotic agents that inhibit cell proliferation by acting on the polymerization dynamics of spindles, which are essential to proper spindle function of microtubules (9). Disruption of microtubule blocks cell cycle progression in many cells at the transition from prometaphase/metaphase to anaphase; this phenomenon is called the mitotic checkpoint. Cell cycle arrest at the mitotic checkpoint is activated by a number of defects in microtubule-kinetochore interactions including microtubule depolymerization, stabilization of microtubule dynamics, absence of tension on kinetochore microtubules, and the presence of kinetochores that are not attached to microtubules (10). There are many chemically diverse compounds that bind to the tubulin–microtubule system. They are broadly classified into two groups: one group called microtubule-stabilizing that stimulates microtubule polymerization (such as taxanes and epothilones) and one group knonwn as microtubule-destabilizing that inhibits microtubule polymerization at high concentrations (such as vincristine, vinblastine, vinorelbine, colchicine, combretastatins) drugs **(Fig.2)** (11).

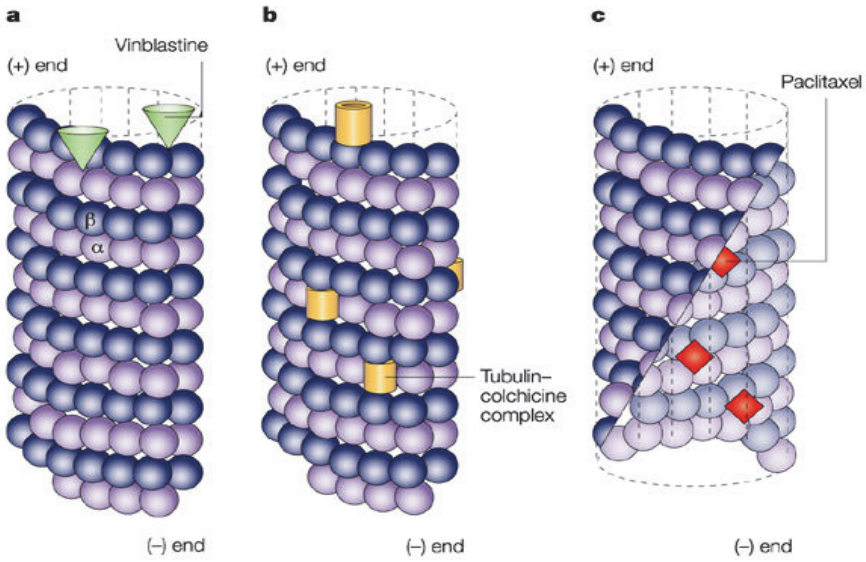

Fig. 2 Antimitotic drugs binds to microtubule at diverse sites. A) Vinblastine binds at the microtubule plus end suffice to suppress microtubule dynamics; b) colchicine forms complexes with tubulin dimers and copolymerizes into the microtubule lattice, suppressing microtubule dynamics; c) paclitaxel binds along the interior surface of the microtubule, suppressing its dynamics (12).

The mechanisms that determine sensitivity or resistance to anti-mitotic agents that target tubulin are not well understood. Studies addressing how the various cellular events associated with cell fate following TBA treatment are influenced by tubulin isotype composition might reveal new information on drug sensitivity. There are multiple α- and ß-tubulin isotypes that are encoded by different genes, located on different chromosomes and that have tissue and cell-specific expression patterns. The structure of tubulin has been highly conserved throughout evolution, and tubulin isotypes share a high degree of aminoacid homology but are distinguished by their unique carboxy-terminal tails (the last 20–27 amino acids). These tubulin isotypes can undergo post-translational modifications, which can alter the interaction of microtubules with microtubule associated proteins and change their function (13).
Understanding the molecular mechanisms that mediate resistance to tubulin-binding agents will be vital to improve the efficacy of these agents.

3.1.3 Citotoxic effect of tubulin binding agents

Both classes of antimitotic drugs suppress microtubule dynamics causing alteration in the spindle organization, with a delay or a block at the metaphase-anaphase transition during mitosis with consequent G2-M cell cycle arrest. Furthermore,

activation of spindle assembly checkpoint in G2 phase and prolonged mitotic arrest provoke apoptosis induction (14). The apoptosis is a programmed cell death characterized by chromatin condensation, DNA fragmentation and activation of caspases. The apoptotic process could be triggered by two pathways called extrinsic and intrinsic pathway. Several works describe that tubulin binding agents induce apoptosis mainly through the intrinsic pathway activation, characterized by the alteration of mitochondrial parameters (such as alteration of membrane potential and ROS production). However, how cell death induction correlates with microtubule destabilization and mitotic arrest still remains unclear and controversial.

The intrinsic pathway of apoptosis is mainly initiated by the release of cytochrome *c* from the mitochondrion. Upon release into the cytoplasm, cytochrome *c* associates with dATP, procaspase-9, and the adaptor protein APAF-1, leading to the sequential activation of caspase-9 and effector caspases (15).

The release of apoptosis-inducing proteins from the mitochondria is regulated by pro- and antiapoptotic members of the Bcl-2 family. Antiapoptotic members (Bcl-2, Bcl-XL, and Mcl-1) associate with the mitochondrial outer membrane via their carboxy termini, exposing to the cytoplasm a hydrophobic binding pocket composed of Bcl-2 homology (BH) domains 1, 2, and 3, that is crucial for their activity. Perturbations of normal physiologic processes in specific cellular compartments lead to the activation of BH3-only proapoptotic family members (such as Bad, Bim, Bid, Puma, Noxa, and others). This leads to the altered conformation of the outer-membrane proteins Bax and Bak, which then oligomerize to form pores in the mitochondrial outer membrane resulting in cytochrome *c* release. Therefore, the relative levels of expression of antiapoptotic Bcl-2 family members compared to the levels of proapoptotic BH3-only proteins at the mitochondrial membrane determines the activation state of the intrinsic pathway. It has been demonstrated that many microtubules binding agents can induce phosphorylation in serine residues of Bcl2 antiapoptotic proteins, in cell that are blocked in G2-M phase, leading to loss prosurvival function and to destabilization of mitochondrial potential. Moreover, Bcl2 phosphorylation decreases its binding to the proapoptotic Bax protein, resulting in an increase of free Bax and apoptosis (16).

3.2 Aim of the project

The microtubule system plays an essential role on a variety of cellular processes, such as on maintaining of cell shape, intracellular transport and more importantly on cell cycle division. Therefore, over the years several antitumoural compounds have been developed for targeting tubulin polymerization and thus cell cycle progression in cancer.

Among the synthetic inhibitors of tubulin polymerization, we previously described the synthesis and biological characterization of two series of compounds based on the 2-alkoxycarbonyl-3-(3',4',5'-trimethoxyanilino)benzo[*b*]thiophene and thieno[2,3-*b*]pyridine molecular skeletons (compounds with general structure 2 and 3, respectively) that showed strong antiproliferative activity against a panel of cell lines and act as inhibitors of microtubule polymerization by interfering with the colchicine site of tubulin. To investigate the possible binding mode for this series of compounds, we performed a series of molecular docking simulations in the colchicine site.

Based on these observations, a new series of derivatives with general formulae 4 was designed with the aim to improve their antimitotic activity.

2-ALKOXYCARBONYL-3-ARYLAMINO-5-SUBSTITUTED THIOPHENES AS A NOVEL CLASS OF ANTIMICROTUBULE AGENTS. DESIGN, SYNTHESIS, CELL GROWTH AND TUBULIN POLYMERIZATION INHIBITION ACTIVITY

Romeo Romagnoli, Maria Kimatrai Salvador, Santiago Schiaffino Ortega, Pier Giovanni Baraldi, Paola Oliva, Stefania Baraldi, Luisa Carlota Lopez-Cara, Andrea Brancale, Salvatore Ferla, Ernest Hamel, Jan Balzarini, Sandra Liekens, **Elena Mattiuzzo**, Giuseppe Basso and Giampietro Viola

Submitted to: European Journal of Medicinal Chemistry

3.3 Abstract

Microtubules are recognized as crucial components of the mitotic spindle during cell division, and, for this reason, the microtubule system is an attractive target for the development of anticancer agents.

Continuing our search strategy for novel tubulin targeting-compounds, a new series of 2-alkoxycarbonyl-3-(3',4',5'-trimethoxyanilino)-5-aryl/heteroaryl thiophene derivatives was designed, synthesized and demonstrated to act as tubulin polymerization inhibitors at the colchicine site. A structure-activity relationship study on the phenyl at the 5-position of the thiophene ring was performed by introducing a variety of substituents containing electron-releasing and electron-withdrawing groups, with the 2-alkoxycarbonyl-3-(3',4',5'-trimethoxyanilino) thiophene scaffold being the minimum structural requirement for activity.

Of the tested compounds, derivatives **4a**, **4c**, **4i** and **4k**, possessed the highest overall potency and displayed high antiproliferative activities at submicromolar concentrations, with IC_{50} values ranging from 0.13 to 0.84 μM against four different cancer cell lines. Three agents (**4a**, **4c** and **4i**) in the present series had similar effects, and these were comparable to those of reference compound combretastatin A-4 (CA-4), especially as inhibitors of tubulin assembly. The antitubulin effects correlated with the cytostatic activities and indicate that these compounds inhibit cell growth through inhibition of tubulin polymerization by binding at the colchicine site. Compound **4c**, containing the thien-2'-yl ring at the 5-position of the 2-methoxycarbonyl-3-(3',4',5'-trimethoxyanilino)thiophene scaffold, exhibited substantial antiproliferative activity with a mean IC_{50} value of 140 nM, inhibited tubulin polymerization with an IC_{50} value of 1,2 μM, similar to that of CA-4 (IC_{50}: 1,1 μM), and induced apoptosis in HeLa cells.

***Keywords*:** microtubule, tubulin polymerization inhibitors, antiproliferative agents, colchicine site, structure-activity relationship.

3.4 Materials and methods

Cell culture

All cell lines were purchased from the American Type Culture Collection. Murine leukemia L1210, murine mammary carcinoma FM3A, human T-lymphocyte leukemia CEM were cultured in RPMI 1640 (Life Technologies, Italy) and human cervix carcinoma (HeLa) was cultured in DMEM (Life Technologies, Italy). All mediums were supplemented with 10% fetal bovine serum (FBS), glutamine (2 mM; Life Technologies, Italy), penicillin (100 U/ml; Life Technologies, Italy) and streptomycin (100 µg/ml; Life Technologies, Italy), and maintained at 37°C in a humidified atmosphere with 5% CO_2.

Peripheral blood lymphocytes (PBL) from healthy donors were obtained by separation on Lymphoprep (Fresenius KABI Norge AS) gradient. After extensive washing, cells were resuspended (1.0×10^6 cells/mL) in RPMI-1640 with 10% fetal bovine serum and incubated overnight. For cytotoxicity evaluations in proliferating PBL cultures, non-adherent cells were resuspended at 5×10^5 cells/mL in growth medium, containing 2.5 µg/mL PHA (Irvine Scientific), whereas for cytotoxicity evaluations in resting PBL cultures, non-adherent cells were resuspended (5×10^5 cells/mL). Different concentrations of the test compounds were added, and viability was determined 72 h later by the MTT test.

MTT assay

Proliferation was assessed by MTT ((3-(4,5-dimethylthiazol-2-yl)-2,5-diphenyl tetrazoliuM bromide) assay after treatment. Cells were suspended at 300,000-500,000 cells/mL and plated in triplicate in a 96-well plate. After incubation at 37°C for two (L1210 and FM3A), three (CEM) or 4 days (HeLa), 10 µl of MTT was added (Sigma-Aldrich, St Louis, MO, USA) for 4 h. Absorbance was measured at 560 nm using Victor3TM 1420 Multilabel Counter (PerkinElmer, Waltham, MA, USA). The growth inhibition 50 (GI50=compound concentration required to inhibit cell proliferation by 50%) was calculated by plotting the data as a logarithmic function of (x) when viability was 50%. DMSO-treated cells viability was set to 100%.

Effects on tubulin polymerization and on colchicine binding to tubulin

To evaluate the effect of the compounds on tubulin assembly in vitro (17), varying concentrations of compounds were preincubated with 10 µM bovine brain tubulin in

0.8 M monosodium glutamate (pH adjusted to 6.6 with HCl in a 2 M stock solution) at 30˚C and then cooled to 0˚C. After addition of 0.4 mM GTP, the mixtures were transferred to 0°C cuvettes in a recording spectrophotometer and warmed to 30°C. Tubulin assembly was followed turbidimetrically at 350 nm. The IC_{50} was defined as the compound concentration that inhibited the extent of assembly by 50% after a 20 min incubation. The capacity of the test compounds to inhibit colchicine binding to tubulin was measured as described (18). The reaction mixtures contained 1 μM tubulin, 5 μM [^{3}H]colchicine and 5 μM test compound.

Molecular modeling

All molecular modeling studies were performed on a MacPro dual 2.66 GHz Xeon running Ubuntu 14.04. The tubulin structure was downloaded from the PDB data bank (http://www.rcsb.org/; PDB code 1SA0) (19). Hydrogen atoms were added to the protein, using the Protonate 3D routine of the Molecular Operating Environment (MOE) (Molecular Operating Environment (MOE 2015.10); Chemical Computing Group, Inc; Montreal, Quebec, Canada, 2015; http://www.chemcomp.com.).Ligand structures were built with MOE and minimized using the MMFF94x force field until a RMSD gradient of 0.05 kcal mol^{-1} $Å^{-1}$ was reached. The docking simulations were performed using PLANTS.

Annexin V/Pi assay

Surface exposure of phosphatidylserine on apoptotic cells was measured by flow cytometry with a Coulter Cytomics FC500 (Beckman Coulter) by adding Annexin V conjugated to fluorescein isothiocyanate (FITC) to cells according to the manufacturer's instructions (Annexin V Fluos, Roche Diagnostic). Simultaneously, the cells were stained with PI. Excitation was set at 488 nm, and the emission filters were at 525 and 585 nm, respectively, for FITC and PI.

Flow cytometric analysis of cell cycle distribution

Cell cycle distribution was measured by flow cytometry with a Coulter Cytomics FC500 (Beckman Coulter) by using propidium iodide in propidium iodide/RNase A staining. 5×10^5 HeLa cells were treated with different concentrations of the test compounds for 24 h. After the incubation period, cells were harvested, washed with phosphate-buffered saline solution (PBS) and fixed in 70% EtOH overnight at 4°C. After fixation, cells were washed twice with PBS before resuspension in 0.1% Triton

X-100/propidium iodide/RNase A solution (1mg/mL of PI and 4mg/mL RNase-A). Cells were incubated at room temperature in the dark light for 30 min and then processed for analysis. Samples were analyzed on a Cytomic FC500 flow cytometer (Beckman Coulter). DNA histograms were analyzed using MultiCycle for Windows (Phoenix Flow Systems).

Analysis of mitochondrial potential and reactive oxygen species (ROS)

The mitochondrial membrane potential was measured with the lipophilic cation JC-1 (Molecular Probes, Eugene, OR, USA), while the production of ROS was followed by flow cytometry using the fluorescent dye H_2DCFDA (Molecular Probes), as previously described (20).

Immunoblot analysis

HeLa cells were incubated in the presence of **4c** and, after different times, were collected, centrifuged, and washed two times with ice-cold phosphate buffered saline (PBS). The pellet was then resuspended in lysis buffer. After the cells were lysed on ice for 30 min, lysates were centrifuged at 15,000 x g at 4°C for 10 min. The protein concentration in the supernatant was determined using the BCA protein assay reagents (Pierce, Italy). Equal amounts of protein (10 µg) were resolved using sodium dodecyl sulfate-polyacrylamide gel electrophoresis (SDS-PAGE) (Criterion Precast, BioRad, Italy) and transferred to a Immobilon-P membrane (Millipore). Membranes were blocked with a bovine serum albumin solution (3% in Tween PBS 1X) for at least 2 h at room temperature. Membranes were then incubated with primary antibodies against Bcl-2, PARP, cdc25c, cyclin B, p-cdc2^{Tyr15}, Mcl-1 (all from Cell Signaling) and β-actin (Sigma-Aldrich) and gently rotated overnight at 4°C. Membranes were next incubated with peroxidase labeled secondary antibodies for 60 min. All membranes were visualized using ECL Select (GE Healthcare), and images were acquired using an Uvitec-Alliance imaging system (Uvitec, Cambridge, UK). To ensure equal protein loading, each membrane was stripped and reprobed with anti-ß-actin antibody.

3.5 Results

3.5.1 Molecular modelling

Among the synthetic inhibitors of tubulin polymerization, we previously described the synthesis and biological characterization of two series of compounds based on the 2-alkoxycarbonyl-3-(3',4',5'-trimethoxyanilino)benzo[*b*]thiophene and thieno[2,3-*b*]pyridine molecular skeletons (compounds with general structure 2 and 3, respectively) that showed strong antiproliferative activity against a panel of cell lines and act as inhibitors of microtubule polymerization by interfering with the colchicine site of tubulin (21). To investigate the possible binding mode for this series of compounds, we performed a series of molecular docking simulations in the colchicine site. The results obtained showed that the trimethoxyphenyl unit of these compounds is placed in proximity of βCys241. Furthermore, the formation of an intramolecular hydrogen bonding interaction between the anilino and the carbonyl groups in these series of molecules allows the formation of a hydrogen bond between the ester itself and βAla250. This study indicated that important structural requirements that play a crucial role in enhancing anti-microtubule activity are the presence of an alkoxycarbonyl moiety and a 3',4',5'-trimethoxyanilino function at the 2- and 3-position, respectively, of the thiophene ring fused with benzene or pyridine.

Based on these observations, a new series of 2-alkoxycarbonyl-3-(3',4',5'-trimethoxyanilino)thiophene derivatives with general formulae 4 was designed to explore the role of the benzene and pyridine portion of the benzo[*b*]thiophene and thieno[2,3-*b*]pyridine nucleus, respectively, in binding in the colchicine site of tubulin. We examined the replacement of benzo[*b*]thiophene and thieno[2,3-*b*]pyridine bicyclic systems by a thiophene ring substituted at its 5-position with an aryl or heteroaryl moiety, whereas the 2-methoxycarbonyl group and the 3-(3,4,5-trimethoxyanilino) function were kept unmodified.

To evaluate the influence in the binding in the colchicine site of tubulin of the new structural modifications, preliminary docking studies were performed, following a previous reported method (22). The new derivatives occupy the active site in a similar manner as the co-crystallized DAMA-colchicine (**Fig.3A:** DAMA and 2-methoxycarbonyl-3-(3',4',5'-trimethoxyanilino)-5-phenylthiophene derivative 4a), and their binding is consistent with the one reported previously for the thieno[2,3-*b*]pyridine series (**Fig.3B 4a** and thieno[2,3-*b*]pyridine **3a**). The trimethoxyphenyl ring is in proximity to Cys241, while the 5-phenyl ring is sitting deep in the small

hydrophobic pocket and potentially interacting with hydrophobic amino acids Met259, Thr314, Val181 and others. These interactions are similar to those modeled with the heterocycle of the thieno[2,3-*b*]pyridine series (**Fig.3C** compound **4a** alone). Small substitutions on the 5-phenyl ring could be tolerated and did not affect the binding in a negative manner. As found previously for the benzo[*b*]thiophene and thieno[2,3-*b*]pyridine series, a molecular docking study revealed that the *ortho*-relationship between the alkoxycarbonyl group and the 3,4,5-trimethoxyanilino moiety plays an important role in activity. This allows the formation of an intramolecular hydrogen bond between the hydrogen of the anilino group and the oxygen of carbonyl group, resulting in formation of a hydrogen bond between the ester itself and Ala250, further stabilizing these new compounds in the colchicine site. Encouraged by the activity obtained with compound **4a**, we assessed the effects on biological activity of both the nature and position of electron-withdrawing (F, Cl, CF_3 and NO_2) and electron-releasing (CH_3, OCH_3 and OC_2H_5) substituents on the phenyl at the 5-position of 2-alkoxycarbonyl-3-(3',4',5'-trimethoxyanilino)thiophene system as well as the replacement of the phenyl with the bioisosteric thien-2'-yl.

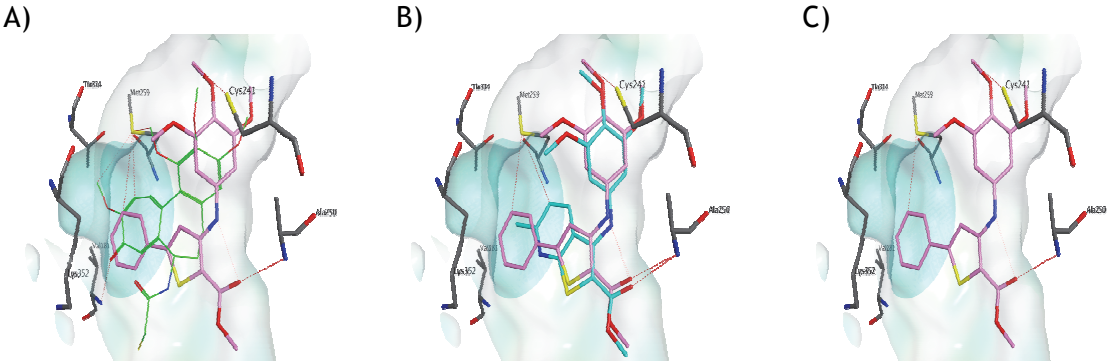

Fig. 3 Proposed binding for compound **4a** in comparison with DAMA-colchicine A) and derivative **3a** B) in the colchicine site. Co-crystallized DAMA-colchicine is shown in green, compound **4a** in magenta, and compound **3a** in turquoise. The hydrophobic subpocket is highlighted with a turquoise surface. C)Proposed binding for compound **4a** alone in the colchicine site. The hydrophobic subpocket is highlighted with a turquoise surface

3.5.2 Chemistry

2-Alkoxycarbonyl-3-(3',4',5'-trimethoxyanilino)-5-aryl/heteroaryl thiophene derivatives **4a-r** were synthesized by a four step procedure summarized in **Scheme 1**. β-Chloroaryl cinnamoniriles **6a-m** were obtained by a modified Vilsmeier reaction of commercially available acetophenones **5a-m** with phosphorus(V)oxychloride ($POCl_3$) in dimethylformamide, followed by treatment with hydroxylamine hydrochloride

($NH_2OH{\cdot}HCl$) (23). The subsequent condensation of compounds **6a-m** with methyl or ethyl thioglycolate using sodium methoxide (MeONa) as base in a mixture of methanol/DMF furnished in mild conditions the corresponding 2-alkoxycarbonyl-3-amino-5-aryl/heteroaryl thiophene derivatives **7a-r** in good yields through the nucleophilic displacement of chlorine, followed by base-induced ring closure in a single step. Subsequent deaminative bromination using modified Sandmeyer conditions of 3-amino thiophenes **7a-r** using *tert*-butyl nitrite (*t*-BuONO) in acetonitrile in the presence of copper(II)bromide ($CuBr_2$) gave the target bromothiophene **8a-r** in excellent yield. Finally, the novel derivatives **4a-r** were obtained using Buchwald-Hartwig conditions, by coupling of bromide **8a-r** with 3,4,5-trimethoxyaniline in a palladium (II)acetate [$Pd(OAc)_2$], 2,2-bis(diphenylphosphino)1,1'-binaphthyl (BINAP) catalytic system in the presence of cesium carbonate (Cs_2CO_3) as base in toluene at 100°C for 18 h.

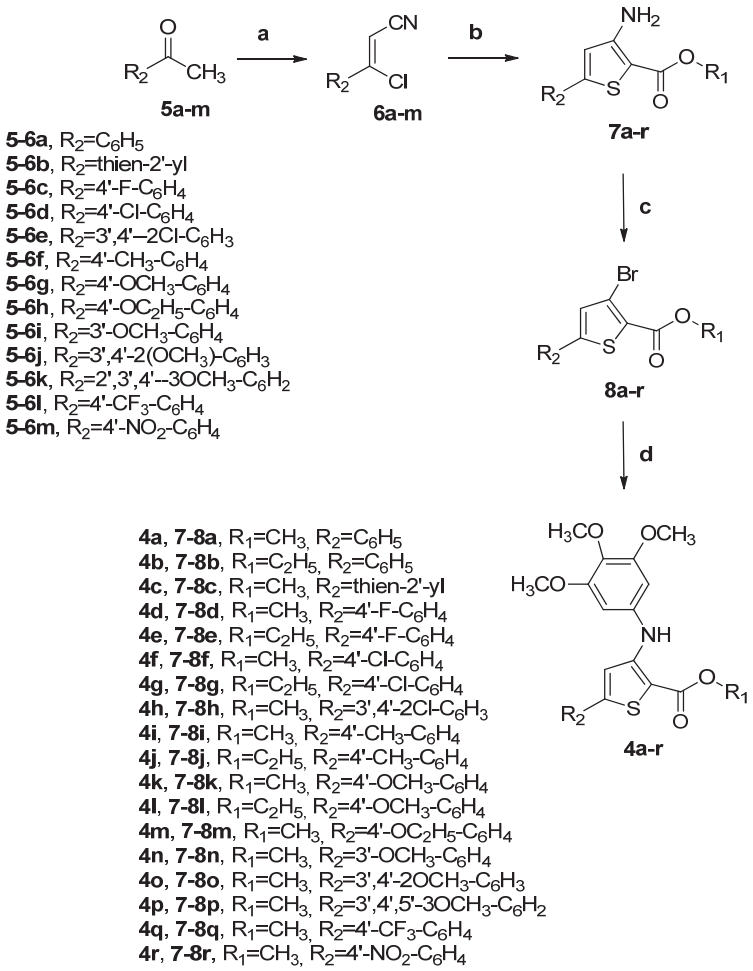

Scheme 1 Reagents: a) POCl3, DMF then NH2OH.HCl; b: HSCH2CO2CH3 or HSCH2CO2C2H5, MeONa, MeOH/DMF, 60°C, 4 h; b) t-BuONO, CuBr2, CH3CN, 0°C then room temperature for 2 h; c) 3,4,5-trimethoxyaniline, Pd(OAc)2, BINAP, Cs2CO3, PhMe, 100°C, 18 h.

3.5.3 In vitro antiproliferative activities

Table 1 summarizes the antiproliferative effects of the 2-alkoxycarbonyl-3-anilino-5-substituted thiophene derivatives **4a-r** against the growth of murine leukemia (L1210), murine mammary carcinoma (FM3A/0), human T-lymphoblastoid leukemia (CEM) and human cervix carcinoma (HeLa) cells as compared with the reference compound CA-4. Comparing compounds which shared a common aryl moiety at the 5-position of the of 2-alkoxycarbonyl-3-(3',4',5'-trimethoxyanilino)thiophene scaffold, the 2-methoxycarbonyl derivatives were more potent than the 2-ethoxycarbonyl counterparts (**4a, 4d, 4f, 4i, 4k** versus **4b, 4e, 4g, 4j, 4l,** respectively). Ignoring compound **4p**, all synthesized compounds possessed significant cell growth inhibitory activity, which was lower than 1 μM for compounds **4a**, **4c-d**, **4i-k**, **4o** and **4r** in all cell lines. Hydrophobic moieties such as phenyl and thien-2'-yl were well tolerated at the 5-position of the 2-alkoxycarbonyl-3-(3',4',5'-trimethoxyanilino)thiophene scaffold, and variation of the phenyl substituents had variable effects on potency. Replacement of the phenyl ring of compound **4a** by the bioisosteric thien-2' ring, to yield derivative **4c**, increased antiproliferative activity 2-4-fold against L1210 and HeLa cells, while the two compounds showed comparable potency against FM3A and CEM cells. Of all the tested compounds, the thien-2'-yl derivative **4c** possessed the highest overall cytostatic potency and inhibited the growth of the four cancer cell lines with IC_{50} values of 0.13-0.16 μM, being 10- to 100-fold more active than the reference compound CA-4. Compound 4i was nearly as active as **4c**.

SAR was elucidated by substitution with electron-releasing and electron-withdrawing groups on the phenyl moiety at the 5-position of the 2-alkoxycarbonyl-3-(3',4',5'-trimethoxyanilino)thiophene system. In general, single modification at the *para*-position of the phenyl ring was well tolerated and *para*-substituted phenyl derivatives showed variable potencies, suggesting an opportunity for further exploration. In comparing the effect of electron releasing (ERG's) or electron witwdrawing groups (EWG's) at the *para*-position of the phenyl ring, in all cell lines compounds **4i** and **4k** with electron-donating methyl or methoxy groups, respectively, were generally more cytostatic than those with the electron-withdrawing fluoro or chloro moieties (derivatives **4d** and **4f**, respectively). The same effect was observed for the 2-ethoxycarbonyl derivatives (**4j** and **4l** *vs.* **4e** and **4g**). Substituents at the *para*-position of the 5-phenyl ring showed antiproliferative activity in the order: Me>OMe>F>Cl=NO_2>CF_3>>OEt.

Potency was reduced from 4- to 7-fold after the weak ERG *p*-methyl (**4i**) was replaced with the EWG trifluoromethyl in compound **4q**. Turning to the effect of ERG's on the phenyl moiety, with the exception of HeLa cells, we found that *para*-tolyl and *para*-methoxyphenyl groups (compounds **4i** and **4k**, respectively) caused only minor changes in antiproliferative activity relative to the unsubstituted phenyl analogue **4a**.

Relative to the activity of the unsubstituted phenyl analogue **4a**, the introduction of the EWG fluorine at the *para*-position of the phenyl ring (compound **4d**) caused a 2-4-fold reduction of antiproliferative activity in three of the four cancer cell lines. Increasing the size of the halogen from fluorine to chlorine (compounds **4d** and **4f**, respectively) reduced the activity on L1210 and CEM cells, while the two compounds were equipotent against FM3A and HeLa cell lines. While a single chlorine atom at the *para*-position of the phenyl group was tolerated for activity (**4f**), double substitution by the introduction of a second chlorine atom to furnish the *meta*, *para*-dichlorophenyl derivative **4h** caused a 4-5-fold reduction of potency relative to **4f** in all cell lines. Replacement of the chlorine atom with even stronger EWG's (trifluoromethyl or nitro; derivatives **4q** and **4r**, respectively) had generally little further effect on activity against the four cell lines.

Replacement of the fluorine atom of **4d** with the weak ERG methyl, resulting in *para*-tolyl derivative **4i**, increased antiproliferative activity by 3-4-fold against all cell lines, with potency similar to that of the thien-2'-yl analogue **4c**.

The number and location of methoxy substitutents on the phenyl ring played a profound role in antiproliferative activity. A comparison between the antiproliferative activities of compounds **4k** and **4n-p**, illustrated the antiproliferative SAR of the number of methoxy groups substituted on the phenyl ring (1>2>>3). The introduction of a single methoxy group at the *para*-position (compound **4k**) caused only minor changes in antiproliferative activity relative to the unsubstituted derivative **4a**. Moving the methoxy group from the *para*- to the *meta*-position, to furnish **4n**, reduced antiproliferative activity 3-4-fold on three of the cancer cell lines. Reduced activity (2-fold) on three cancer cell lines relative to **4k** occurred with the insertion of a second methoxy group, to furnish the *meta*, *para*-dimethoxyphenyl analogue **4o**, while activity was maintained against HeLa cells. This latter compound has antiproliferative activity similar to that of *meta*-methoxy analogue **4n** against HeLa cells and increased potency against the three other cell lines. These results suggest that the optimal position for mono-methoxy substitution

is the *para*-position, as in compound **4k**. Adding a third methoxy group, to yield derivative **4p**, abolished antiproliferative activity.

These results suggested that the space for accepting substituents on the phenyl at the 5-position of 2-alkoxycarbonyl-3-(3',4',5'-trimethoxyanilino)thiophene system is highly limited and that the phenyl ring is specifically recognized by tubulin in a highly specific manner. In an effort to further understand the steric effect of the alkoxy substitution at the *para*-position of the phenyl ring, replacement of the *para*-methoxy with a *para*-ethoxy homologue (compound **4m**) resulted in a 5-20-fold reduction of cytostatic activity in all cell lines.

Table 1 In vitro inhibitory effects of compounds **4a-r** and CA-4 against the proliferation of murine leukemia (L1210), murine mammary carcinoma (FM3A), human T-lymphocyte leukemia (CEM) and human cervix carcinoma (HeLa) cells

Compounds	IC_{50} μM			
	L1210	FM3A/0	CEM	HeLa
4a	0.24 ± 0.01	0.21 ± 0.03	0.20 ± 0.08	0.67 ± 0.40
4b	1.1 ± 0.0	0.98 ± 0.13	0.93 ± 0.08	1.4 ± 0.7
4c	0.13 ± 0.07	0.16 ± 0.01	0.16 ± 0.08	0.16 ± 0.02
4d	0.56 ± 0.38	0.72 ± 0.19	0.53 ± 0.38	0.88 ± 0.16
4e	1.1 ± 0.0	1.0 ± 0.2	0.99 ± 0.24	2.1 ± 1.1
4f	1.1 ± 0.1	0.88 ± 0.08	0.87 ± 0.18	0.87 ± 0.13
4g	6.0 ± 0.0	5.1 ± 0.5	4.6 ± 0.6	9.8 ± 5.0
4h	5.7 ± 0.1	4.6 ± 0.6	3.3 ± 1.7	5.0 ± 1.3
4i	0.15 ± 0.08	0.18 ± 0.01	0.18 ± 0.04	0.26 ± 0.10
4j	0.82 ± 0.31	0.82 ± 0.23	0.76 ± 0.38	0.78 ± 0.06
4k	0.27 ± 0.03	0.25 ± 0.04	0.23 ± 0.10	0.84 ± 0.10
4l	1.2 ± 0.1	1.2 ± 0.1	1.1 ± 0.3	2.3 ± 1.5
4m	6.3 ± 0.0	5.7 ± 0.5	5.4 ± 1.3	4.4 ± 0.2
4n	1.1 ± 0.1	0.99 ± 0.10	0.69 ± 0.46	0.80 ± 0.06
4o	0.48 ± 0.27	0.43 ± 0.29	0.47 ± 0.35	0.89 ± 0.08
4p	>250	>250	>250	162 ± 25
4q	1.2 ± 0.1	1.1 ± 0.1	0.81 ± 0.33	1.3 ± 0.2
4r	0.99 ± 0.13	0.93 ± 0.08	0.76 ± 0.21	1.0 ± 0.3
CA-4 (nM)	3 ± 1	42 ± 6	2 ± 1	2 ± 1

IC_{50} = compound concentration required to inhibit tumour cell proliferation by 50%. Data are expressed as the mean ± SD from three independent experiments

3.5.4 Evaluation of cytotoxicity of 4a, 4c and 4i compounds in human noncancer cells

To obtain a preliminary indication of the cytotoxic potential of these derivatives in normal human cells, three of the most active compounds (**4a, 4c** and **4i**) were evaluated *in vitro* against peripheral blood lymphocytes (PBL) from healthy donors **(Table 2).** All compounds were practically devoid of a significant citotoxic activity in quiescent lymphocytes being the GI_{50} in the range of 30-85 μM, while in the presence of the mitogenic stimulus phytohematoaglutinin (PHA), the GI_{50} slightly increase to about 20-30 μM.

Nevertheless, these values, even in proliferation conditions, are more than 100 times that found in the two lines of T lymphoblastic leukemia (L1210 and CEM) reported in **Table 2**. These results indicate that these compounds are endowed with a very modest effect in rapidly proliferating cells but not in quiescent cells.

Table 2. Cytotoxicity of compounds **4a**, **4c** and **4i** for human peripheral blood lymphocytes (PBL)

	GI_{50} (μM) [a]		
	4a	**4c**	**4i**
$PBL_{resting}$[b]	45.7 ± 10.9	85.7 ± 8.9	31.7 ± 2.0
PBL_{PHA}[c]	19.0 ± 1.7	29.3 ± 1.2	20.0 ± 1.1

[a]Compound concentration required to reduce cell growth inhibition by 50%.

[b] PBL not stimulated with PHA.

[c] PBL stimulated with PHA.

Values are the mean ± SEM from two separate experiments.

3.5.5 Inhibition of tubulin polymerization and colchicine binding

To investigate whether the activities of these molecules were related to an interaction with the microtubule system, the more active compounds (**4a**, **4c-d**, **4i**, **4k** and **4o**) and reference compound CA-4 were evaluated for their *in vitro* tubulin polymerization inhibitory activity as well as for their inhibitory effects on the binding of [^{3}H]colchicine to tubulin (in the latter assay, the compounds and colchicine were at 5 μM, and tubulin was at 1 μM) **(Table 3).** In the tubulin polymerization assay, these compounds showed IC_{50} values in a relatively narrow range (1,2-2,7 μM). Three compounds (**4a**, **4c** and **4i**) showed the best tubulin polymerization assembly inhibition ability (IC_{50}: 1,2-1,3 μM), which is comparable to the IC_{50} of 1,1 μM obtained with CA-4, while derivatives **4d**, **4k** and **4o** were about half as potent as CA-4. Derivatives **4a**, **4c** and **4i** also displayed the most potent activities against the panel of four cancer cell lines. The results obtained demonstrated that antiproliferative activity correlated well with inhibition of tubulin polymerization.

In the colchicine binding studies, compounds **4a**, **4c** and **4i** were also the best inhibitors of the binding of [^{3}H]colchicine to tubulin. None, however, was quite as potent as CA-4, which in these experiments inhibited colchicine binding by 99%. The potent inhibition observed with these compounds indicated that **4a**, **4c** and **4i** bind to

tubulin at a site overlapping the colchicine site. This group of compounds were all highly potent in the biological assays (inhibition of cell growth, tubulin assembly and colchicine binding), and there was a good correlation between the three assay types. We conclude that the antiproliferative activity of these derivatives derives from an interaction with the colchicine site of tubulin and interference with cellular microtubule assembly.

Table 3 Inhibition of tubulin polymerization and colchicine binding by compounds **4a**, **4c-d**, **4i**, **4k**, **4o** and CA-4.

Compound	Tubulin assembly[a] IC_{50} ± SD (μM)	Colchicine binding[b] % ± SD
4a	1.3 ± 0.2	57 ± 5
4c	1.2 ± 0.1	62 ± 1
4d	2.2 ± 0.3	41 ± 5
4i	1.2 ± 0.0	70 ± 3
4k	2.0 ± 0.3	46 ± 4
4o	2.7 ± 0.0	30 ± 3
CA-4	1.1 ± 0.1	99 ± 3

A)Inhibition of tubulin polymerization. Tubulin was at 10 μM; b) inhibition of [^{3}H]colchicine binding. Tubulin, colchicine and tested compound were at 1, 5 and 5 μM, respectively.

3.5.6 Effects of 4a, 4c and 4i on the cell cycle

The effect of compounds 4a, 4c and 4i on cell cycle progression was examined by flow cytometry in Hela cells. After a 24 h treatment (**Fig.4**), the three compounds induced a G2-M arrest that became evident at the highest concentration used (500 nM). A concomitant reduction of cells in the G1 phase was also observed, while S phase cells remained essentially constant, although there was a slight increase in S phase cells that occurred at 500 nM with all compounds.

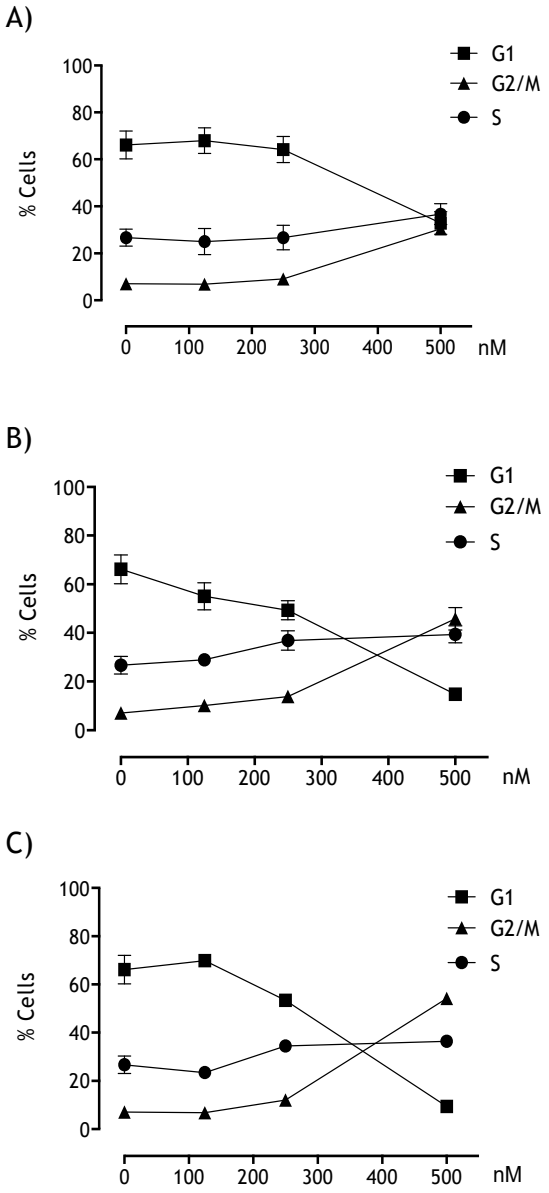

Fig. 4 Compounds 4a, 4c, 4i induce G2-M arrest in Hela cells. Percentage of cells in each phase of the cell cycle in HeLa cells, treated with compounds **4a** (A), **4c** (B) and **4i** (C) at the indicated concentrations for 24 h. Cells were fixed and labeled with PI and analyzed by flow cytometry as described in the Experimental Section. Data are presented as mean of two independent experiments ± SEM.

We also studied the association between **4c**-induced G2-M arrest and alterations in G2-M regulatory protein expression in HeLa cells. As shown in **Fig.5**, compound **4c** caused, in a concentration-dependent manner, an increase in cyclin B1 expression after 24 h, followed by a marked reduction at 48 h, indicating an activation of the mitotic checkpoint following drug exposure (24). This effect was confirmed by a remarkable reduction in the expression of phosphatase cdc25c after a 24 h

incubation, even at the lowest concentration used (100 nM). The phosphorylation of cdc25c directly stimulates its phosphatase activity, and this is necessary to activate cdc2(CDK1)/cyclin B on entry into mitosis (25). Accordingly, we observed a decrease in the phosphorylated form of cdc2 (CDK1) kinase after 24 h and 48 h treatments at 250 nM.

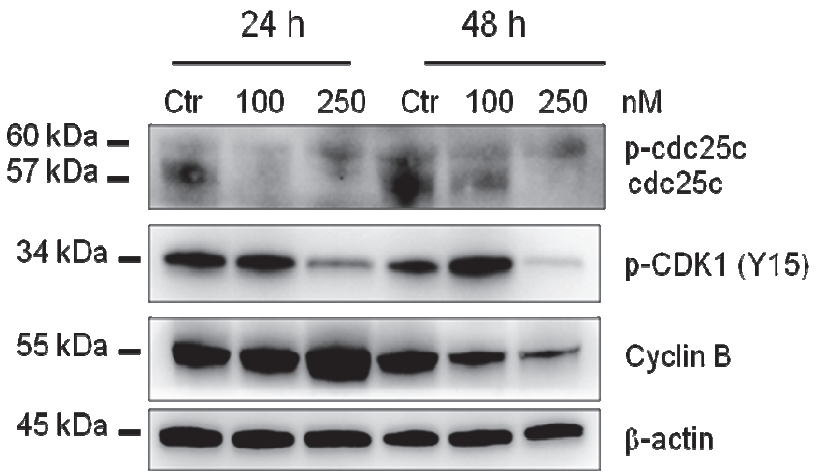

Fig. 5 Effect of compound 4c on cell cycle checkpoint proteins. HeLa cells were treated for 24 or 48 h with the indicated concentrations of **4c**. The cells were harvested and lysed for detection of the expression of the indicated proteins by western blot analysis. To confirm equal protein loading, each membrane was stripped and reprobed with anti-β-actin antibody.

3.5.7 Compounds 4a, 4c and 4i induce apoptosis

To evaluate the mode of cell death, we treated HeLa cell with compounds **4a**, **4c** and **4i**, and, after 24 and 48 h incubations, we performed a biparametric cytofluorimetric analysis using propidium iodide (PI) and annexin-V-FITC, which stain DNA and phosphatidylserine (PS) residues, respectively. As shown in **Fig.6**, the three compounds induced a significant proportion of apoptotic cells after the 24 h incubation, and this proportion increase markedly at 48 h. The most active compounds appear to be **4c** and **4i**, in good agreement with the antiproliferative results presented in **Table 1**.

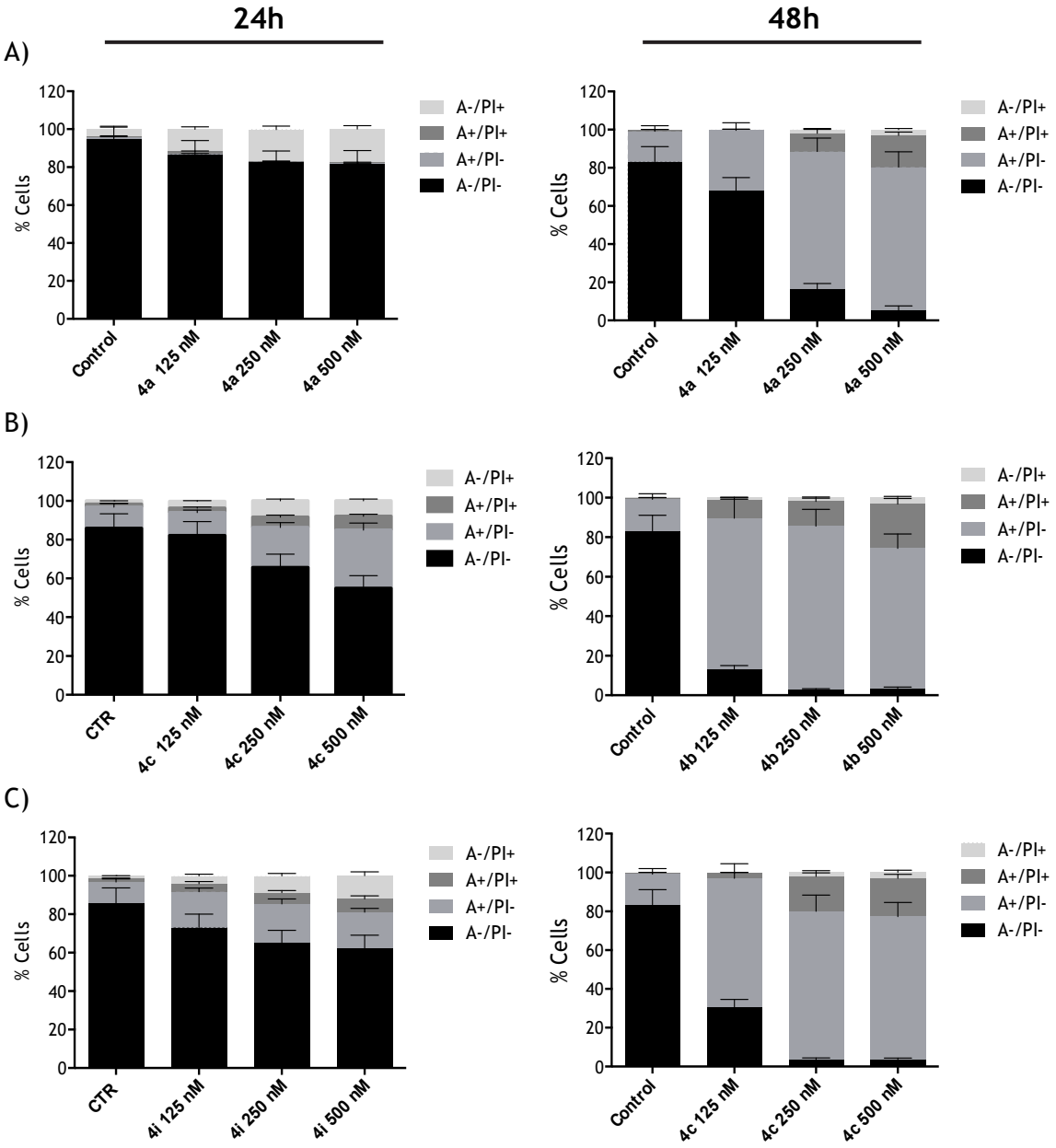

Fig. 6 Flow cytometric analysis of apoptotic cells after treatment of HeLa cells with **4a** (A), **4c** (B) and **4i** (C) at the indicated concentrations after incubation for 24 or 48 h. The cells were harvested and labeled with annexin-V-FITC and PI and analyzed by flow cytometry. Data are presented as mean ± SEM of three independent experiments.

3.5.8 Compound 4c induces mitochondrial depolarization and ROS production

It is well known that mitochondria are involved in the initiation of apoptosis, since, at an early stage, apoptotic stimuli alter the mitochondrial transmembrane potential ($\Delta\psi_{mt}$) (26,27). To determine whether the cells treated with compound **4c** underwent mitochondrial depolarization, we assessed the changes in $\Delta\psi_{mt}$ in HeLa cells by flow cytometry using the fluorescent dye JC-1. HeLa cells treated with compound **4c** (100-

250 nM) showed a time-dependent increase in the percentage of cells with low $\Delta\psi_{mt}$ (**Fig.7A**). The depolarization of the mitochondrial membrane is associated with the appearance of annexin-V positivity in the treated cells when they are in an early apoptotic stage (28). One of the major consequences of the increase of mitochondrial membrane permeability is the release into the cytosol of pro-apoptotic factors such as procaspases and, in particular, cytochrome c (29) This release triggers ROS production at the mitochondrial level during the later stages of the cell death program. We therefore investigated whether ROS production increased after treatment with compound **4c**. We analyzed ROS production by flow cytometry, using the fluorescence indicator H_2-DCFDA. As shown in **Fig.7B**, compound **4c** induced significant production of ROS starting after a treatment of 12-24 h at 250 nM, in good agreement with the mitochondrial depolarization described above.

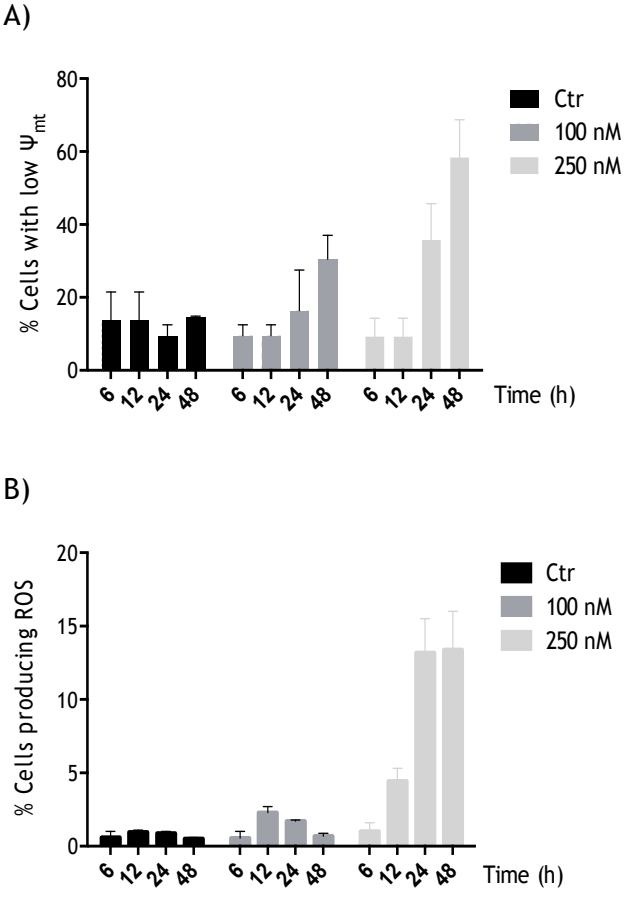

Fig. 7 Compound 4c induces mitochondrial depolarization and ROS production.

(A) Hela cells were treated with the indicated concentration for 6, 12, 24 or 48 h and then stained with the fluorescent probe JC-1 for analysis of mitochondrial potential. Cells were then analyzed by flow cytometry as described in the experimental section. Data are presented as mean ± SEM of three independent experiments.

(B) Cells were treated with the indicated concentration for 6, 12, 24 or 48 h and then stained with H_2-DCFDA for evaluation of ROS levels. Cells were then analyzed by flow cytometry as described in the Experimental Section. Data are presented as mean ± SEM of three independent experiments.

3.5.9 Compound 4c induced PARP activation and decreased expression of anti apoptotic proteins

To further investigate the mechanism of apoptosis induction by **4c**, we analyzed the

expression of poly (ADP-Ribose) polymerase (PARP), a protein involved in late stage apoptosis, and the expression of two anti-apoptotic proteins belonging to the Bcl-2 family. As shown in **Fig.8**, compound **4c** in HeLa cells caused a concentration- and time-dependent cleavage of PARP confirming the pro-apoptotic properties of **4c**.

We also investigated the expression of anti-apoptotic proteins such as Bcl-2 and Mcl-1. It is well known that antimitotic agents can modulate both expression levels and activity of many proteins of the Bcl-2 family (30, 31, 32) Our results **(Fig.8)** showed that the expression of both anti-apoptotic proteins Bcl-2 and Mcl-1 were decreased starting after 24 h of treatment, even at the lowest **4c** concentration used (0.1 μM). These studies underline the importance of Mcl-1 phosphorylation and its subsequent degradation in response to antimitotic agents and that this event potentiates cell death (33).

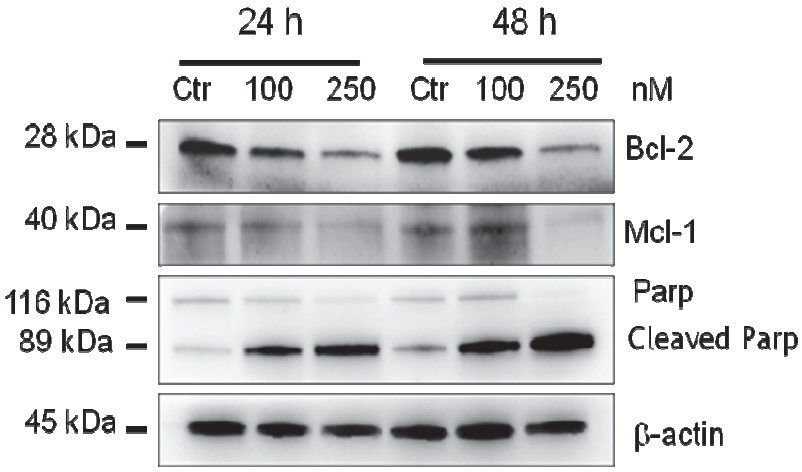

Fig. 8 Western blot analysis of, Bcl-2, Mcl-1 and PARP after treatment of HeLa cells with **4c** at the indicated concentrations and times. To confirm equal protein loading, each membrane was stripped and reprobed with anti-β-actin antibody.

3.6 Discussion

We have discovered a new class of simple synthetic inhibitors of tubulin polymerization based on the molecular skeleton of 2-alkoxycarbonyl-3-(3',4',5'-trimethoxyanilino)thiophene. These derivatives were designed and synthesized based on modification of benzo[b]thiophene and thieno [2,3-b]pyridine analogues previously published. The results demonstrated that the aryl or 2-thienyl moieties at the 5-position of the 2-alkoxycarbonyl-3-(3',4',5'-trimethoxyanilino)thiophene system could replace either the benzene or the pyridine portion of benzo[b]thiophene and thieno [2,3-b]pyridine derivatives with general structure 2 and 3, respectively. We explored SAR by examining various substitutions with EWGs and ERGs on the phenyl at the 5-position of the 2-alkoxycarbonyl-3-(3',4',5'-trimethoxyanilino)thiophene scaffold. The presence of ERGs such as methyl or methoxy was beneficial for antiproliferative activity, as these compounds proved to be more potent than the corresponding derivatives with the EWGs fluorine or chlorine. Generally, it was found that most substituents in the para-position resulted in lower activity as compared to the unsubstituted parent compound **4a**, with the least deleterious being methyl and methoxy moieties (compounds **4i** and **4k**, respectively).

It is clear that the substitution pattern on the phenyl at the 5-position of the 2-methoxycarbonyl-3-(3',4',5'-trimethoxyanilino)thiophene system plays an important role for antitubulin and antiproliferative activities, and this was supported by the molecular docking studies. SAR studies showed that the 2-methoxycarbonyl-3-(3',4',5'-trimethoxyanilino)-5-phenylthiophene derivative **4a**, its bioisosteric thien-2'-yl analogue **4c** as well as the para-tolyl and para-methoxyphenyl analogues **4i** and **4k**, respectively, displayed high antiproliferative activities, with IC_{50} values 0.13-0.24, 0.16-0.25, 0.16-0.23 and 0.16-0.84 μM, respectively, against the L1210, FM3A, CEM and HeLa cell lines. Of all the tested compounds, derivative **4c** possessed the highest overall cytostatic potency with IC_{50} values ranging from 0.13 to 0.16 μM against the panel of four cancer cell lines. The antiproliferative activity was considerably increased by replacing the EWG fluorine with the ERG methyl group (compounds **4d** and **4i**, respectively), with the latter compound being about 3-6-fold more active than the former. By comparing **4d** and **4f**, replacement of the para-fluoro group in **4d** with the chloro (derivative **4f**) led to little change in activity against FM3A and HeLa cells, while **4f** was less potent than **4d** in L1210 and CEM

cells. Replacement of the EWG para-chlorine atom of **4f** with the ERG para-methyl moiety, to furnish derivative **4i**, resulted in 4-6-fold enhancement in antiproliferative activity against the four cancer cell lines. Replacement of the methyl with a methoxy group (derivative **4k**) produced a 2- and 3-fold reduction in potency against L1210 and HeLa cells, respectively, while the difference between **4i** and **4k** were minimal in FM3A and CEM cells.

The antiproliferative activity of the thiophene derivatives **4k** and **4n-p** can be further characterized in terms of the substitution pattern and the number of methoxy groups on the phenyl ring. The introduction of a single methoxy group at the para-position caused only minor changes in antiproliferative activity relative to the unsubstituted derivative **4a**. Reduced activity occurred in three of the four cancer cell lines when the methoxy substituent was moved from the para- to the meta-position (**4n**), with the exception of HeLa cells. As previously observed comparing the activities of para-chloro and meta, para-dichloro derivatives **4f** and **4h**, respectively, the introduction of a second methoxy group at the meta-position of para-methoxyphenyl derivative **4k**, to furnish the meta, para-dimethoxyphenyl analogue 4o, decreased potency in three of the four cancer cell lines by 2-fold, with the exception of the HeLa cells. The 3',4',5'-trimethoxyphenyl derivative **4p** was not active, and this result suggested the space for accepting substituents on the phenyl ring at the 5-position of the 2-alkoxycarbonyl-3-(3',4',5'-trimethoxyanilino)thiophene scaffold is highly limited. This conclusion was supported by comparing the reduced activity (on average 20-fold) of the para-ethoxy homologue **4m** relative to the para-methoxy analogue **4k**.

The results we obtained indicated that compound **4c** could induce tumour cell apoptosis through reducing the mitochondrial membrane potential and regulating the expression of apoptosis-related proteins in tumour cells.

3.7 References

1) Pettit G.R., Temple C. Jr., Narayanan, V.L., Varma, R., Boyd M.R., Rener, G.A., Bansal, N. (1995) Antineoplastic agents 322. Synthesis of combretastatin A-4 prodrugs *Anti-Cancer Drug Des* 10: 299-309
2) Van Vuuren R.J., Visagie M.H., Theron A.E., Joubert A.M. (2015) Antimitotic drugs in the treatment of cancer *Cancer Chemother Pharmacol* 76: 1101-1112
3) Akhmanova A., Steinmetz M.O. (2015) Control of microtubule organization and dynamics: two ends in the limelight Nat Rev Mol Cell Biol 16: 711-726
4) Siemann D. W., Chaplin D. J., Walike P. A. (2009) A review and update of the current status of the vasculature-disabling agent combretastatin-A4 phosphate (CA4P) *Expert Opin Investig Drugs* 18: 189-197
5) Romagnoli R., Baraldi P., G. Carrion M. D., Cruz-Lopez O., Lopez-Cara C., Basso G., Viola G., Khedr M., Balzarini J., Mahboobi S., Sellmer A., Brancale A., Hamel E. (2009) 2-Arylamino-4-amino-5-aroylthiazoles. "One-pot" synthesis and biological evaluation of a new class of inhibitors of tubulin polymerization *J Med Chem* 52: 5551-5555
6) Das U., Sharma R. K., Dimmock J. R. (2009) 1,5-diaryl-3-oxo-1,4-pentadienes: a case for antineoplastics with multiple targets *Curr Med Chem* 16: 2001-20
7) "Microtubule and filaments" *Essentials of Biology Unit 3 - Nature education*
8) Parker L.A., Kavallaris M., McCarroll A. J. (2014) Microtubules and Their Role in Cellular Stress in Cancer *Front Oncol* 4: 153
9) Mukhtar E., Adham V.M.i, Mukhtar H. (2014) Targeting Microtubules by Natural Agents for Cancer Therapy *Mol Cancer Ther* 13: 275–284
10) Jordan M.A., Wilson L. (1998) Microtubules and actin filaments: dynamic targets for cancer chemotherapy *Curr Opin Cell Biol* 10:123-30
11) Jordan M. A. and Wilson L. (2004) Microtubules as a target for anticancer drugs *Nature Reviews Cancer* 4: 253-265
12) Kavallaris M. (2010) Microtubules and resistance to tubulin-binding agents *Nat Rev Cancer* 10: 194-204
13) Hamel E. (2003) Evaluation of antimitotic agents by quantitative comparisons of their effects on the polymerization of purified tubulin *Cell Biochem Biophys* 38:1-21
14) Lange J. H. M., van Stuivenberg H. H., Coolen H. K. A. C., Adolfs T. J. P., McCreary A. C., Keizer H. G., Wals H. C., Veerman W., Borst A. J. M., de Looff

W., Verveer P. C., Kruse C. G. (2005) Bioisosteric replacements of the pyrazole moiety of rimonabant: Synthesis, biological properties, and molecular modeling investigations of thiazoles, triazoles, and imidazoles as potent and selective CB1 cannabinoid receptor antagonists *J Med Chem* 48: 1823-1838

15) Thomae D., Perspicace E., Hesse S., Kirsch G., Seck P. (2008) Synthesis of substituted [1,3]thiazolo[4,5-*d*][1,2.3]triazines *Tetrahedron* 64: 9306-9314

16) Webb R. L., Eggleston D. S., Labaw C. S., Lewis J. J., Wert K. (1987) Diphenyl cyancarbonimidate and dichlorodiphenoxymethane as synthons for the construction of heterocyclic systems of medicinal interest *J Heterocycl Chem* 24: 275-278

17) Verdier-Pinard P., Lai J-Y, Yoo H-D., Yu J., Marquez B., Nagle D. G., Nambu M., White J.D., Falck J. R., Gerwick W. H, Day B. W., Hamel E. (1998) Structure-activity analysis of the interaction of curacin A, the potent colchicine site antimitotic agent, with tubulin and effects of analogs on the growth of MCF-7 breast cancer cell *Mol Pharmacol* 53: 62-67

18) O. Korb, T. Stützle, T. E. Exner. PLANTS: Application of ant colony optimization to structure-based drug design. In *Ant Colony Optimization and Swarm Intelligence*, 5th International Workshop, ANTS 2006, Brussels, Belgium, Sep 4-7, 2006. M. Dorigo, L.M. Gambardella, M. Birattari, A.; Martinoli, R. Poli, T. Sttzle. Eds.; Springer: Berlin, 2006; LNCS 4150, 247-258

19) Ravelli R. B. G., Gigant B., Curmi P. A., Jourdain I., Lachkar S., Sobel A., Knossow M. (2004) Insight into tubulin regulation from a complex with colchicine and a stathmin-like domain *Nature* 428

20) Ferlin M. G., Bortolozzi R., Brun P., Castagliuolo I., Hamel E., Basso G., Viola G. (2010) Synthesis and in vitro evaluation of 3*H*-pyrrolo[3,2-*f*]-quinolin-9-one derivatives that show potent and selective anti-leukemic activity *Chem Med Chem* 5: 1373-1385

21) Romagnoli R., Baraldi P. G., Salvador M. K., Preti D., Aghazadeh Tabrizi M., Bassetto M., Brancale A., Hamel E., Castagliuolo I., Bortolozzi R., Basso G., Viola G. (2013) Synthesis and biological evaluation of 2-alkoxycarbonyl-3-Anilino benzo[*b*]thiophenes and thieno[2,3-*c*]pyridines as new potent anticancer agents *J Med Chem* 56: 2606-2618.

22) Romagnoli R., Baraldi P. G., Salvador M.K., Camacho M.E., Preti D., Aghazadeh Tabrizi M., Bassetto M., Brancale A., Hamel E., Bortolozzi R., Basso G., Viola G. (2012) Synthesis and biological evaluation of 2-substituted-4-(3',4',5'-

trimethoxyphenyl)-5-aryl thiazoles as anticancer agents *Bioorg Med Chem* 20: 7083-7094

23) Romagnoli R., Baraldi P. G., Remusat V., Carrion M. D., Lopez Cara C., Preti D., Fruttarolo F., Pavani M. G., Aghazadeh Tabrizi M., Tolomeo M, Grimaudo S., Balzarini J., Jordan M. A., Hamel E. (2006) Synthesis and biological evaluation of 2-(3',4',5'-trimethoxybenzoyl)-3-amino 5-aryl thiophenes as a new class of tubulin inhibitors *J Med Chem* 49: 6425-6428
24) Weaver B. A. A., Cleveland D. W. (2005) Decoding the links between mitosis, cancer, and chemotherapy: the mitotic checkpoint, adaptation, and cell death *Cancer Cell* 8: 7-12
25) Clarke P. R., Allan L. A. (2009) Cell-cycle control in the face of damage- a matter of life or death *Trends Cell Biol* 19: 89-98.
26) Tsujimoto Y., Shimizu S. (2007) Role of the mitochondrial membrane permeability transition in cell death *Apoptosis* 12: 835-840
27) Xiong S., Mu T., Wang G., Jiang X. (2014) Mitochondria-mediated apoptosis in mammals *Protein Cell* 5: 737-749
28) Zamzami N., Marchetti P., Castedo M., Decaudin D., Macho A., Hirsch T., Susin S. A., Petit P. X., Mignotte B., Kroemer G. (1995) Sequential reduction of mitochondrial transmembrane potential and generation of reactive oxygen species in early programmed cell death *J Exp Med* 182: 367-377
29) Cai J., Jones D. P. (1998) Superoxide in apoptosis. Mitochondrial generation triggered by cytochrome c loss *J Biol Chem* 273: 11401-11404
30) Rovini A., Savry A., Braguer D., Carré M. (2011) Microtubule-targeted agents: when mitochondria become essential to chemotherapy *Biochim Biophys Acta - Bioenerg* 6: 679–688
31) Romagnoli R., Baraldi P.G., Lopez-Cara C., Preti D., Aghazadeh Tabrizi M., Balzarini J., Bassetto M., Brancale A., Xian-Hua F., Gao Y., Li J., Zhang S.-Z., Hamel E., Bortolozzi R., Basso G., Viola G. (2013) Concise synthesis and biological evaluation of 2-aroyl-5-amino benzo[*b*]thiophene derivatives as a novel class of potent antimitotic agents J Med Chem 56: 9296-9309
32) Romagnoli R., Baraldi P.G., Kimatrai Salvador M., Schiaffino Ortega S., Prencipe F., Brancale A., Hamel E., Castagliuolo I., Mitola S., Ronca R., Bortolozzi R., Porcù E., Basso G., Viola G. (2015) Design, Synthesis, in vitro and in vivo anticancer and antiangiogenic activity of novel 3-arylamino benzofuran derivatives targeting the colchicine site on tubulin J Med Chem 58: 3209-3222

33) Haschka M. D., Soratroi C., Kirschnek S., Häcker G.,. Hilbe R, Geley S., Villunger A., Fava L.L. (2015) The NOXA-MCL1-BIM axis defines lifespan on extended mitotic arrest *Nat Commun* 6: 6891